KfK 5359
Oktober 1994

On the Estimation of the Steam Generator Maintenance Efficiency by the Means of Probabilistic Fracture Mechanics

L. Cizelj
Institut für Materialforschung

Kernforschungszentrum Karlsruhe

Kernforschungszentrum Karlsruhe
Institut für Materialforschung

KfK 5359

On the Estimation of the Steam Generator Maintenance Efficiency by the Means of Probabilistic Fracture Mechanics

L.Cizelj

"Jožef Stefan" Institute, Reactor Engineering Division
Ljubljana, Slovenia

Kernforschungszentrum Karlsruhe GmbH, Karlsruhe

Als Manuskript gedruckt

Kernforschungszentrum Karlsruhe GmbH
Postfach 3640, 76021 Karlsruhe

ISSN 0303-4003

PREFACE

This report is an english version of the Ph.D Thesis entitled *Ocenjevanje uspešnosti vzdrževanja uparjalnikov s pomočjo verjetnostne mehanike loma*, which was accepted by the University of Ljubljana, Slovenia, in 1993. It is based on the *Short English Version* which was given in Appendix C of the original thesis. Some editing and slight expansion of the text was enhanced by the translation of the complete set of figures and tables, which are now included in the text. This resulted in a report which is shorter than original in Slovene, but contains the most important information about research performed.

The author wishes to express his gratitude to the supervisor Prof.Dr.Borut Mavko ("Jožef Stefan" Institute, Ljubljana, Slovenia) and cosupervisor Prof.Dr.Peter Vencelj (University of Ljubljana, Slovenia). Special thanks are due to Dr.Angelika Brückner-Foit (University of Karlsruhe, Germany) who actually wrote the *Short English Version* after my sometimes puzzled explanations of the Slovene original and Dr.Heinz Riesch-Oppermann (Kernforschungszentrum Karlsruhe, Germany) who introduced me to his ZERBERUS code.

I am further greatly indebted to the excellent teams of Reactor Engineering Division of "Jožef Stefan" Institute and Institut für Materialforschung II and their heads Prof.Dr.Borut Mavko and Prof.Dr.Dietrich Munz for the opportunity to share their experience.

Financial support granted by Ministry of Science of Republic of Slovenia, Nuklearna elektrarna Krško, Slovenia, The International Office of KFA Jülich, Germany and International Atomic Energy Agency is gratefully acknowledged.

ABSTRACT

Steam generator tubing represents a substantial part of the second fission product barrier in a pressurized water reactor nuclear power plant. Various ageing processes might significantly decrease its structural reliability. In particular, stress corrosion cracking of Inconel-600 tubes results in deep, often through-wall axial cracks which initiate in the areas dominated by the residual stresses.

In order to maintain an acceptable level of the steam generator reliability, different maintenance strategies have been developed and implemented. Usually, the non-destructive examination of tubes is performed followed by plugging excessively damaged tubes, which on the other hand reduces the heat transfer and steam generator life-time. The definition of the allowable tube damage criteria implicitly defines the efficiency of the maintenance both in terms of steam generator reliability and life-time. The world praxis recognized two approaches, based on either allowable defect depth or length.

In this report, an original probabilistic model aimed to assess the efficiency of particular maintenance strategy in terms of tube failure probability is proposed. The model concentrates on axial through wall cracks in the residual stress dominated tube expansion transition zone. It is based on the recent developments in probabilistic fracture mechanics and accounts for scatter in material, geometry and crack propagation data. Special attention has been paid to model the uncertainties connected to non-destructive examination technique (e.g., measurement errors, non-detection probability). First and second order reliability methods (FORM and SORM) have been implemented to calculate the failure probabilities. This is the first time that those methods are applied to the reliability analysis of components containing stress-corrosion cracks.

In order to predict the time development of the tube failure probabilities, an original linear elastic fracture mechanics based crack propagation model has been developed. It accounts for the residual and operating stresses together. Also, the model accounts for scatter in residual and operational stresses due to the random variations in tube geometry and material data. Due to the lack of reliable crack velocity vs load data, the non-destructive examination records of the crack propagation have been employed to estimate the velocities at the crack tips.

Abstract

Two numerical examples are provided. The first correlates the performance of the model to some earlier work. In particular, a numerical example with results obtained by different numerical techniques has been employed. Qualitative agreement of the results was satisfactory despite the significant differences in the crack propagation and maintenance models employed.

The second numerical example considered the Krško NPP steam generator number 1 after the 1992 refuelling maintenance. The potential of the crack length based plugging criterion to reduce the tube failure probability for a few orders of magnitude is shown, whereas the possible failure probability reduction depends strongly on the reliability of the non-destructive examination technique applied. Furthermore, concentrating the plugging on tubes with longer cracks significantly reduces the probability of multiple tube rupture. Comparing the performance of the crack length and crack depth based maintenance strategies showed that the crack depth plugging criterion may miss the majority of the long cracks, which leads to a high probability of multiple tube rupture following a hypothetical feed line break.

Based on the overall performance of the model, some comments concerning the risk-based steam generator life-time optimisation are given.

ZUSAMMENFASSUNG

EFFIZIENZBETRACHTUNGEN FÜR DIE INSTANDHALTUNG VON DAMPFERZEUGERN UNTER VERWENDUNG VON METHODEN DER PROBABILISTISCHEN BRUCHMECHANIK

Rohre in Dampferzeugern sind wesentlicher Teil der äußeren Barriere zur Rückhaltung von Spaltprodukten in Druckwasserreaktoren. Ihre Zuverlässigkeit kann durch verschiedene Alterungsprozesse beträchtlich vermindert werden. Besonders bei Rohren aus dem Werkstoff Inconel-600 können durch Spannungsrißkorrosion tiefe, oft durchgehende axiale Risse entstehen, vorzugsweise in jenen Bereichen, wo hohe Eigenspannungen vorhanden sind.

Zur Sicherstellung eines vertretbaren Zuverlässigkeitsniveaus wurden verschiedene Instandhaltungsstrategien entwickelt und verfolgt. Üblicherweise werden zerstörungsfreie Untersuchungen durchgeführt und Rohre die starke Schäden aufweisen, werden durch Pfropfen verschlossen. Das führt jedoch andererseits zu verringertem Wärmeübergang und reduzierter Lebensdauer des Dampferzeugers. Bei der Festlegung eines Kriteriums für zulässige Schädigung eines Dampferzeugerrohrs muß deshalb sowohl Ansprüchen an die Zuverlässigkeit des Dampferzeugers als auch an seine Lebensdauer Rechnung getragen werden. Weltweit existieren zwei Ansätze, die auf tolerierbarer Fehlertiefe (Rißtiefe) oder Fehlerlänge basieren.

In der vorliegenden Arbeit wird ein eigenes probabilistisches Modell vorgeschlagen, das zur Abschätzung der Effektivität einer bestimmten Instandhaltungsstrategie die Wahrscheinlichkeit für das Versagen von Rohren verwendet. Das vorgeschlagene Modell beschreibt durchgehende axiale Risse in der von hohen Eigenspannungen charakterisierten Übergangszone in der Nähe der Befestigung der Dampferzeugerrohre am Einlaß des Dampferzeugers. Dabei finden neuere Entwicklungen der probabilistischen Bruchmechanik Anwendung. Streuende Materialkennwerte, Geometriegrößen und Rißwachstumskennwerte können modelliert werden. Außerdem wurden Unsicherheiten in Verbindung mit zerstörungsfreien Prüfverfahren berücksichtigt (wie z.B. Meßfehler, Nichtentdeckungswahrscheinlichkeit von Fehlern). Zur Berechnung der Ausfallwahrscheinlichkeiten wurden Zuverlässigkeitsverfahren erster (FORM) und zweiter Ordnung (SORM) implementiert. Damit wurden diese Methoden zum ersten Mal zur Zuverlässigkeitsanalyse von Bauteilen im Bereich der Spannungsrißkorrosion angewandt.

Zusammenfassung

Um den zeitlichen Verlauf der Ausfallwahrscheinlichkeit für die betrachteten Rohre vorherzusagen, wurde ein eigenes bruchmechanisches Rißwachstumsmodell entwickelt. Es erlaubt die gemeinsame Berücksichtigung sowohl von Eigenspannungs- als auch von Betriebsbelastungen. Außerdem berücksichtigt das Modell von zufälligen Schwankungen in der Geometrie der Rohre und in den Materialkennwerten herrührende Streuungen der Eigenspannungs- und Betriebsbelastungen. Da keine verläßlichen Daten zur Rißgeschwindigkeit in Abhängigkeit von der Belastung existieren, wurden Aufzeichnungen aus zerstörungsfreien Untersuchungen des Rißwachstums verwendet, aus denen die Rißgeschwindigkeiten an den jeweiligen Rißenden abgeschätzt wurden.

Die vorgeschlagenen Verfahren wurden anhand von zwei Beispielen durchgeführt. Das erste Beispiel bestätigt die Leistungsfähigkeit des Modells anhand eines Vergleichs mit früheren Arbeiten. Bei diesem Beispiel wurden verschiedene numerische Verfahren angewendet. Es zeigt sich, daß die Übereinstimmung der Ergebnisse zufriedenstellend war, obwohl die verwendeten Modelle für Rißwachstum und Instandhaltung beträchtliche Unterschiede aufweisen.

Im zweiten Beispiel wurde der Dampferzeuger Nr. 1 des Krško Kernkraftwerks in Slowenien betrachtet, wobei die Daten der im Rahmen eines Brennelementwechsels 1992 stattfindenden Wartung verwendet wurden. Es wird gezeigt, daß das verwendete auf der Rißlänge basierende Kriterium zur Außerbetriebsetzung von Rohren eine Reduzierung der Ausfallwahrscheinlichkeit um einige Größenordnungen erlaubt, wobei das Ausmaß der zu erreichenden Reduzierung stark von der Zuverlässigkeit der zerstörungsfreien Prüfverfahren abhängt. Darüberhinaus ist zu sehen, daß durch Beschränkung der Außerbetriebsetzung auf Rohre mit längeren Rissen die Wahrscheinlichkeit des gleichzeitigen Bruches mehrerer Rohre signifikant verringert wird. Vergleicht man rißlängen- und rißtiefenorientierte Instandhaltungsstrategien, so zeigt sich, daß durch rißtiefenorientierte Kriterien zur Außerbetriebsetzung von Rohren ein Großteil langer Risse nicht erfaßt wird, was zu einer hohen Wahrscheinlichkeit für Mehrfachbrüche infolge eines hypothetischen Bruchs der Zuleitung führt.

Abschließend werden einige Überlegungen formuliert, die sich aus der Leistungsfähigkeit des Modells im Hinblick auf eine Risiko-basierte Optimierung der Lebensdauer von Dampferzeugern ergeben.

TABLE OF CONTENTS

Table of contents

LIST OF FIGURES

List of figures

LIST OF TABLES

LIST OF SYMBOLS

Uppercase

A	real crack length; random variable
A_1, A_2	tube cross-section before (1) and (2) after the rolling process
C, C_{-a}, C_{+a}	constant term in crack propagation law
D	event describing the detection of a crack
$\mathbf{D}$	matrix, transformation of standardized normal (u) into rotated (y) space
E	Youngs modulus
E_1, E_2	events
E_{app}	apparent activation energy
E_T	Tangent modulus (strain hardening parameter)
F_A	fraction of tubes without cracks
F_i	c.d.f. of i-th basic variable
F_{in}	fraction of inspected tubes (≤ 1)
F_M	fraction of tubes where cracks have been detected
F_{pl}	fraction of plugged tubes (subfraction of inspected tubes)
$\mathbf{G}_y$	matrix of failure function second order partial derivatives in rotated (y) space
$\mathbf{I}$	unit matrix
K, K_{-a}, K_{+a}	stress intensity factor
K_{ISCC}	stress corrosion crack propagation threshold
L	location of the crack centre in the residual stress filed
$\dot{\mathrm{L}}$	velocity of the crack centre relative to the residual stress field origin
L_{init}	location of the peak hoop residual stress value
M	measured crack length; random variable
N, N_{SG}	number of tubes in the steam generator
N_M	number of tubes with detected cracks
$P(i)$	probability of having i tubes ruptured
$P(i=1)$	single tube rupture probability
$P(i\geq 1)$	tube rupture probability
$P(i\geq 2)$	multiple tube rupture probability
$P(\cdot)$	probability of event $\cdot$
P_f	probability of failure of a component containing exactly one crack; fraction of failed components
PL	plugging limit (the longest crack to remain in operation)

P_{OD}	probability of defect detection (given the tube has been inspected)
$P_{OD}(a)$	probability of detecting a crack of half-length a
$P_{pl}(a)$	probability of plugging a tube containing a crack with half length a
Q	ratio of multiple $P(i \geq 2)$ to single $P(i=1)$ tube rupture probability
R	mean tube radius; random variable
R	gas constant
R^2	an estimate of the response surface fit quality
Re[]	real part of the complex number
RF	tube sheet reinforcing factor
R_{in}	inside tube radius
R_h	radius of the tube-sheet hole
R_{out}, $R_{out,\,1}$, $R_{out,\,2}$	outside tube radius, also before (1) and after (2) rolling
R_{pl}	reliability of plugging procedure
R_{TS}	equivalent tube-sheet radius in the axisymmetrical model
S_1, S_3, S_3	elements of the failure probability (SORM)
T	temperature
ΔT	temperature difference on the tube inside and outside surfaces
$T(r)$	radial distribution of the temperature in the tube wall
T_{in}	inside tube surface temperature
$T_{in,\,\infty}$	inside tube surface coolant temperature
T_{out}	outside tube surface temperature
$T_{out,\,\infty}$	outside tube surface coolant temperature
T_∞	remote fluid temperature
U	realisation of basic variables in standardized normal (u) space (vector)
U_i	realisation of the i-th basic variable in standardized normal space
W	parameter of statistical crack propagation model
X_i	realisation od the i-th basic variable in the physical space
Y	realisation of basic variables in the rotated (y) space

Lowercase

$\dot{a}$	average half-crack velocity
$\vec{a}$	failure function gradient (normalized)
Δa	half-crack growth
a	half-crack length
a_0	initial crack half-length
a_1	crack half-length after the inspection

a_c	critical crack half-length
a_e	crack half-length measurement error
a_g	half crack growth
a_m	measured crack half-length
c	clearance between the tube and the tube sheet
d_i^1, d_i^2	inside tube diameter before (1) and after (2) the rolling
da	infinitesimal crack (half) growth
dt	infinitesimal time step
$f(\vec{x})$	joint probability density of basic variables
$f(\omega)$, ω	function of electro-chemical parameters at stress corrosion
$f(l)$	distribution of crack length indications
$g(\vec{x})$	failure function
g_u	failure function in standardized normal space
h, h_{in}, h_{out}	heat transfer coefficient
$h(\Delta l)$	distribution of crack indications growth
i	counter
k	heat conductivity
l	length of the crack indication
Δl	length of the crack indication growth
l_0	initial crack indication length
m	measured crack length; exponent in the crack propagation law
m_F	Folias' bulging factor
n	number of basic variables; the dimension of the standardized normal space
o	apparent tube wall thickness reduction
p	pressure
Δp	pressure difference
$p_A(a)$	pdf of real crack lengths
$\tilde{p}_A(a)$	$p_A(a)$ including the 0-length cracks assumed to be in the tubes without cracks
$p_{A,M}(a, m)$	joint probability density of real and measured crack lengths
$p_{A\|D}(a)$	pdf of detected crack lengths, assuming perfect detection
pH	level of acid in the solution
$p_M(m)$	pdf of measured crack lengths
$p_{M\|A}(m\|a)$	conditional probability of measuring the length m given crack of length a
$p_R(a)$	pdf of cracks remaining in the steam generator tubes after the plugging

$\tilde{p}_R(a)$	$p_R(a)$ including the 0 crack lengths assumed to be in the tubes without cracks
r	radius
t	tube wall thickness
t_1, t_2	tube wall thickness before (1) and after (2) the rolling
$\vec{u}$	position of a point in the standardized normal space
$\vec{u}^*$	design point in the standardized normal space
$\vec{x}$	vector of basic variables (x_1, x_2, ..., x_n)
$\vec{x}^*$	design point in physical space
$\vec{y}^*$	design point in rotated space
z	step correction in the design point search algorithm (FORM)

Greek

$\vec{\alpha}^*$	sensitivity factors of basic variables (FORM)
α, α_i, $\alpha(l)$	shape factor, Gamma distribution
α_T	linear temperature expansion coefficient
β, β_i, $\beta(l)$	scale parameter, Gamma distribution
β	reliability index
$\Gamma()$	Euler's Gamma function
$\delta(a)$	Dirac's delta function
$\delta_{l,0}$	average indication growth given initial indication length l_0
δ_T	coefficient of operational temperature on the material parameters
$\dot{\varepsilon}_{ct}$	local strain rate
ε_{OD}	fraction of non-detected cracks (e.g., human errors)
ϵ_{pl}	probability of missing a long crack during plugging
ε_{PL}	fraction of non-plugged tubes (e.g., human error)
η	local crack coordinate system axis; $1/\eta$ fraction of inspected tubes
Θ	function of heat conductivity and tube geometry
κ	flow stress factor
$\boldsymbol{\kappa}$	vector of failure function curvatures at design point (SORM)
ξ	local crack coordinate system axis; uniform random variable
ρ_C	ratio of both crack tip velocities
$\sigma\|_{x\to\infty}$	far end stress solution
$\sigma(x)$	axial stress distribution
σ_ϕ	membrane hoop stress
$\sigma_{\phi,\Delta T}(r)$	thermal gradient induced hoop stress

σ_f	flow stress
σ_M	ultimate tensile strength
$\sigma_{R,\,max}$	peak residual hoop stress value
σ_Y	yield strength
υ	Poisson ratio
Φ	cdf of standard normal distribution
χ^2	χ^2-test
φ	standard normal distribution

Other

I, II, III	stress corrosion crack propagation phases
$\partial/\partial x_i$	partial derivative
∇	gradient

1 INTRODUCTION

Steam generators in nuclear power plants with pressurized water reactors have to transfer heat from the primary to secondary coolant, which vaporizes. The boundary between both coolants is a bundle of thin-walled tubes, which represent the major part of the reactor coolant pressure boundary. The tube bundle should be designed and manufactured to satisfy both of its main functions:

- The largest possible heat transfer. Due to large thermal convection from the primary coolant to the tube and from the tube to the secondary coolant, the conduction through the tube wall controls the heat transfer rate.

- The integrity of the reactor coolant pressure boundary prevents the penetration of the radioactive reactor coolant into the secondary coolant. General design criteria for nuclear power plants ([95], criterion 14) requires that reactor coolant pressure boundary is "*...designed, fabricated, erected and tested so as to have an extremely low probability of abnormal leakage, of rapidly propagating failure, and of gross rupture.*". Thicker tube walls therefore represent larger safety against overloading and ruptures.

Optimal fulfillment of both contradictory requests is possible by the appropriate choice of material and manufacturing process.

1.1 Steam generator description

The description of steam generators, ageing processes and maintenance strategies is limited to the steam generators with vertical U-shaped tubes, made of Inconel 600. Such steam generators accumulated the majority of the operational experience and the problems related to ageing [10, 27] and are also installed in Slovenian nuclear power plant at Krško. This limitation does not restrict the theoretical investigations of this study, but enables direct comparison of theoretical assumptions and findings with the data base describing the state of Krško steam generators.

A cross-section of a steam generator is shown in Fig. 1-1. Each of Krško steam generators contains 4586 tubes. Their total heat transfer surface represents more than half of the reactor coolant pressure boundary. The operational pressure of the reactor coolant is 155.6 bar at

the average temperature of 305.9°C. The outside diameter of tubes is 19.05 mm, the tube wall thickness of 1.09 mm which is extremely thin in comparison with other parts of the reactor coolant pressure boundary. The straight part of the tubes is 7181.9 mm long and guided by 11 support plates. Tube bends are manufactured with radii between 57.2 and 1352.6 mm. They are supported by 4 groups of anti-vibration bars. Tubes are made of nickel based alloy with commercial name Inconel 600 [99].

The design capacity of a steam generator is 510 kg/s of saturated steam at 63.4 bar. Feedwater temperature is 221°C. The heat flux through the tube walls is about 190 kW/m^2, which is only possible in the two-phase fluid flow conditions and at extremely thin tube walls.

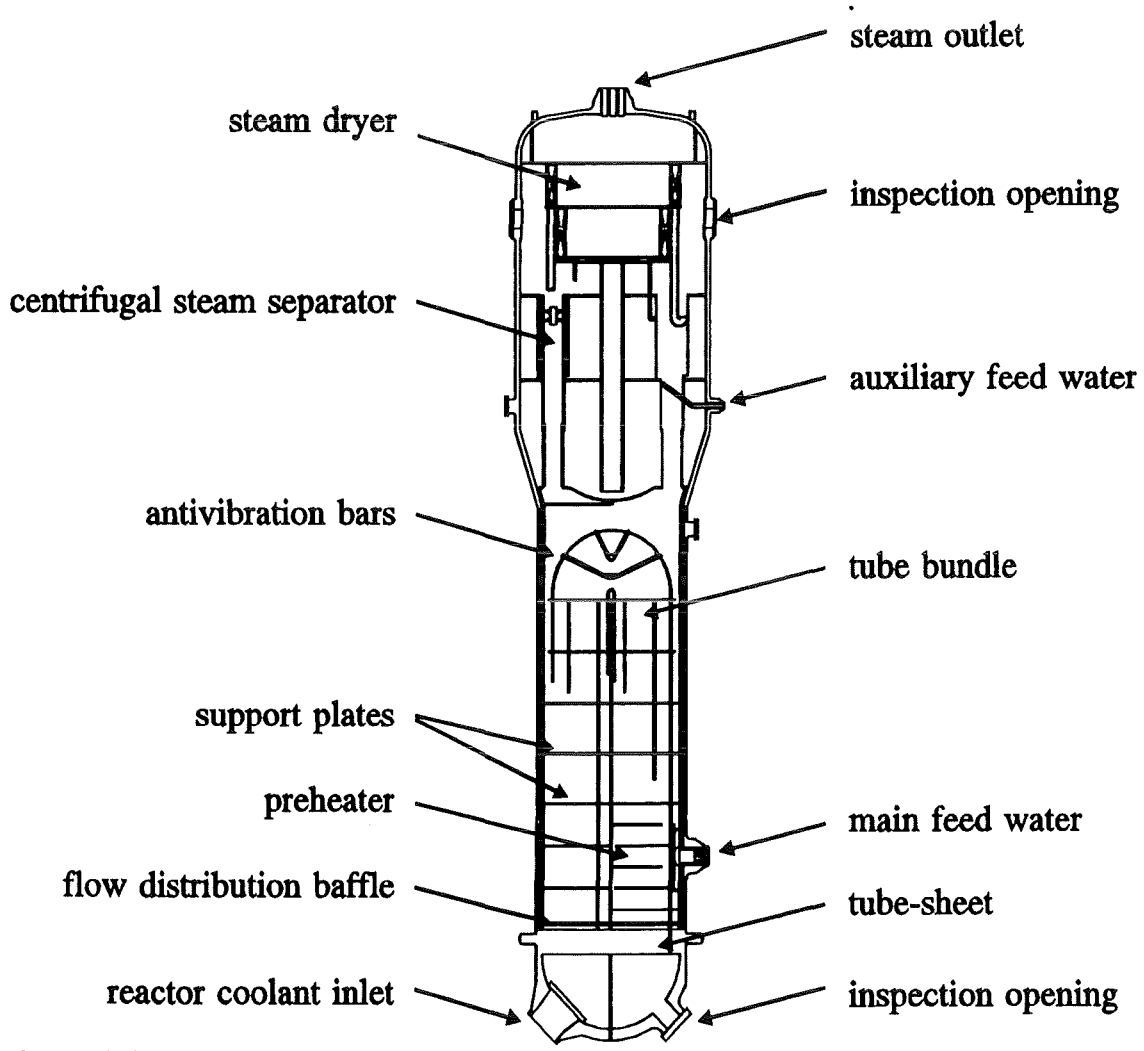

Figure 1-1 Cross-section of a steam generator

1.2 Aging mechanisms

Fig. 1-2 gives an overview of the ageing mechanisms which are causing damage in the tubes. They are caused by chemical, thermal and mechanical effects. Those effects can interfere and tend to reduce the load carrying capacity of some tubes. Detailed descriptions of ageing processes are given elsewhere [10], [36].

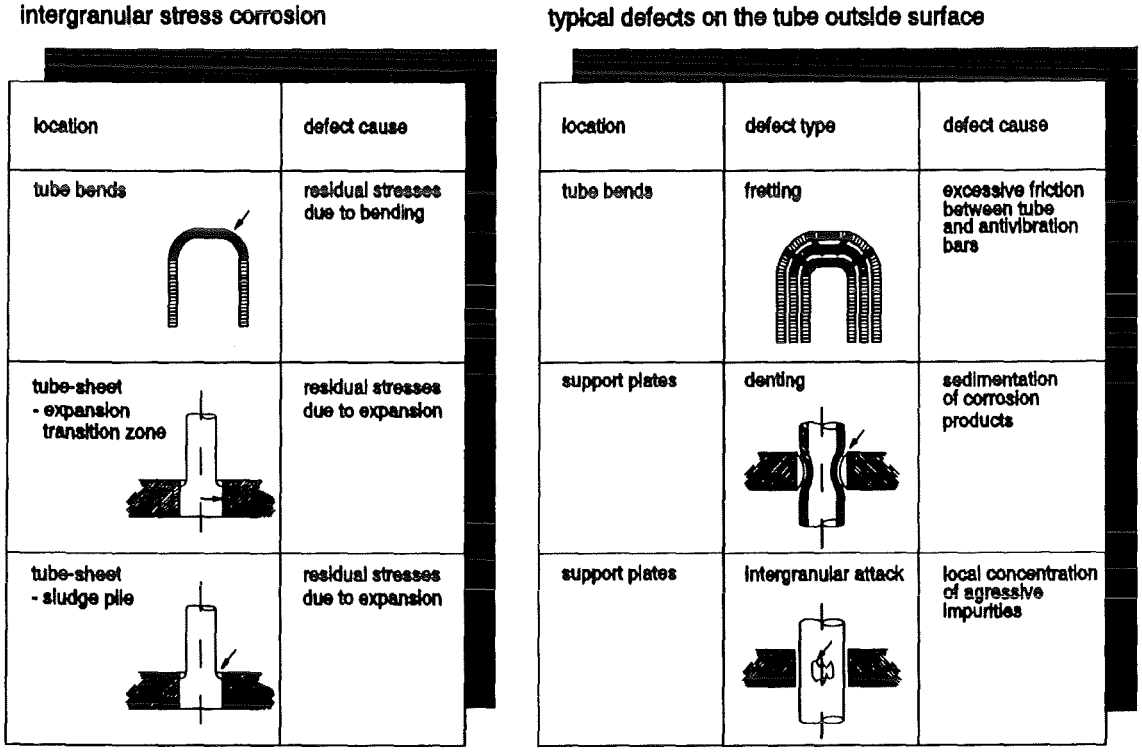

Figure 1-2 The most common steam generator tube ageing mechanisms

1.2.1 Intergranular stress corrosion cracking

This is one of the most frequently observed damage mechanism. It results in the initiation and propagation of cracks, mainly in the areas with high tensile stresses, such as residual stress dominated expansion transition area at the top of tube-sheet (Fig. 1-3). Axial cracks initiate in this area and propagate out of it as nearly through-wall cracks. Up to 1/3 of the tubes in a steam generator may be affected [56].

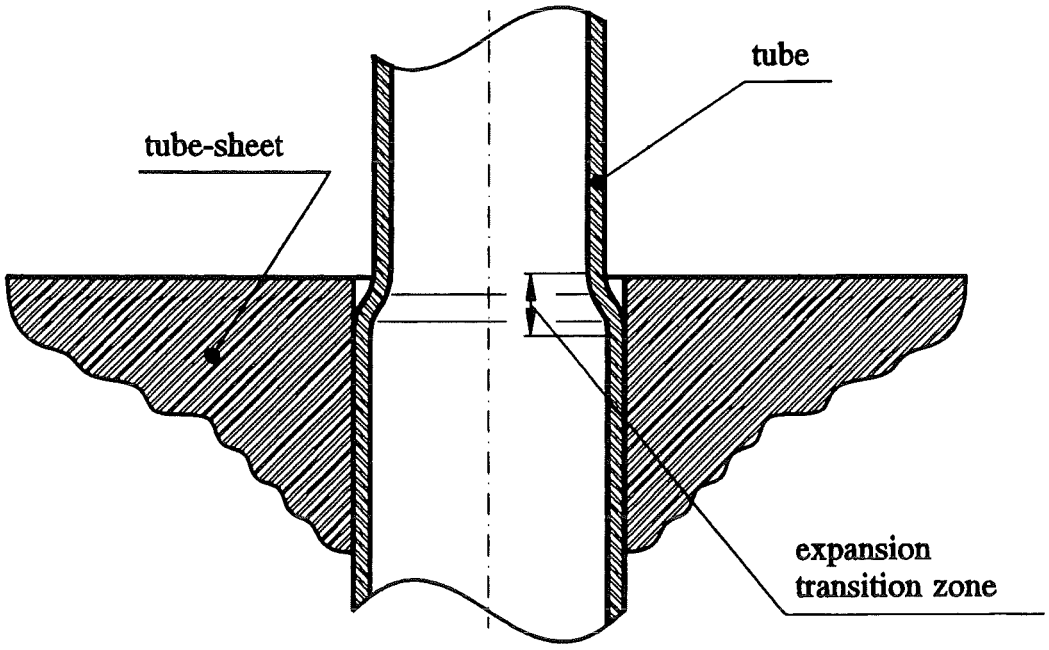

Figure 1-3 Tube expansion transition area

1.2.2 Intergranular attack

This is another important degradation mechanism (see Fig. 1-2) and develops mainly at the intersections of tubes and support plates. It is caused by high local concentrations of aggressive impurities and results in a random crack pattern. It is not further studied in this report.

1.2.3 Denting

This degradation mechanism is caused by the sedimentation of the corrosion products in the crevice between tubes and support plates (see Fig. 1-2). Due to different thermal expansion of tubes and support plates, tubes affected can be plasticaly deformed during steam generator heat cycles. It is not further studied in this report.

1.2.4 Importance of particular ageing mechanisms

Fig. 1-4 shows the percentage of causes for plugging of tubes in Krško plant during the period from 1985-1992. The decrease of the number of plugged tubes which were affected by SCC can be related to the fact that the plugging criteria after 1990 allowed for small cracks whereas all cracked tubes were plugged in the previous years. In recent years, the

defects at the tube to tube support plate intersections tend to dominate the plugging process. Those defects and their impact on the plant safety are not considered in this study.

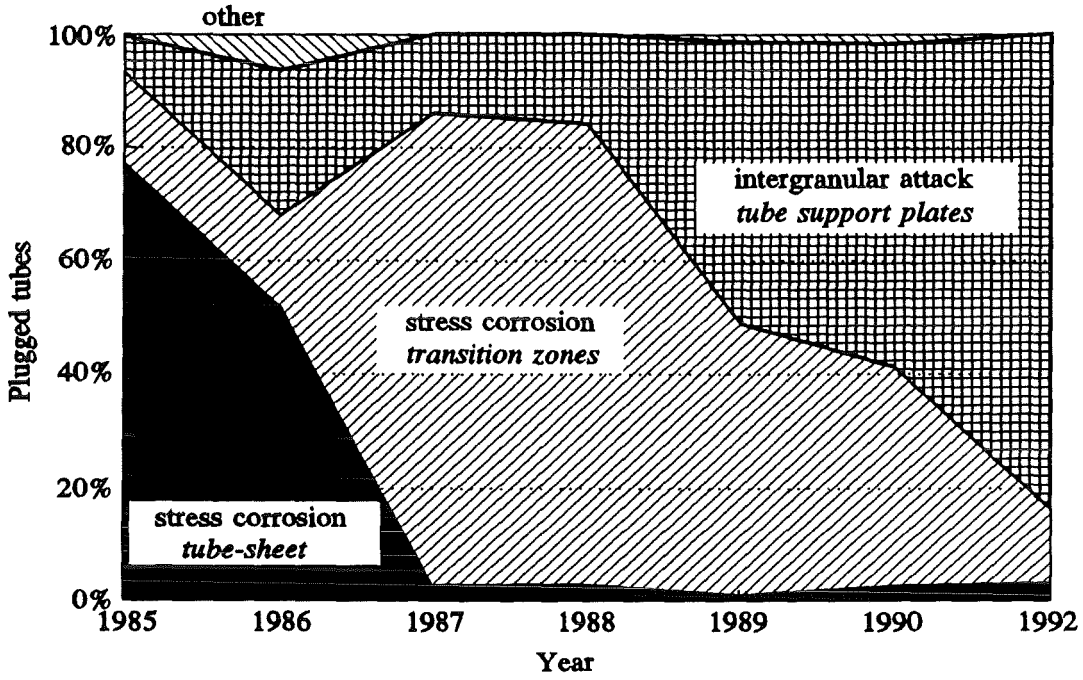

Figure 1-4 Krško NPP tube plugging history

1.3 Maintenance of steam generator tubes

In the following, the preventive and corrective actions are described which are mainly used in the steam generator maintenance practice. Corrective actions are those, which remove a cracked tube from operation. It should be noted, that such corrective actions in the vast majority of cases occur before the actual tube (and consequently steam generator) failure.

1.3.1 Preventive actions

Measures taken to reduce the rate of stress corrosion cracking are chemical control of the coolant, removal of sludge, relieving of residual stresses by shot peening.

The effects of preventive actions are not explicitly addressed in this study. They are however incorporated in the model through the crack growth rates.

1.3.2 Corrective actions

Excessively degraded tubes are plugged in order to avoid tube rupture. Alternate possibility is to instal sleeves, which are then welded to the tube below and above the damaged area.

The magnitude of defects is determined by periodic non-destructive examinations. A plugging criterion defines tolerable defects [27]. In some cases a destructive examination of tubes pulled out of steam generator is also required [27, 60, 85].

Plugging criterion should be conservative for safety reasons. On the other hand the efficiency of the plant is reduced by plugging because of reduced heat transfer. For example, a typical design margin for the heat transfer capability is in the order of 20%. This means that about 20% of tubes could be plugged without reducing the plant power. Exceeding such margin requires the reduction of the plant power or major modifications like replacement of steam generators.

1.3.3 Plugging criterion

The plugging criterion defines the largest acceptable defect. The criterion which has been used traditionally was based on the assumption that the defects found were part-through. The critical defect depth (in the order of 50% of the initial wall thickness) was calculated using a limit load criterion [93]. The defect depth was determined by the analysis of eddy current signal obtained from bobbin coil [27, 36].

Hence the uncertainty of the defect depth determined by inspection is very high. Due to the large number of tubes a sampling plan has been set up [94] in order to reduce the inspection time. However this plan was not very well-defined and could lead to non-conservative inspection results [22].

The use of the defect depth criterion has been enhanced by its simplicity and conservativity. For example, it does not require the determination of defect morphology. However, as the large number of tubes have been affected by stress corrosion cracking [59], the strict use of such criterion would require immediate shut down of affected steam generators.

One of possible solutions which emerged was the development of defect specific plugging criteria. Accounting for specific properties of the defect and implementation of a dedicated inspection method could relax the plugging criterion considerably without jeopardizing the

plant safety. Crack length based criterion was therefore implemented in the case of axial stress corrosion cracks [96].

1.4 Defect length based plugging criteria

A new plugging criterion has been introduced using the critical crack length $2a_c$ for plastic collapse of through-wall axial cracks in the tube expansion zone [49]. The plugging limit is defined by [96]:

$$\frac{1}{2}PL = a_c - a_e - a_g \qquad (1\text{-}1)$$

The uncertainty $2a_e$ of the inspection is mainly caused by problems in controlling the velocity of the dedicated motorized rotating pancake (MRPC) probe. It is reported to be in the order of $\pm$ 1.5 mm [29, 43].

The amount of crack growth between to inspections $2a_g$ has been analyzed in [56] on the basis of compiled inspection data.

1.5 Impact of plant maintenance strategy on plant safety

The main goal of every maintenance strategy is to assure the reliability of steam generator and consequently the plant safety. The basic measure of reliability is the probability of having one or more tubes failed. This section contains a review of existing probabilistic analyses on failure of steam generators.

- Pitner [77] performed a probabilistic safety analysis using a systems approach. The goal was to determine the number of tubes to be inspected. The uncertainty of the inspection was not taken into account.

- Hernalsteen [56] was concerned with leakage caused by the through-wall cracks. Using probabilistic methods, leak rate and tube failure probability were predicted. He did a very profound statistical analysis of crack growth based on inspection data. This kind of analysis can only be used to predict the expected crack growth between two inspection intervals and does not allow any extrapolation beyond this interval.

- Granger et al. develop the code COMPROMIS to assist at steam generator maintenance. Information on this code is only available in rather general conference papers [40, 52, 78]. Apparently a probabilistic analysis is performed including the influence of inspection uncertainty. A semi-empirical crack propagation law [51] has been applied, which can apparently not account for the scatter of the residual stress field. The excessive leak rates are incorporated as the second steam generator failure mode.

- Gunsell [53] performed a probabilistic safety assessment (system approach) using second moment analysis. The number and lengths of cracks to be left in operation were related to the failure probability.

- Mavko et al. [68] performed an analysis of tube failure using probabilistic fracture mechanics. The empirical crack growth law of [56] was employed as well as a simplified model for inspection uncertainly.

Conclusions about state-of-the art: the French analysis (Pitner et al [40, 52, 78]) probably is the most advanced analysis but has some weak points (scatter of residual stress field not accounted for, semi-empirical crack propagation model). All others used simplified models.

1.6 Scope and limitations of this research

A method to assess the safety consequences of plugging criteria will be developed. The analysis will be limited to axial stress corrosion cracks in the expansion transition zone. The following points will be addressed:

- Probabilistic fracture mechanics model, which deals with all parameters influencing the tube failure probability (Section 2).

- Parametric residual stress analysis in the tube expansion transition zone (Section 3).

- Model describing propagation of cracks in residual stress field (Section 4).

- Reliability methods (Section 5).

- Applications (Section 6).

The study considers only through-wall axial stress corrosion cracks in the tube expansion transition zone. However, the basic concept allows for extensions incorporating other damage mechanisms.

2 PROBABILISTIC FRACTURE MECHANICS MODEL

Probabilistic fracture mechanics (PFM) deals with the reliability analysis of cracked components. It has mainly been applied to reactor and aerospace components. A review of nuclear application was given by G. Johnston [62].

2.1 Theoretical background

The failure integral is the probability content of the failure domain defined by values of the failure function $g(\vec{x})<0$:

$$P_f = \int_{g(\vec{x})<0} f(\vec{x})\, d\vec{x} \tag{2-1}$$

Only independent random variables $\vec{x}=(x_1, x_2, \ldots, x_n)$ will be considered here. Numerical evaluation of the failure integral will be discussed in chapter 5.

2.2 Failure function

$g(\vec{x})$ depends on the tube failure mode, crack propagation and the maintenance strategy implemented.

2.2.1 Assumptions

Cracks develop at the inside of tubes as axial through wall cracks. Only rupture of tubes is considered, developments of leaks and leak-detection are not considered. Each tube contains exactly one crack (which may have length zero to simulate crack-free tubes). Failure of a complete steam generator is represented by a failure of at least one steam generator tube.

2.2.2 Failure of an axially cracked tube

The failure functions is defined by the limit load model:

$$g(\vec{x}) = \sigma_f - m_F \cdot \sigma_\phi \tag{2-2}$$

where σ_f is the flow stress, σ_ϕ is the pressure induced hoop stress and the bulging factor m_F is given by [35]:

$$m_F = 0.614 + 0.386e^{\left(-2.25\frac{a_1}{\sqrt{Rt}}\right)} + 0.866\left(\frac{a_1}{\sqrt{Rt}}\right) \quad (2\text{-}3)$$

a_1, R and t being the crack half-length at the end of inspection cycle, the tube mean radius and the tube wall thickness, respectively. The flow stress σ_f is defined by the yield strength σ_Y and the ultimate tensile strength σ_M and adjusted to the operating temperature conditions by application of the correction coefficient δ_T, where appropriate:

$$\sigma_f = \kappa(\sigma_Y + \sigma_M)\delta_T \quad (2\text{-}4)$$

κ represents the experimentally determined constant which actually describes the degree of strain hardening behavior of the tube material. The membrane stress perpendicular to the crack direction σ_ϕ is the pressure (p) induced tube hoop stress:

$$\sigma_\phi = \Delta p\left(\frac{R}{t} - \frac{1}{2}\right) \quad (2\text{-}5)$$

2.2.3 Tube-sheet reinforcement

The tubes are fixed into a tube sheet which provides additional circumferential rigidity and obstructs bulging. The *Tube Sheet Reinforcing Factor* (*RF*) has been proposed to account for this effect [43]. It is defined as correction coefficient to the flow stress factor κ at the critical crack length (see eq. (2-4)):

$$RF(a_c) = 1 + 10\exp\left[-1.8\frac{a_c}{\sqrt{R\,t}}\right] \quad (2\text{-}6)$$

a_c represents the critical crack length in a free span tube and can be obtained by setting $\sigma_f - m_F\sigma_\phi = 0$ and inverting eq. (2-3). Unfortunately, its use is restricted to the cracks tangent to the tube sheet, which may not be true for the numerous cracks propagating out of the tube sheet.

2.3 Distribution of crack lengths

In a previous paper [68] the crack length a_1 at the subsequent inspections which determines the value of the bulging factor m_F (eq. (2-3)) was calculated from the following relation:

$$a_1 = a_g + \begin{cases} a_m + a_e,\ a_m + a_e < PL/2 \\ a_m + a_e,\ a_m + a_e \geq PL/2 \text{ in } \xi \geq P_{OD} \\ 0 \text{ otherwise} \end{cases} \tag{2-7}$$

The sizing uncertainty was taken into account by introducing the error term a_e which was assumed to be independent of the measured crack length a_m, a_g accounted for the crack growth. PL represents the plugging limit and P_{OD} the crack detection probability.

Hence the maintenance strategy was taken into consideration by replacing a_1 by the corresponding random variables.

A more advanced analysis should take into account the correlation between real and measured crack size and the efficiency of the inspection. Those quantities will affect the distribution of the crack length which in turn affects the integrand of the failure integral (eq. (2-1)). The analysis presented in the following section was first given in [6].

2.3.1 Probability of detection

According to Bayes' theorem the conditional probability of event E_1 to take place under the condition that event E_2 has already occurred follows from:

$$P(E_1 \mid E_2) = \frac{P(E_2 \mid E_1)\ P(E_1)}{P(E_2)} \tag{2-8}$$

If E_1 denotes the event that the random crack length A assumes values in the interval $[a, a+da)$ and E_2 is the event D denoting detection of a crack of arbitrary size, we have:

$$P(a \leq A < a+da \mid D) = \frac{P(D \mid a \leq A < a+da)\ P(a \leq A < a+da)}{P(D)} \tag{2-9}$$

which yields the following expression for the probability densities:

$$p_{A|D}(a) = \frac{P_{OD}(a)\ p_A(a)}{\int_0^\infty p_A(a')\ P_{OD}(a')\ da'} \tag{2-10}$$

where P_{OD} is sometimes called the detection probability, $p_A(a)$ is the probability density function of the actual crack length and $p_{A|D}(a)$ is the probability density function of the detected cracks provided that there is no sizing error.

2.3.2 Sizing errors

Let M be the random variable for the measured crack length which assumes values denoted by m. If $p_{A,M}$ denotes the joint probability density function of actual and measured crack length, we can derive the following expression for the marginal distribution functions:

$$p_M(m) = \int_0^\infty p_{A,M}(a, m)\, da \tag{2-11}$$

for the p.d.f. of the measured crack length and

$$p_A(a) = \int_0^\infty p_{A,M}(a, m)\, dm \tag{2-12}$$

for the p.d.f. of the actual crack length. $p_{A,M}(a,m)$ is generally only specified for the detected cracks; this effect will be taken into account at the end of this section. This difficulty can be circumvented if non-detected cracks have $m=0$.

Again using Bayes' theorem leads to the conditional p.d.f. of finding a value of m giving an actual crack of length a:

$$P_{M|A}(m|a) = \frac{p_{A,M}(a, m)}{p_A(a)} \tag{2-13}$$

Solving for $p_{A,M}(a,m)$:

$$p_{A,M}(a, m) = p_{M|A}(m|a)\, p_A(a) \tag{2-14}$$

and integrating over a leads to an expression of the p.d.f. of measured crack length:

$$p_M(m) = \int_o^\infty p_{M|A}(m, a)\, p_A(a) da \tag{2-15}$$

If the possibility of missing a crack is explicitly included in eq. (2-15) $p_A(a)$ has to be replaced by the p.d.f. of detected cracks (eq. (2-10)). Hence the following expression is obtained:

$$p_M(m) = \frac{\int_0^\infty p_{M|A}(m|a)\ p_A(a)\ P_{OD}(a)\ da}{\int_0^\infty p_A(a')\ P_{OD}(a')\ da'} \qquad (2\text{-}16)$$

relating the p.d.f. of the measured crack lengths to that of the actual crack lengths.

Inverting eq. (2-16) gives a possibility to determine the $p_A(a)$ from $p_M(m)$. This represents of course a difficult problem which is solved numerically using a procedure proposed by Barnier et al [6]. First the functional form of $p_A(a)$ is selected. Then $p_M(m)$ is calculated using eq. (2-16) which depends on the unknown parameters of the assumed p.d.f. These can be determined by fitting calculated values of $p_M(m)$ to the empirical distribution of measured crack lengths which can be done by minimizing χ^2. More details are found in ref. [6].

2.3.3 Effect of plugging

Let F_{in} denote the fraction of tubes inspected:

$$F_{in} = 1/\eta \qquad (2\text{-}17)$$

If PL denotes the plugging limit, a given crack of size a is supposed to exceed the plugging limit with probability:

$$P(M > PL|a) = \int_{PL}^\infty p_{M|A}(m|a)\ dm \qquad (2\text{-}18)$$

The probability that a crack of size a is found during the inspection and has a measured crack size larger than the plugging limit is equal to:

$$P(M>PL,\ D|a) = P_{OD}(a)\ P(M>PL|a) \qquad (2\text{-}19)$$

The plugging procedure has a reliability:

$$R_{pl} = 1 - \epsilon_{pl} \qquad (2\text{-}20)$$

As each tube contains exactly one crack, an inspected tube containing a crack of length a is successfully plugged with probability:

$$P_{pl}(a) = (1 - \epsilon_{pl})\ P_{OD}(a)\ P(M>PL|a) \tag{2-21}$$

Multiplying this equation by the inspection probability F_{in} eq. (2-17) yields the probability that a tube containing crack of length a is plugged:

$$P_{pl}(a) = 1/\eta\ P_{OD}(a) \int_{PL}^{\infty} p_{M|A}(m|a)\ dm\ (1 - \epsilon_{pl}) \tag{2-22}$$

The fraction of plugged tubes follows from:

$$F_{pl} = \int_{0}^{\infty} p_A(a)\ P_{pl}(a)\ da \tag{2-23}$$

The quantity:

$$p_A(a)\ \left(1 - P_{pl}(a)\right) \tag{2-24}$$

corresponds to the probability that a tube contains a crack of length a and the tube is not plugged. Dividing this quantity by the fraction of non-plugged tubes leads to the probability density function of remaining cracks (Bayes theorem):

$$p_R(a) = \frac{p_A(a)\ \left[1 - P_{pl}(a)\right]}{\int_{0}^{\infty} p_A(a')\ \left[1 - P_{pl}(a')\right]\ da'} \tag{2-25}$$

2.3.4 Tubes without cracks

To account for tubes without cracks, the procedure proposed in [83] has been used:

$$p_A(a) = F_A\ \delta(a) + \tilde{p}_A(a) \tag{2-26}$$

F_A represents the fraction of tubes containing zero length cracks. $\delta(a)$ is Dirac function and $\tilde{p}_A(a)$ the probability density of real crack lengths.

From the normalization property of probability distributions:

$$1 = \int_0^\infty \left(F_A \delta(a) + \tilde{p}_A(a)\right) da = F_A + \int_0^\infty \tilde{p}_A(a)\, da \tag{2-27}$$

the relation between $p_A(a)$ and $\tilde{p}_A(a)$ is determined as:

$$\tilde{p}_A(a) = \left(1 - F_A\right) p_A(a) \tag{2-28}$$

Fractions of cracked tubes F_A and those with detected cracks F_M can be estimated from the inspection data and parameters:

$$F_A = 1 - \frac{F_M}{F_{OD}} \tag{2-29}$$

$$F_M = \frac{N_M}{N_{SG}} \tag{2-30}$$

where N_M represents the number of tubes with detected cracks and N_{SG} the total number of tubes in a steam generator.

2.3.5 Stable crack growth

Stable crack growth has been found to be the most important factor affecting the tube failure probability [25] and will be discussed in detail in Section 4. It affects the failure function by the crack length a_1.

2.4 Multiple tube rupture

All tubes contain exactly one crack which fails with probability P_f. Hence the probability that i tubes fail is equal to:

$$p(i) = \frac{(N P_f)^i}{i!} e^{-NP_f}; \quad i = 0, 1, ..., N \tag{2-31}$$

where N is the total number of tubes and advantage has been taken of the fact that the number of tubes is large. The probability that at least one tube fails follows from eq. (2-31):

$$P(i \geq 1) = 1 - e^{-N P_f} \tag{2-32}$$

At least two tubes fail with probability

$$P(i \geq 2) = 1 - \left(1 + NP_f\right) e^{-N P_f} \tag{2-33}$$

Hence the ratio of multiple tube failure to single tube failure is given by:

$$Q = \frac{P(i \geq 2)}{P(i = 1)} = \frac{1 - \left(1 + N P_f\right) e^{-N P_f}}{N P_f e^{-N P_f}} \tag{2-34}$$

3 STRESSES IN STEAM GENERATOR TUBES

Classification of stresses according to their origin was performed by Flesch et al [39]:

- residual stresses from manufacturing process such as bending and drawing of tubes;
- residual stresses from expanding tubes into tube sheet;
- operational stresses caused by thermal loading and pressure difference;
- sludge induced stresses.

The residual stresses due to the expansion of tubes into tube sheet and operational stresses have the most pronounced effect on the propagation of axial cracks. They are further investigated below.

3.1 Residual stresses

3.1.1 Origin of residual stresses

Tubes are expanded into tube sheet (see Fig. 3-1) by plastic deformation to obtain a leak tight joint. The procedure used is mechanical rolling (as illustrated in Fig. 3-2). In Krško plant a one-step rolling procedure is used (see Fig. 3-3a) as opposed to two-step rolling (Fig. 3-3b).

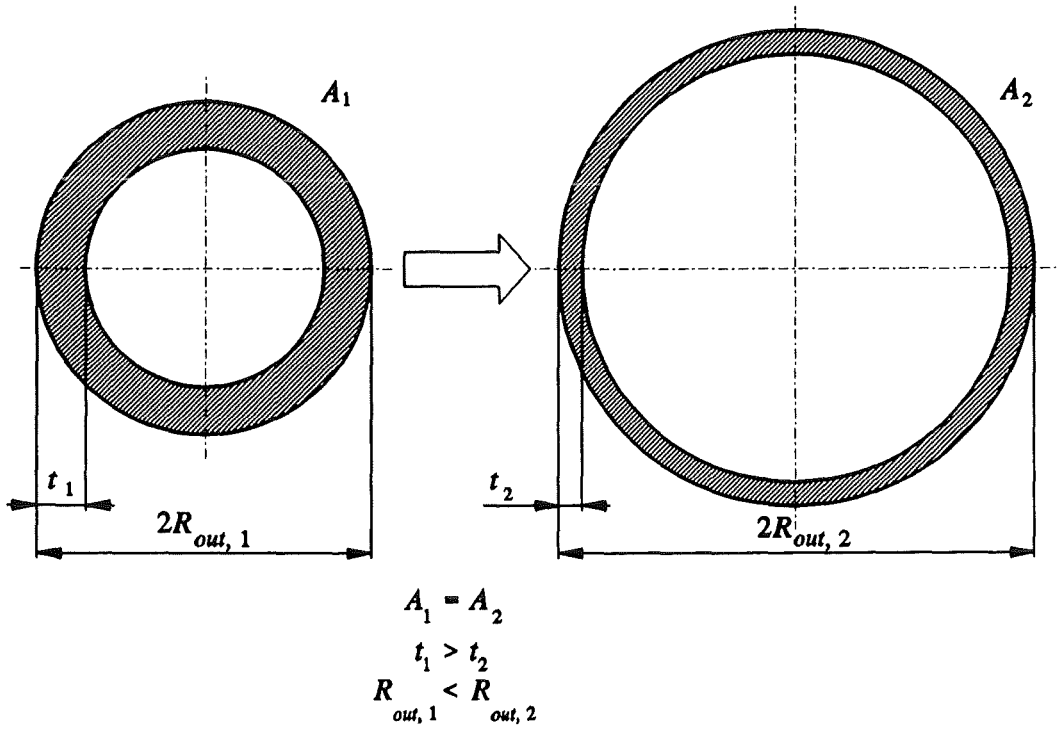

Figure 3-1 Expansion of tube into tube-sheet

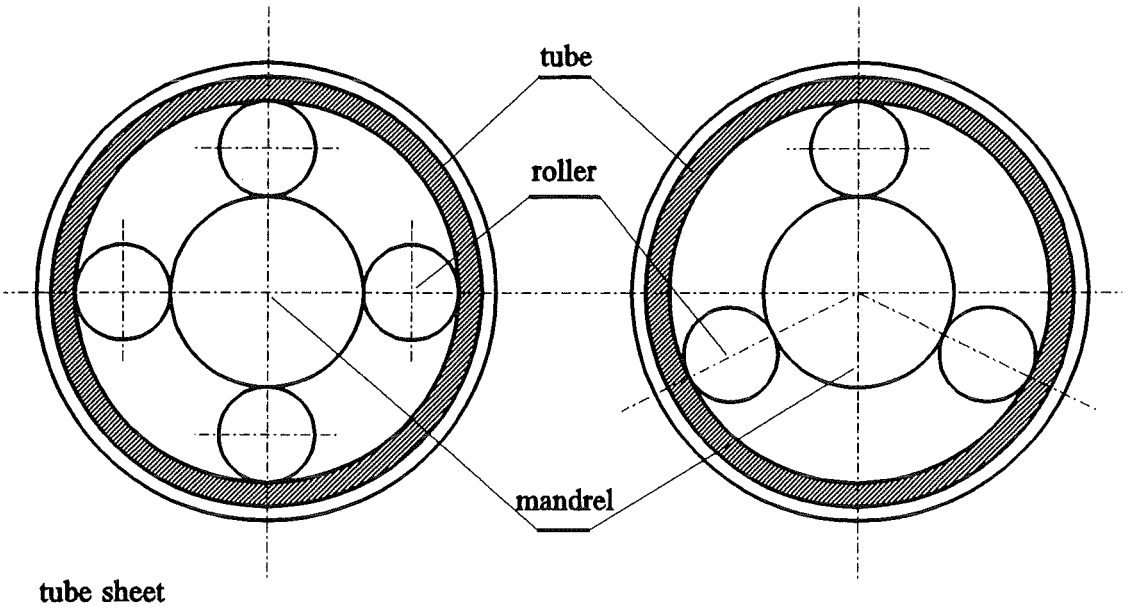

Figure 3-2 Tooling for tube-to-tube-sheet rolling

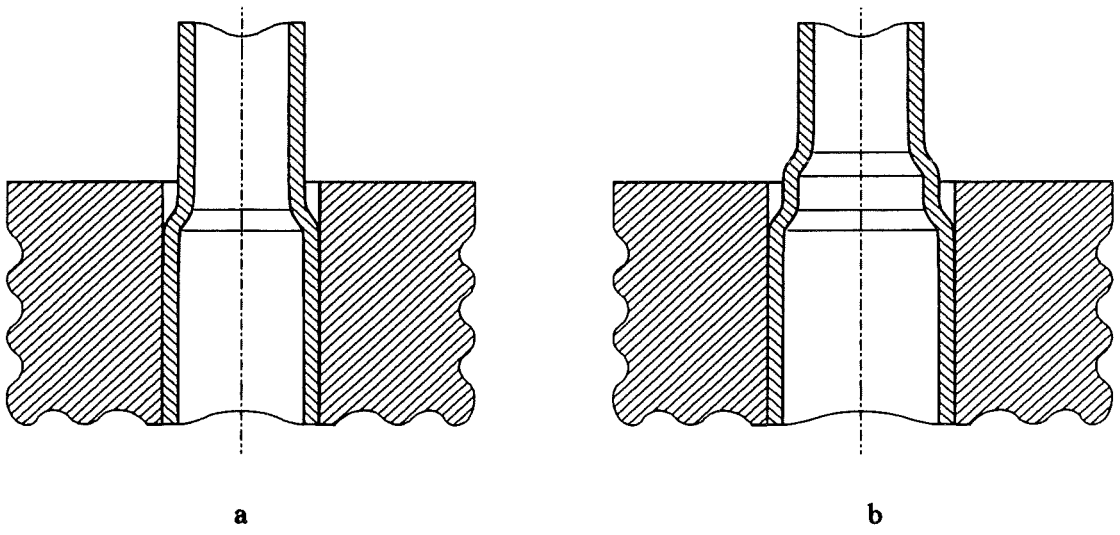

Figure 3-3 One- and two-step rolling

The main control parameter of the rolling process is torque [100]. Its value is preset to achieve the 20 bar residual contact pressure between tube and tube sheet. Another important technological parameter is the apparent wall reduction o [63]:

$$o = \frac{d_i^2 - \left(d_i^1 + 2c\right)}{2t} * 100 \qquad [\%] \qquad (3\text{-}1)$$

The optimal value is of the order of 3-6% [63], experimental data lead to o=5% [67].

3.1.2 Estimating the residual stresses

First attempts aimed at estimating the residual stresses far away from the expansion zone [61 and 63]. Middlebrooks et al [72] performed a non-linear finite element analysis (**ABAQUS**) for hydraulic expansion of tubes. An axisymmetric model was considered to be adequate. Flesh et al. [39] experimentally determined residual stresses in tubes for some French nuclear power plants (different geometry compared to Krško plant). The values obtained in the expansion zone were 370 MPa for the hoop stress and 340 MPa for the axial stress.

Duc et al [33] performed a non-linear FE-analysis for this case using an axisymmetric model. They got good agreement with [39] but overestimated the axial stresses as compared to the experiment (see discussion in 3.1.5). Also, a good qualitative agreement with [72] was obtained.

No parametric study is available which takes into account the variation of the residual stresses with variation of the input parameters.

3.1.3 Finite element model

A finite element analysis with the **ABAQUS** code was performed in order to simulate tube expansion. The axisymmetric meshes are shown in Fig 3-5 (coarse mesh) and Fig. 3-6 (fine mesh). The rolling tools were modelled as rigid surfaces which were pushed on to the tube surface until a residual contact pressure of 20 bar is reached. The friction coefficients (rolling tools-tube 0.1, tube-tube sheet 0.2) were taken from [67] and [72]. The tube was long enough to model the far-field solution at the far end. The tube sheet was modelled as a very thick tube with a wall thickness corresponding to the average distance between tubes (see Fig. 3-4b) which is in agreement with recommendations in [72].

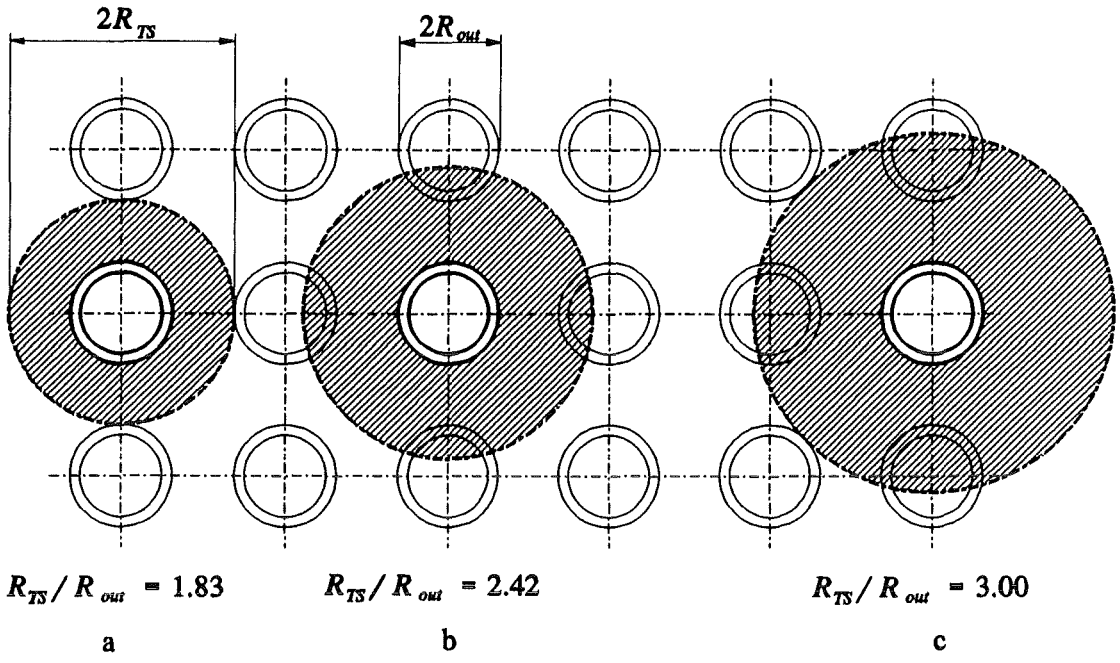

Figure 3-4 Possibilities for the axisymmetrical simulation of tube to tube-sheet joint

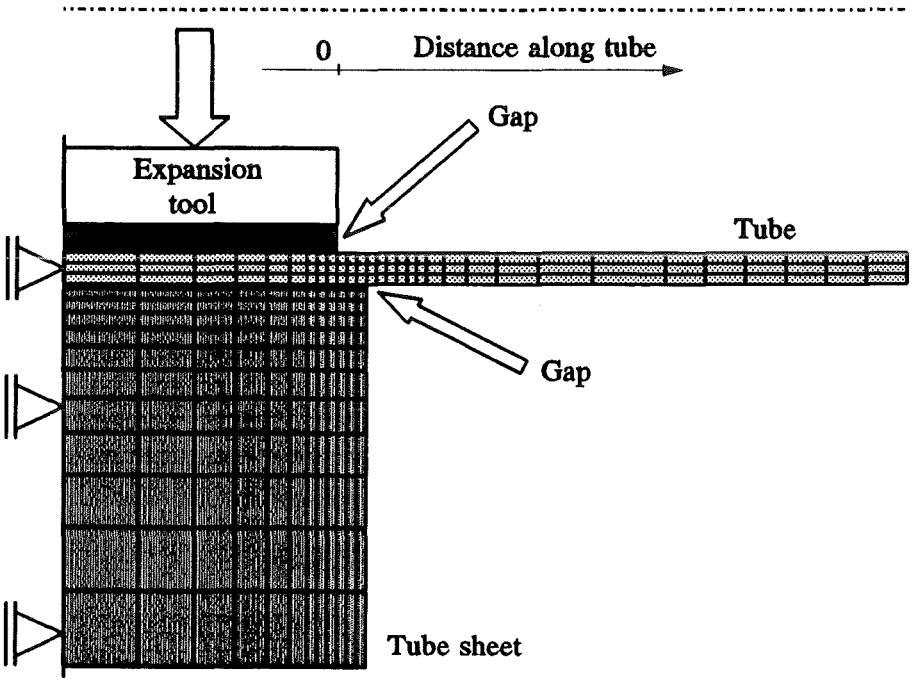

Figure 3-5 Model of the tube to tube-sheet joint (coarse mesh)

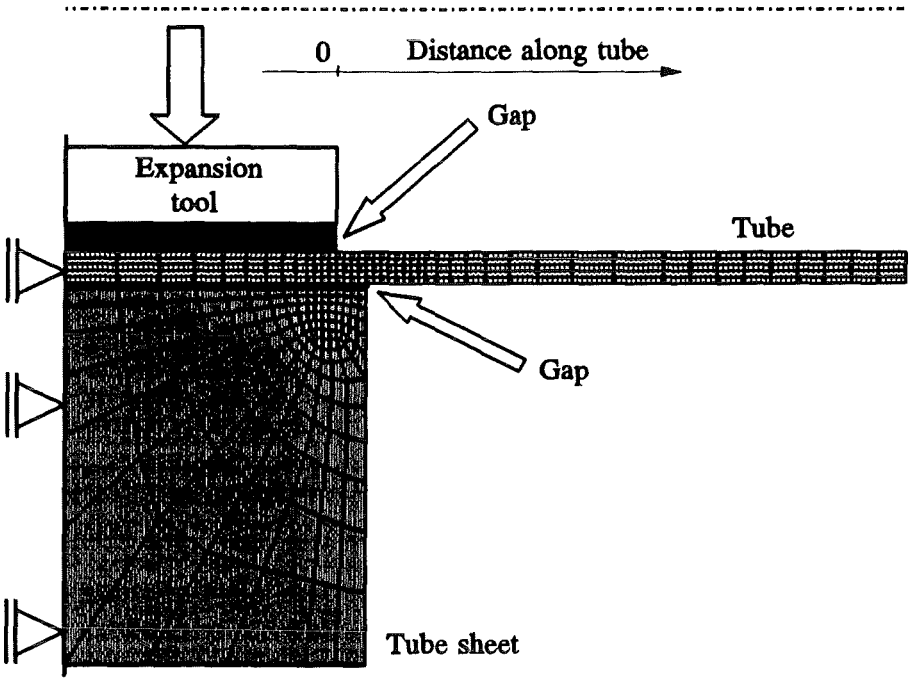

Figure 3-6 Model of tube to tube-sheet joint (fine mesh)

The elements used allow thermal as well as mechanical loading. The stress-strain curve was bilinear. The von Mises yielding condition and isotropic hardening was used as well as the Prandtl-Reuss law for plastic flow. Material data are given in Table 3-I.

Table 3-I Material parameters for tube and tube sheet

Material	Temp. [°C] T	Youngs modulus [GPa] E	Tangent modulus** [Gpa] E_T	Poisson ratio [-] ν	Conductivity* [W/mK] k	Thermal expansion* [10^{-6}/K] α_T
Tubes Inconel 600 [98, 4]	20.	200.	3.00	0.3	(20.)	(14.04)
	340.	190.	(3.00)	0.3	20.	14.04
Tube-sheet SA 508 [4]	20.	192.	2.88	0.3	(40.)	(13.10)
	340.	168.	(2.88)	0.3	40.	13.10

* Thermal properties at 20°C were not relevant for the present analysis.

** Tangent modulus after ref. [33]. Its value at 340°C unknown and does not affect the results of the present analysis.

3.1.4 Finite element results

Fig. 3-7 shows the profile of the inner wall of the tube after completion of the rolling. Both meshes yield identical results. Fig. 3-8 shows the residual hoop stresses at the inner and the outer side of the tube, whereas Fig. 3-9 shows the residual stress field obtained for the axial stresses. In all areas both meshes yield virtually the same results. At the transition between the expanded tube and the expansion zone there are some oscillations in the residual stress field which can be attributed to the discontinuous boundary conditions in the expansion process (end of tool). Comparatively high tensile residual stresses develop in the expansion zone at the inner wall of the tube, whereas the other wall is under compression. The absolute values of the axial stresses inside and outside are approximately the same, i.e. the axial load in the expansion process correspond to bending. The maximum values of the axial stresses are higher than those of the hoop stresses. This would imply that circumferential cracks are formed in contradiction to what is observed in real steam generator tube which contain mostly axial cracks.

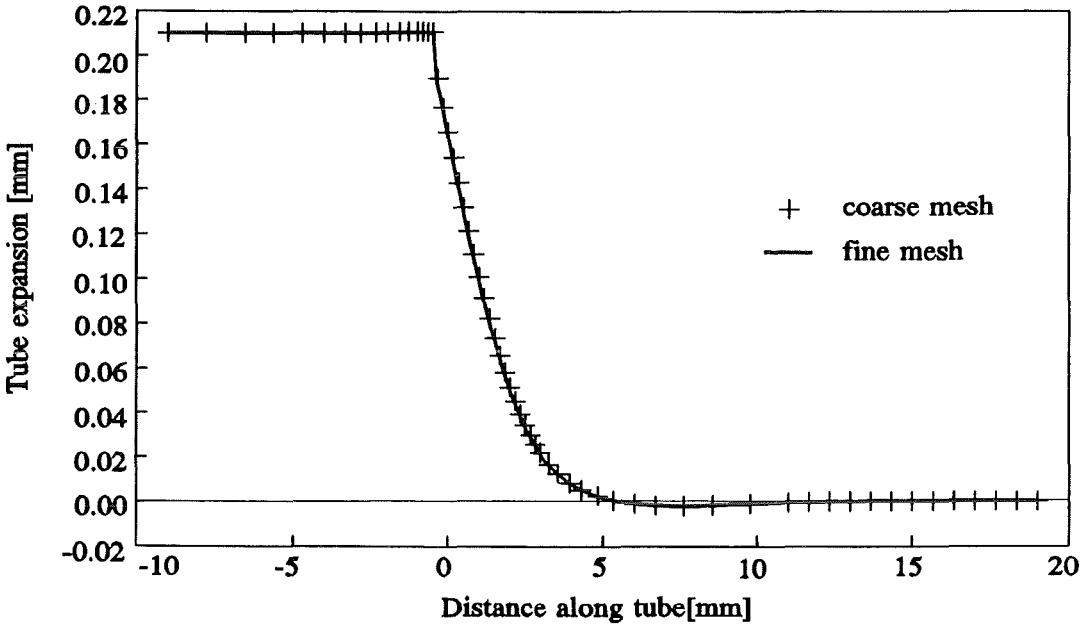

Figure 3-7 Calculated tube internal surface profile

Fig. 3-10 shows the variation of the residual hoop stress across the wall thickness. Almost 70% of the wall is subjected to tensile residual stresses.

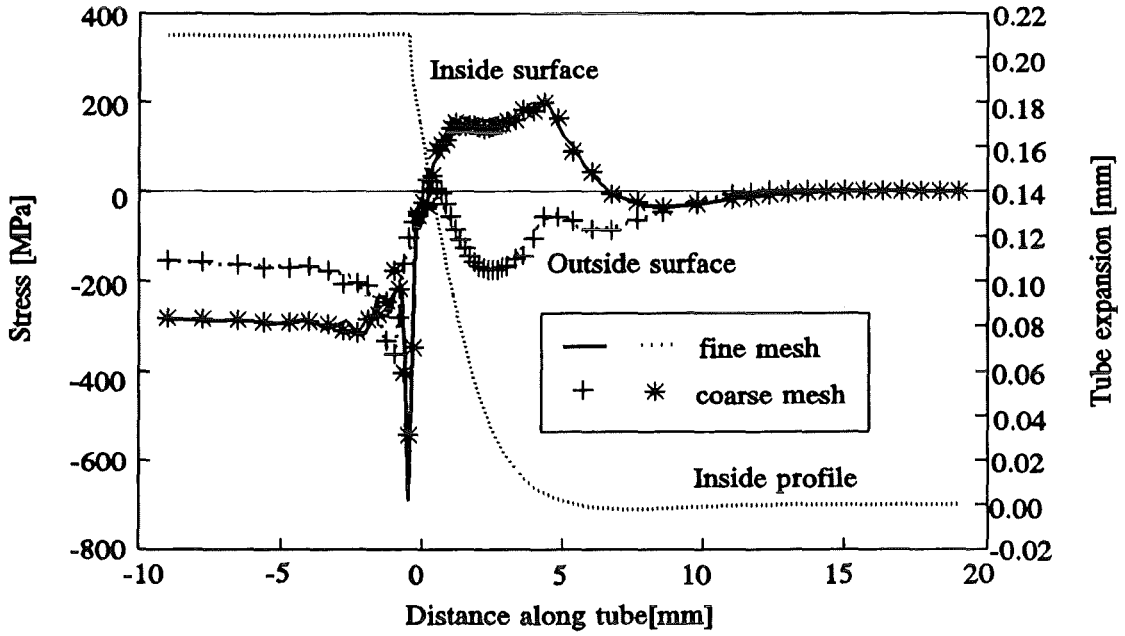

Figure 3-8 Residual hoop stress - comparison of meshes

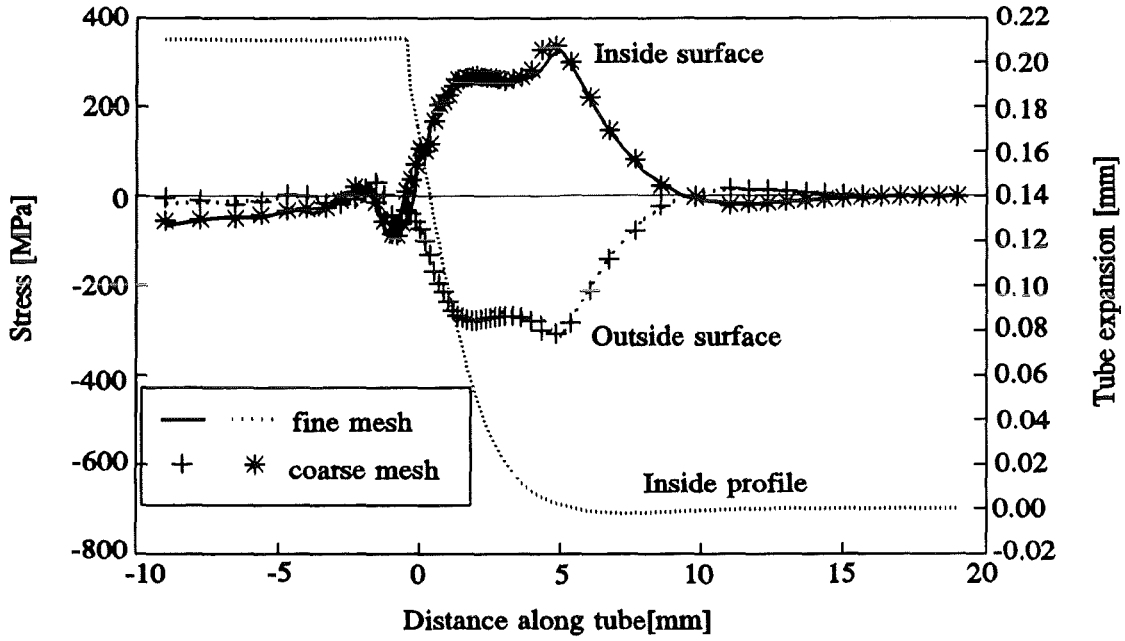

Figure 3-9 Axial hoop stress - comparison of meshes

Fig. 3-11 summarizes the distributions of the residual stress field in the expanded zone. A 3-D model would be more adequate but does not seem to be feasible at the time being.

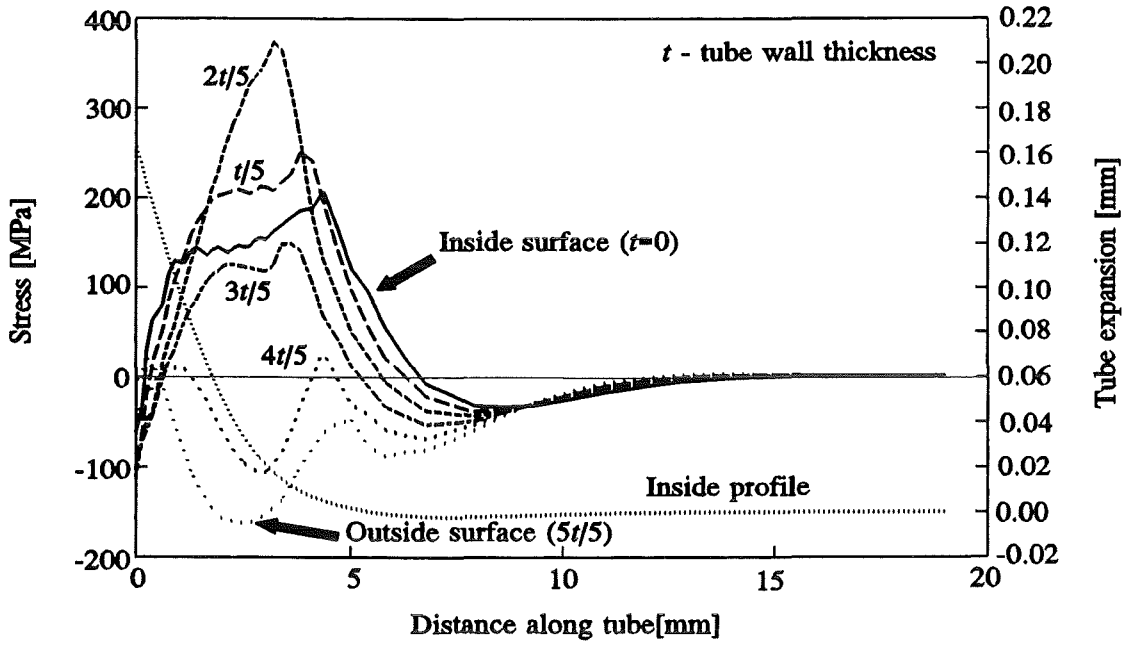

Figure 3-10 Distribution of hoop residual stresses through the wall thickness

3.1.5 Discussion of results

The high values of the axial residual stresses have been also observed by Duc et al [33] and can be attributed to the effect of axisymmetric modelling. There are two versions for this. First the real tube material flows in axial direction during the expansion process which is not observed for the FE model. Second the axisymmetric model assumes constant displacement along the circumference, whereas in reality, local tube thinning occurs depending on the position of the roles. The tube sheet cannot be made stiff enough to account for this effect in an axisymmetric model.

3.2 Operational stresses

Table 3-II summarizes the temperatures and pressures which are present in the tubes and the tube sheet under normal operating conditions. It also contains the heat transfer coefficients which were assumed in the analysis for tubes and the tube sheet with and without sludge.

The operational loads were applied immediately after the release of the expansion load, i.e. the validity of the superposition principle could be checked.

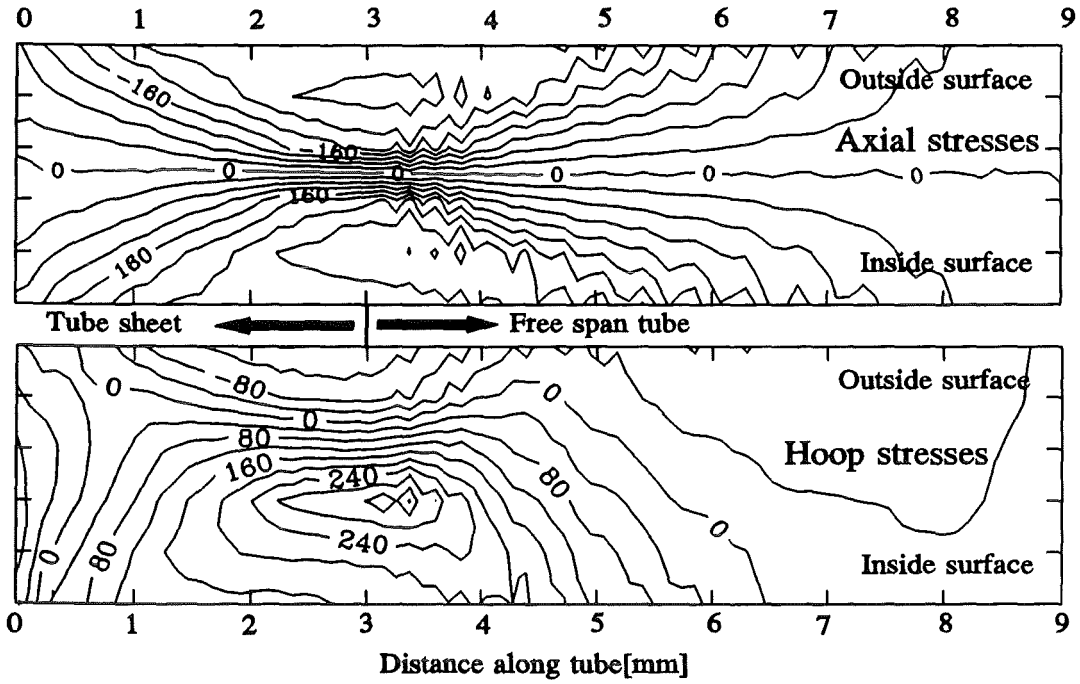

Figure 3-11 Comparison of axial and hoop residual stresses

Table 3-II Basic tube operational loading data

Location		Pressure [bar] p	Temperature [°C] T_∞	Film coeff. h [kW/m²K]	
				Without sludge	With sludge
Tube	Reactor coolant	155.6	325.1	25.	25.
	Secondary coolant	63.4	279.1	20.	$5.\cdot10^{-3}$
Tube-sheet		63.4	279.1	5.	$2.\cdot10^{-3}$

3.2.1 Operational tube loads

The pressure difference inside and outside the tube can be determined from Table 3-II. In the FE-model the effect of the pressure difference on the gap between the tube and the tube sheet is simulated. Both mechanical and thermal expansion are taken into account. For the thermal loads, the convectional heat transfer is assumed. In the gap, the heat transfer depends on the gap distance. In the presence of sludge the heat transfer to the secondary coolant is severely restricted, whereas full heat transfer is observed for clean tubes.

3.2.2 Stresses in sludge region

Figure 3-12 shows the total hoop stress at the inner and the outer tube wall where it was assumed that sludge hampers heat transfer. The coarse and the fine FE mesh show some disagreement (10%), and only the results obtained with the fine mesh will be considered in the following.

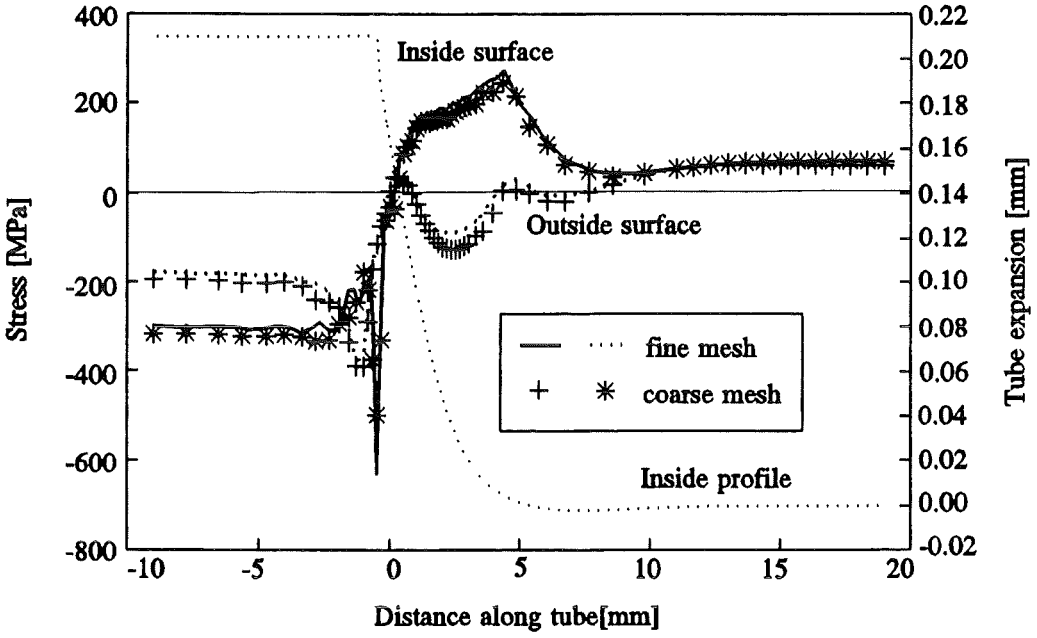

Figure 3-12 Total hoop stresses under sludge

The operational stresses are obtained by subtracting the residual stresses obtained in the previous analysis from the total stresses. Fig. 3-13 shows the variation of the operational hoop stresses along the tube including the expansion zone. The oscillations observed in the expansion zone are probably caused by numerical effects because the total stresses are almost equal to the residual stresses.

At far end of the tube, outside and inside stresses are almost equal indicating the absence of thermal stresses.

3.2.3 Stresses in clean tubes

Fig. 3-14 contains the total hoop stresses at the inner and the outer wall of the tube. Again there is some difference in the results obtained using the course mesh and the fine mesh

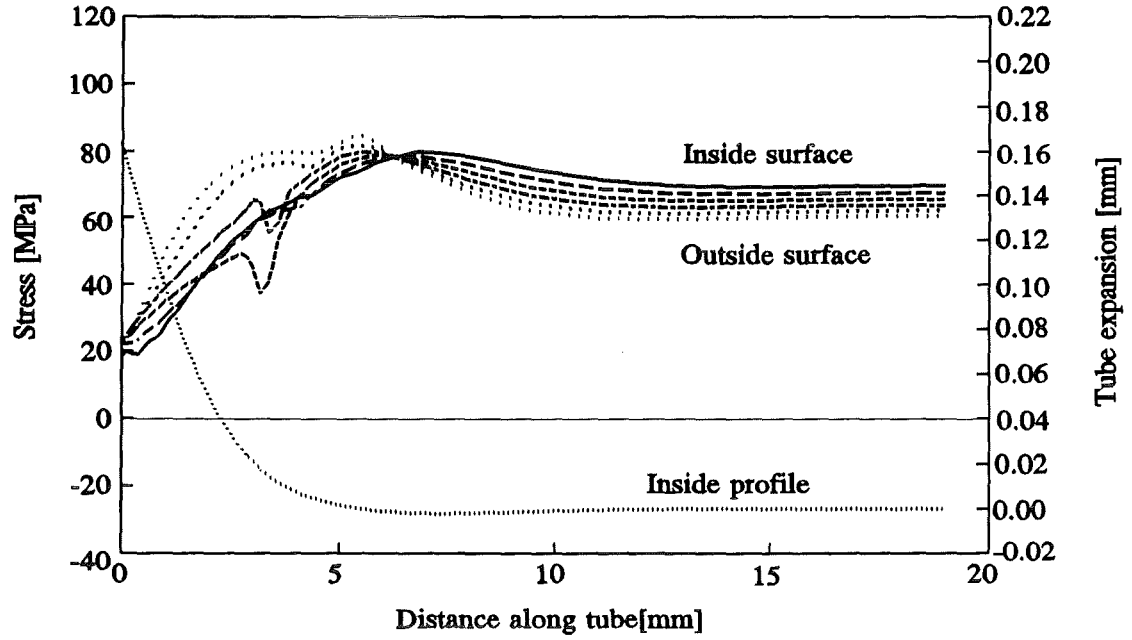

Figure 3-13 Operational stresses under sludge

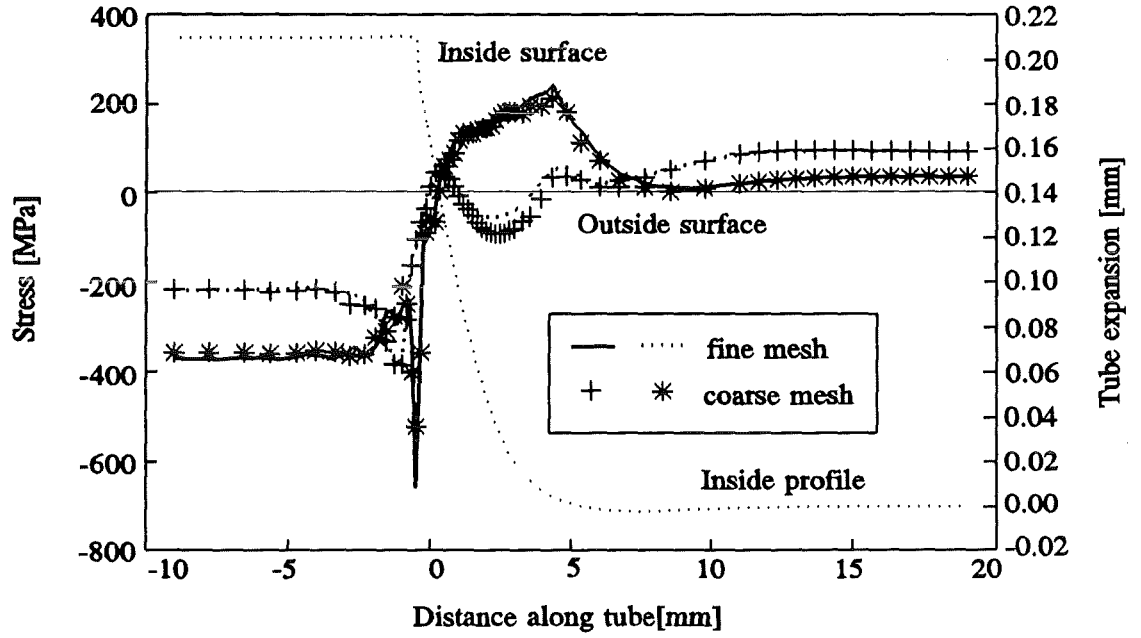

Figure 3-14 Total hoop stresses in a clean tube

which will be used in the following. Inside and outside hoop stress at far end are different because of thermal loading. This can also be seen in Fig. 3-15 which shows the operational stresses obtained by subtracting the residual hoop stresses from the total hoop stresses. The

oscillations of the operational stress in the expansion zone are again attributed to numerical effects.

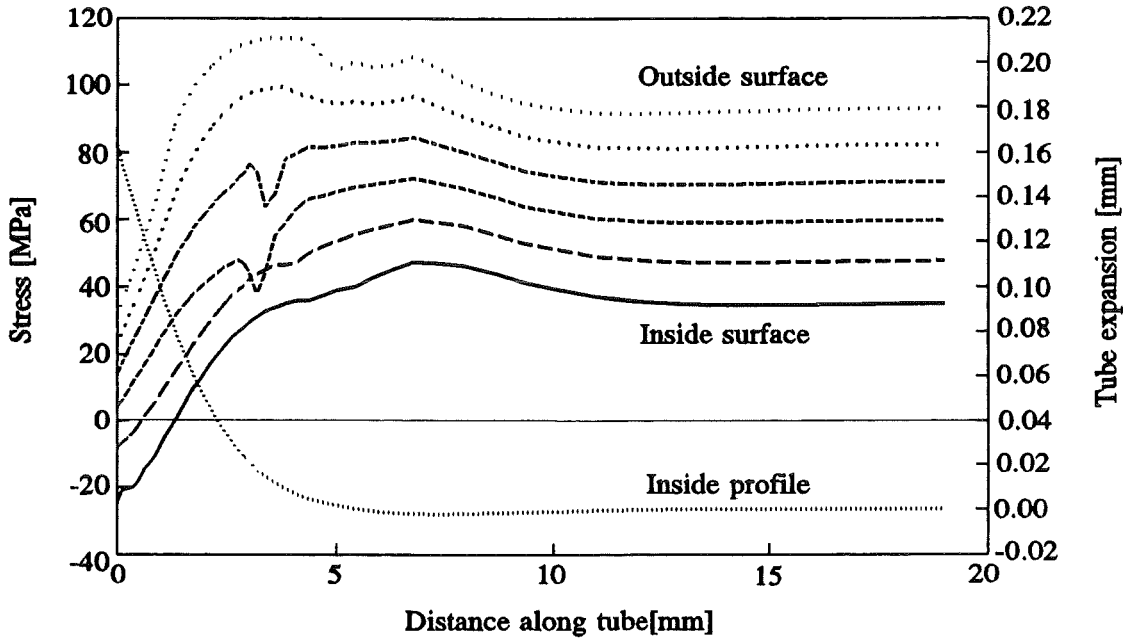

Figure 3-15 Operational hoop stresses in a clean tube

The tensile stresses at the inner wall are higher when sludge is present than for clear tubes.

3.2.4 Discussion of results

The values of the operational stresses determined in the FE analysis agree very well with the results obtained by Garud [48] who calculated the operational stresses and did not analyze the expansion process. This implies that the superposition principle is valid. Figs. 3-16 and 3-17 summarize the hoop stress distribution obtained for tubes with sludge and clean tubes. In addition the shape of an axial through-wall crack is shown which was found by destructively inspecting a tube. The stress profile agrees very well with the crack shape especially for the case with sludge. This is considered to be an experimental confirmation of the stress analysis for the hoop stress.

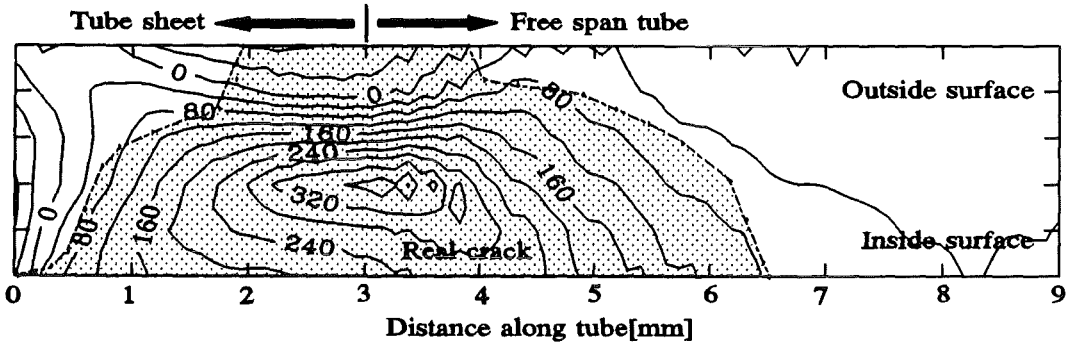

Figure 3-16 Typical crack shape and total hoop stresses in the sludge region

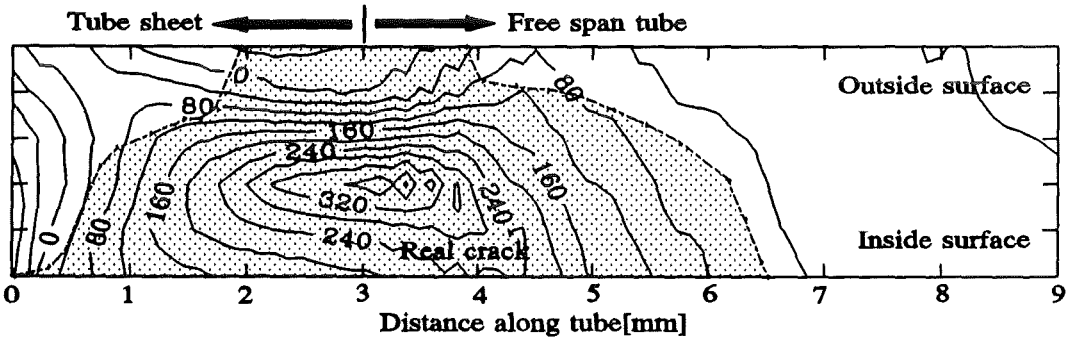

Figure 3-17 Typical crack shape and total hoop stresses in a clean tube

3.3 Parametric stress analysis

The stress field depends on the geometry of the tubes and the material properties. A variation of these input parameters will affect the stress field. This becomes important in reliability analyses where the scatter of the input parameters has to be taken into account.

A detailed sensitivity analysis within the framework of a reliability analysis is not feasible because a non-linear FE analysis has to be performed for each combination of input parameters. A parametric analysis is performed instead in order to find simple formula for interpolation of the stress field.

3.3.1 Residual stresses

Middlebrooks et al [72] performed a parametric study for the case of an axisymmetric model with hydraulic tube expansion. He identified three dominant input parameters. The yield strength of the tube, the thickness of the tube and the initial clearance between tube and tube sheet.

Table 3-III Design matrix for the residual hoop stress calculations

Analysis number	Real parameter values			Coded parameter values*		
	t [mm]	c [mm]	σ_Y [MPa]	t	c	σ_Y
1	0.9906	0.1016	276	-1	-1	-1
2	0.9906	0.1016	448	-1	-1	1
3	0.9906	0.2921	276	-1	1	-1
4	0.9906	0.2921	448	-1	1	1
5	1.1938	0.1016	276	1	-1	-1
6	1.1938	0.1016	448	1	-1	1
7	1.1938	0.2921	276	1	1	-1
8	1.1938	0.2921	448	1	1	1
9	1.0922	0.1969	362	0	0	0
10	0.9687	0.1969	362	-1.216	0	0
11	1.2158	0.1969	362	1.216	0	0
12	1.0922	0.08011	362	0	-1.216	0
13	1.0922	0.3127	362	0	1.216	0
14	1.0922	0.1969	257	0	0	-1.216
15	1.0922	0.1969	467	0	0	1.216

* parameters are coded in the following way: coded value 0 represents the mean value while -1 and +1 the lower and upper limit of the interval considered.

It is assumed that these parameters are also relevant in the analysis presented here (axisymmetric model with tube expansion by mechanical rolling).

An orthogonal experimental design plan (see [74]) was used to determine a quadratic response surface for the hoop stresses. The contribution of input parameters selected is summarized in Table 3-III. A non-linear finite element analysis was performed for all 15 cases. Figures 3-18, 3-19 and 3-20 illustrate the variation of the residual stresses at the inside surface of the tube wall. Whereas a variation of the wall thickness shifts the maximum tensile residual stress by about 1 mm (Fig. 3-18), a variation of the clearance width leads to a shift of about 2 mm (Fig. 3-19). The yield strength changes the peak height considerably (Fig. 3-20).

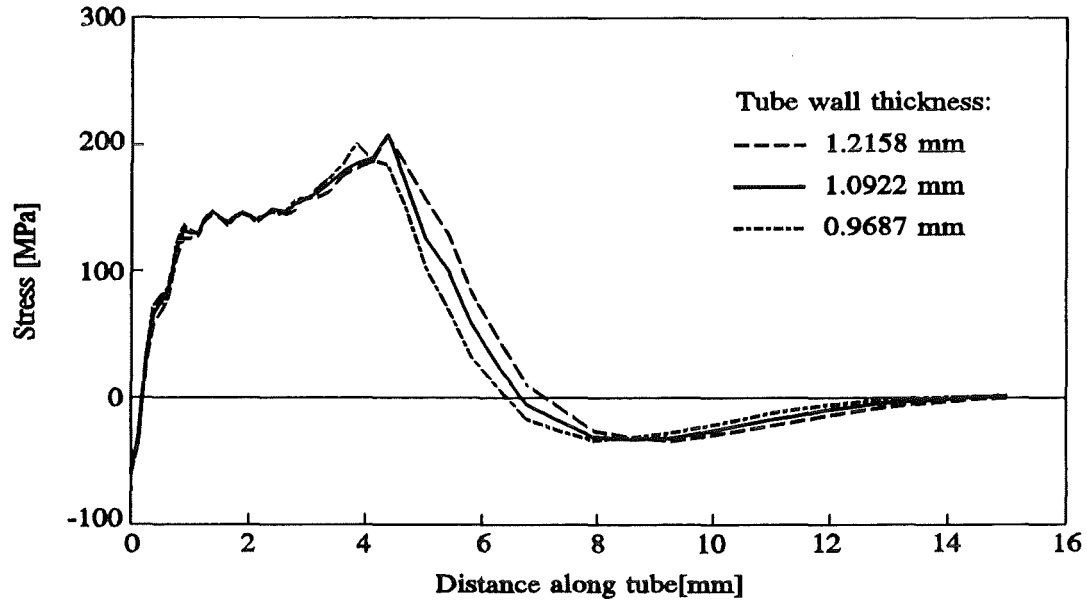

Figure 3-18 Sensitivity of the residual hoop stress to the wall thickness

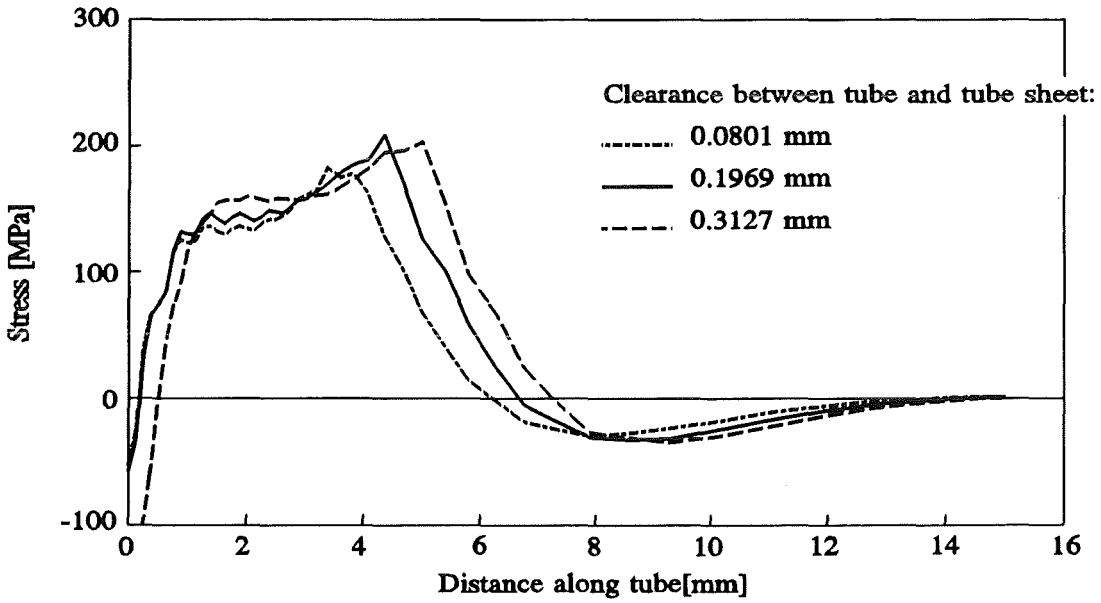

Figure 3-19 Sensitivity of the residual hoop stresses on the initial tube to tube-sheet clearance

3.3.2 Modelling residual stresses by response surface technique

The FE-results were used to fit an independent quadratic response surface to the residual hoop stresses obtained for each node. The correlation coefficient of the fitting was better than

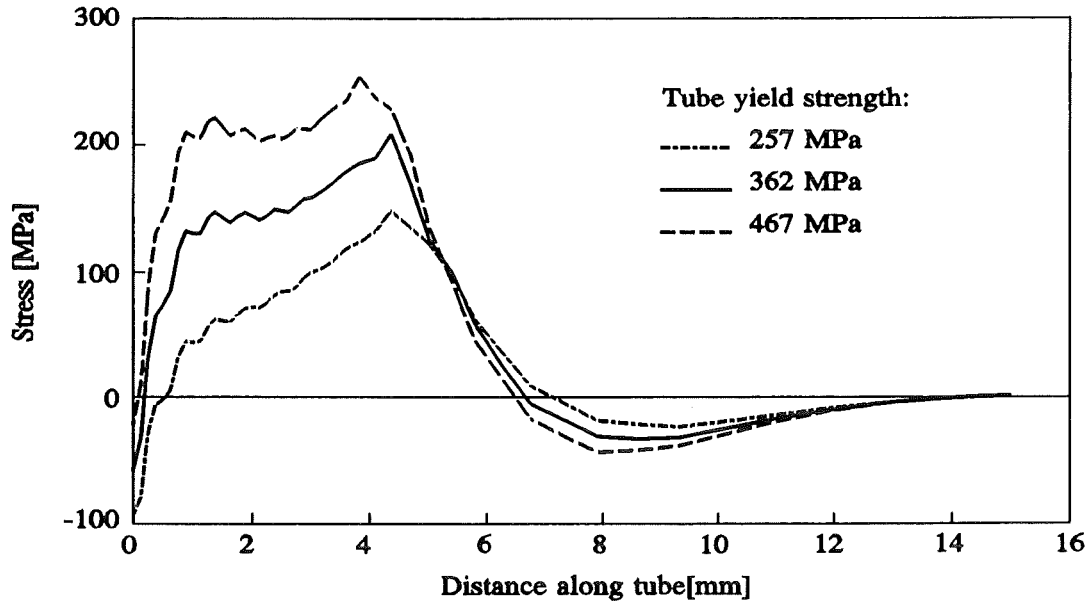

Figure 3-20 Sensitivity of the residual hoop stresses on the tube yield strength

99.6%. Spline interpolation was used to obtain the stresses between the nodes. The peak residual stress value $\sigma_{R,\,max}$ and its position along the tube axis L_{init} are defined by:

$$\begin{aligned}\sigma_{R,\,max} &= 361. + 1.421\,t + 16.566\,c + 73.955\,\sigma_Y - \\ &- 0.104\,t^2 - 11.612\,c^2 - 2.473\,\sigma_Y^2 + \\ &+ 0.500\,tc - 1.250\,t\sigma_Y + 9.500\,c\sigma_y\end{aligned} \tag{3-2}$$

$$\begin{aligned}L_{init} &= 3.324 + 0.126\,t + 0.465\,c - 0.217\,\sigma_Y + \\ &+ 0.0778\,t^2 + 0.0786\,c^2 + 0.091\,\sigma_Y^2 + \\ &+ 0.0355\,tc - 0.0257\,t\sigma_Y + 0.0270\,c\sigma_y\end{aligned} \tag{3-3}$$

To assure continuous first and second order partial derivatives, a cubic spline stress field interpolation was introduced as shown in Fig. 3-21. The error at the stress intensity factor level (see chapter 4.4.1) was below 1%.

3.3.3 Operational stresses

The distribution of operational stresses was approximated by:

$$\sigma(x) = \left(1 - e^{-0.6\,x}\right)\,\sigma\,|_{x\to\infty} \tag{3-4}$$

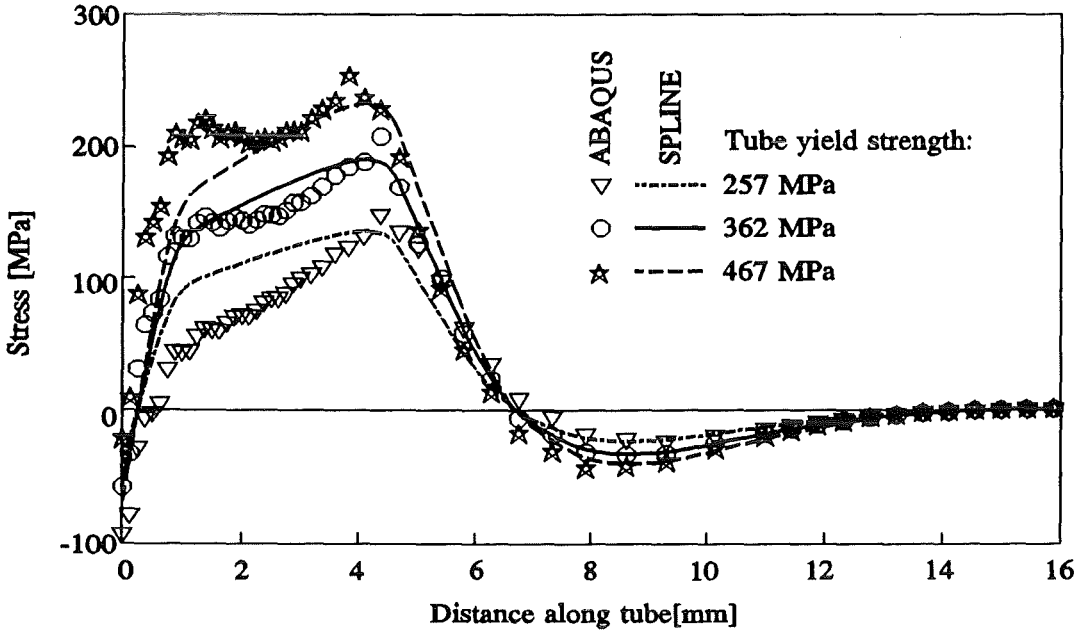

Figure 3-21 Cubical *spline* interpolation of the residual stresses along the tube length

where $\sigma|_{x\to\infty}$ represents the far field solution. This ignores the slight maximum of the operational stresses obtained in the expansion zone (see Fig. 3-13 and 3-15). This seems to be justified by the fact that the stress field is dominated by the residual stresses in this area.

Eq. (2-5) has been used to estimate the pressure induced stresses. Thermal stresses are calculated according to eqs. (3-5) to (3-10) given below. Both analytically obtained values confirm the numerical results obtained by ABAQUS code.

Thermal stresses

Assuming the radial temperature distribution in the form:

$$T(r) = \frac{\Delta T}{\ln(R_{out} / R_{in})} \ln(R_{out} / r) \qquad (3\text{-}5)$$

where ΔT is the temperature difference between the inner (R_{in}) and outer (R_{out}) surface, the hoop stress follows as [92]:

$$\sigma_{\phi,\Delta T}(r) = \frac{\alpha_T E \Delta T}{2(1-\nu)\ln(R_{out}/R_{in})}\left[1 - \ln\frac{R_{out}}{r} - \frac{R_{in}^2}{R_{out}^2 - R_{in}^2}\left(1 + \frac{R_{out}^2}{r}\right)\ln\frac{R_{out}^2}{R_{in}^2}\right] \qquad (3\text{-}6)$$

E and α are Youngs modulus and linear thermal expansion coefficient (Table 3-I) and ν the Poisson's ratio. Temperature difference ΔT is obtained by setting convective boundary conditions at both tube surfaces [73]:

$$\Delta T = T_{in} - T_{out} \tag{3-7}$$

with:

$$T_{out} = \frac{\Theta T_{in,\infty} + \frac{h_{out}}{h_{in}} \frac{R_{out}}{R_{in}} \Theta T_{out,\infty} + h_{out} R_{out} T_{out,\infty}}{h_{out} R_{out} + \frac{h_{out}}{h_{in}} \frac{R_{out}}{R_{in}} \Theta + \Theta} \tag{3-8}$$

and:

$$T_{in} = T_{in,\infty} + \frac{h_{out}}{h_{in}} \frac{R_{out}}{R_{in}} \left(T_{out} - T_{out,\infty} \right) \tag{3-9}$$

$T_{in,\infty}$ are $T_{out,\infty}$ temperatures of primary and secondary coolants, h_{in} and h_{out} are the corresponding heat transfer coefficients. Θ is defined by the means of thermal conductivity of the tube k:

$$\Theta = \frac{k}{\ln\left(\frac{R_{out}}{R_{in}} \right)} \tag{3-10}$$

Constants $T_{in,\infty}$, $T_{out,\infty}$, h_{in}, h_{out} are given in Table 3-II and k in Table 3-I. Both tube radii are considered as random variables.

4 STRESS CORROSION CRACK PROPAGATION

Stress corrosion cracking determines the lifetime of the steam generator tubes. Further, crack propagation has a dominant influence on the failure probability [25]. This chapter contains a review of the database for stress corrosion cracking in Inconel-600. The crack propagation law used in the subsequent calculations is derived. Only through-wall axial cracks in the tubes will be considered.

4.1 Basic facts about stress corrosion cracking

Stress corrosion cracks are known to develop in a reactive environment at relatively low sustained stress levels. Thus, loads which are safely applied to a structure in an inert environment could cause catastrophic failure at the presence of a reactive gas or fluid. Generally, stress corrosion crack growth strongly depends on the materials and temperatures involved. On the micro scale, a lot of different processes or their combinations cause the crack initiation and propagation. In this subsection, only a very brief review of basic facts is given.

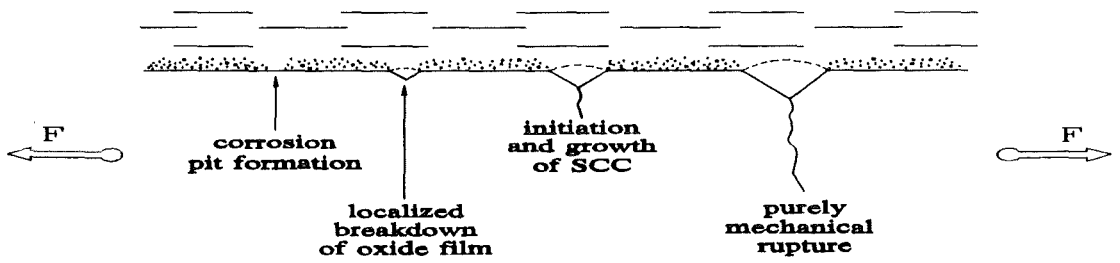

Figure 4-1 Initiation and propagation of stress corrosion cracks

Fig. 4-1 depicts the sequence of events in stress corrosion [70]. First, the oxide layer on the surface breaks, then a corrosion pit is formed from which a crack is initiated. The rate of stress corrosion crack propagation depends on temperature and loading for a given combination medium/base material. The loading is given in terms of stress intensity factor K. Three different crack growth regimes are generally observed: chemical dissolution of base

material in region I, diffusion controlled crack growth in region II, and mechanical breaking in region III (see Fig. 4-2). The temperature dependence in region II is shown in Fig. 4-3 and can be described by the Arrhenius equation (eq. (4-1)):

$$\left(\frac{da}{dt}\right)_{II} \propto e^{-E_{app}/(RT)} \qquad (4\text{-}1)$$

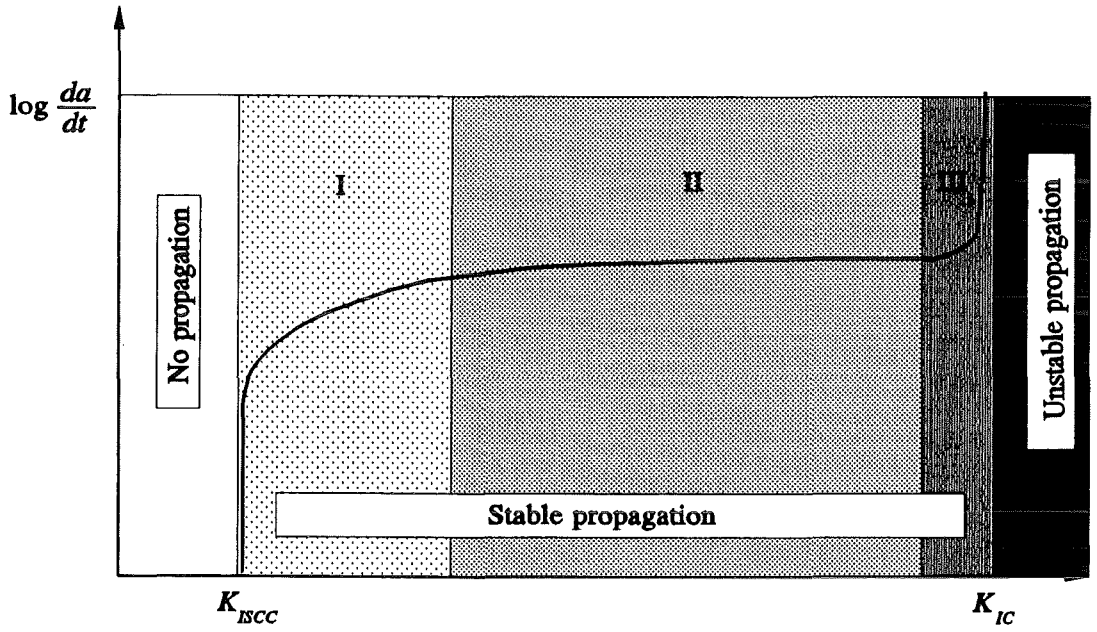

Figure 4-2 Crack tip velocity as a function of load

4.2 Stress corrosion cracking in Inconel-600

The chemical composition of Inconel-600 is given in Table 4-I. Stress corrosion cracking occurs in hot water for temperatures higher than approx. 300°C. A review of the influence parameters is given in [5, 19].

4.2.1 Basic mechanisms of stress corrosion cracking in Inconel-600

There is no agreement about the dominant mechanisms of stress corrosion cracking in Inconel 600 [8, 9]. Some reports are briefly reviewed below.

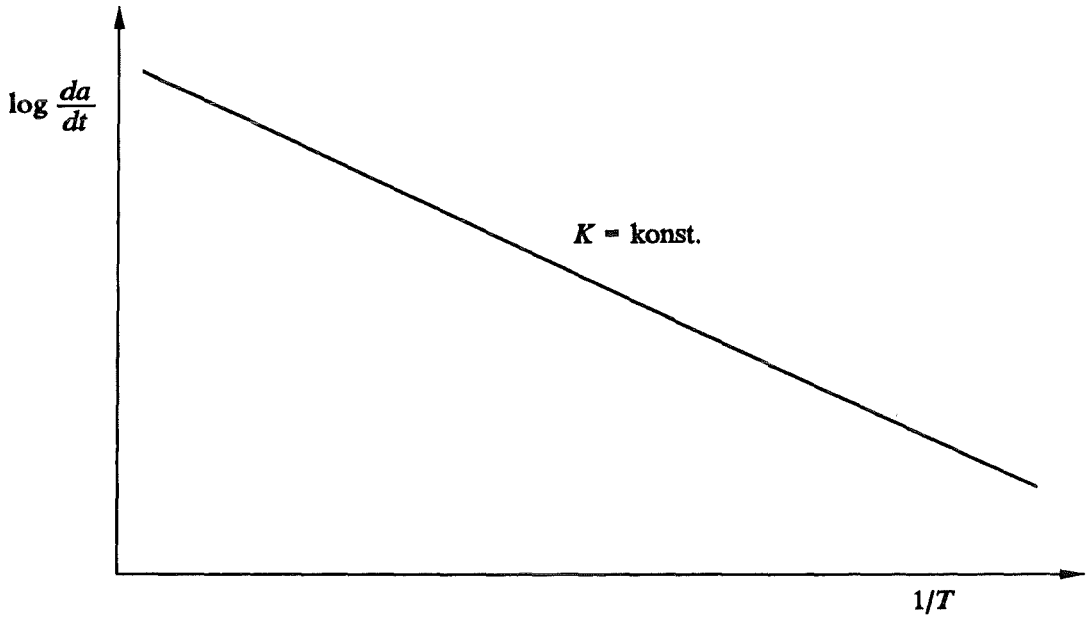

Figure 4-3 Crack tip velocity (*da/dt*) as a function of temperature (*T*)

Table 4-I Chemical composition of Inconel 600

Source	Chemical composition in % (the rest is Ni)							
	Cr	Fe	Si	Mn	Cu	Mo	C	S
ASME SB 163 specification [4]	14.00 – 17.00	6.00 – 10.00	max 0.50	max 1.00	max 0.50	N/A*	max 0.15	max 0.015
Krško NPP min [98]	14.00	6.43	0.04	0.10	0.02	N/A	0.01	0.001
Krško NPP max [98]	16.83	10.0	0.40	0.52	0.49	N/A	0.06	0.012
Speidel [89]	15.60	8.40	0.32	0.24	0.18	0.13	0.10	0.004

* no data available.

Shen and Shewmon [87, 88] reported that the dominant damage mechanism is hydrogen (H_2) diffusion which is enhanced by the presence of methane (CH_4). In steam generator tubes, methane is formed from the free carbon (C) in the metal and free hydrogen in the water. This was found at rather high stress intensity factor values ($K \approx 72\text{-}80$ MPa $m^{1/2}$), which are not typical for normal operation.

Rebak et al [81] report that the crack propagation is affected simultaneously by three different mechanisms: nickel dissolution, hydrogen diffusion and creep. Further, the variations of the reactor coolant chemical composition (pH between 6.9 and 7.4) appeared not to have any influence on the crack tip velocity.

Another damage mechanism suggested in the literature (formation of carbides on the grain boundaries and subsequent nickel dissolution [5, 42]) seems to be less important for the Krško plant, because it mainly occurs in sensitized material, whereas the tubes in Krško steam generators are from non-sensitized material. It should be noted here that sensitized and non-sensitized Inconel 600 are typically affected only in BWR and PWR conditions, respectively.

The following is a summary of stress corrosion mechanisms in a Inconel-600 steam generator tube (PWR environment):

- crack propagation is faster if the carbides do not precipitate on the grain boundaries;
- the crack velocity is enhanced by increasing the partial pressure of hydrogen in water up to 1 bar. At 10 bar, a decrease of the crack velocity has been observed;
- crack tip velocity is very sensitive to the increase in temperature. Activation energy in eq. (4-1) is reported to be between 74 and 138 kJ/mol [87, 89];
- plastic deformation enhances the crack velocity [87, 88, 89];
- expected Ph values of reactor coolant are between 6.9-7.4. In this range, the change of pH does not significantly affect the crack velocity.

4.2.2 Availability and reliability of crack velocity data

Most of the data available in the literature are concerned with time to crack initiation, not with crack propagation. Only recently some attempts to determine the crack tip velocities have been published. An overview of the data on crack propagation is given in [19]. The results are summarized in Fig. 4-4 for the reactor coolant temperature of 330°C. The reasons for large scatter in the experimental data are difficulties in determining the crack initiation time and controlling the loading during the experiment [19].

The threshold for crack propagation is of the order of 5-10 MPa $m^{1/2}$. The transition between region I and region II occurs at about 30 MPa $m^{1/2}$. The upper limit of region II occurs at 100 MPa $m^{1/2}$. The plateau velocity with prior plastic deformation is approximately equal to 9.5 mm/year; without prior plastic deformation this value is reduced to 1.6 mm/year. this is important since the cracks considered in this report develop inside the cold-worked tube and propagate towards the non-deformed tube.

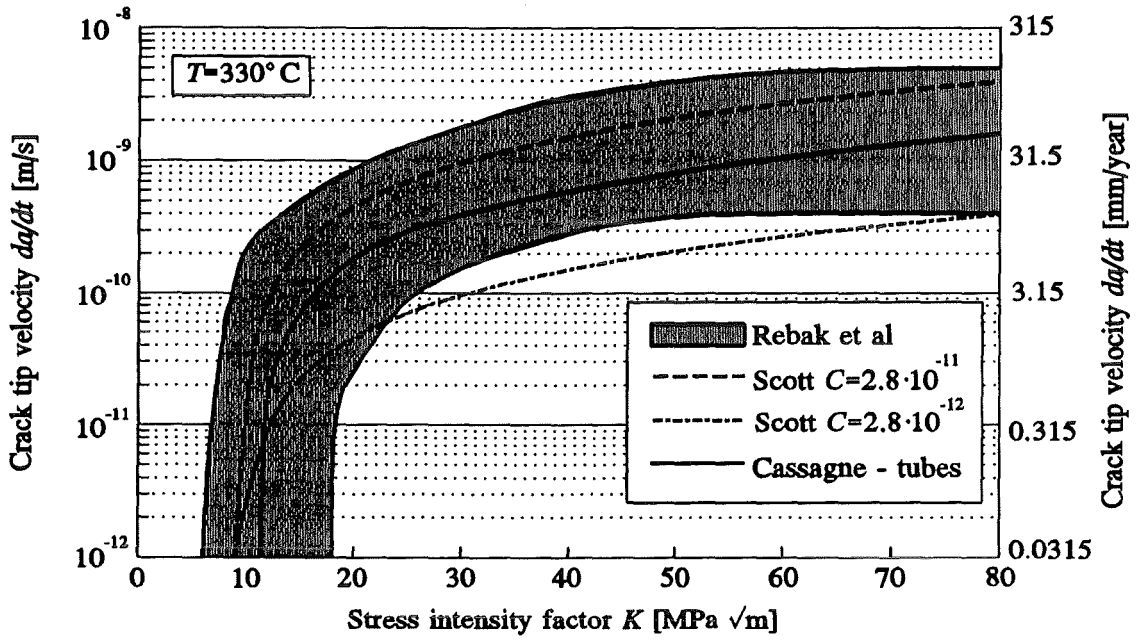

Figure 4-4 Range of reported crack tip velocities (Rebak et al [81], Cassagne [19] in Scott [86])

4.3 Overview of crack propagation models

Three different approaches are used in the literature:

- statistical analysis of non-destructive measurements,
- linear elastic fracture mechanics and
- local strain rate.

Further details on each of them are given below.

4.3.1 Statistical analysis of results of non-destructive examination

A Gamma distribution was introduced in [56, 58, 59] for the distribution of measured crack indication length:

$$f(l) = \frac{\beta^{\alpha}\, l^{\alpha-1}\, e^{-\beta l}}{\Gamma(\alpha)} \tag{4-2}$$

where Γ represents the Eulers Gamma function:

$$\Gamma(\alpha) = \int_0^{\infty} x^{\alpha-1}\, e^{-x}\, dx \tag{4-3}$$

The amount of crack indication growth between two inspections is described by an exponential distribution:

$$h(\Delta l) = \beta\, e^{-\beta\, \Delta l} \tag{4-4}$$

The crack indication length distribution of inspection number $j+1$ follows from the data of the j^{th} inspection using:

$$f_{j+1}(l) = \int_0^{l} f_j(x)\, h(l - x)\, dx \tag{4-5}$$

The parameters α, β of $f(l)$ (eq. (4-2)) and $h(\Delta l)$ (eq. (4-4)) are determined as follows:

$$\left.\begin{aligned} \alpha(l) &= \delta_{l,0}^2 \\ \beta(l) &= \delta_{l,0} \end{aligned}\right\} \tag{4-6}$$

Those parameters depend on the initial crack indication length l_0, defined as:

$$\delta_{l,0} = W + 3.0 \cdot e^{-0.45 \cdot l_0} \tag{4-7}$$

The parameter W has to be inferred form the experimental data.

The parameters of the distribution describing previously non-detected cracks are defined as:

$$\left.\begin{aligned} \alpha_i &= (W+3.0)^2 \\ \beta_i &= W+3.0 \end{aligned}\right\} \qquad (4\text{-}8)$$

However, this model is not able to predict the number of new cracks.

The statistical approach is very well suited to evaluate an existing database but it can not be extrapolated to other load cases where $f(l)$ and $h(\Delta l)$ may not be known with sufficient accuracy.

4.3.2 Linear elastic fracture mechanics

Scott [86] described the crack growth rate as:

$$\frac{da}{dt} = C\left(K - K_{ISCC}\right)^m \qquad (4\text{-}9)$$

The constants were determined as $m=1.16$, $2.8 \cdot 10^{-12} < C < 2.8 \cdot 10^{-11}$ and $K_{ISCC}=9$ MPa $m^{½}$ in typical reactor coolant. The crack growth curve is shown in Fig. 4-4 together with other relevant data available.

These constants were found by fitting experimental results in [71]. The stress distribution in the tube expansion transition zone was modelled as shown in Fig. 4-5, which corresponds to a sum of residual and operational stresses. The fracture mechanics model is restricted to one-way crack propagation, i.e. cracks can only propagate outside the tube sheet. The scatter of the stress field was not taken into account in [86].

A similar model for crack propagation is used in the COMPROMIS code [52, 78], which also accounts for the scatter observed in inspection data. However, the details of the model are not clear from the published literature.

4.3.3 Local strain rate

Ford and Andresen [42] developed a semi-empirical model for stress corrosion crack propagation in sensitized stainless steels. The basic mechanism assumed was the breaking of the oxide film at the crack tip. Hence, the crack velocity is related to the strain rate which is responsible for film breaking (*film rupture model*). The crack growth rate is determined by:

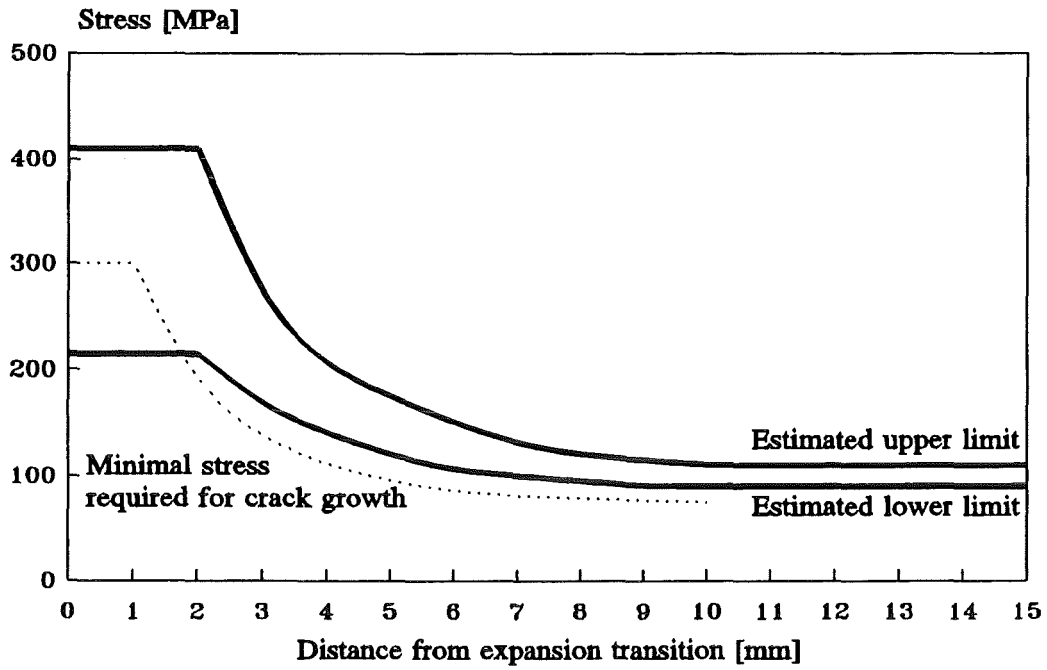

Figure 4-5 Total residual and operational hoop stresses in a tube (Scott [86])

$$\frac{da}{dt} = f(\omega)\ \dot{\varepsilon}_{ct}^{\omega} \tag{4-10}$$

where ω accounts for the electro-chemical properties of the system under consideration and $\dot{\varepsilon}_{ct}$ is the local strain rate at the crack tip. An empirical relation between the local strain rate and the stress intensity factor K is proposed by Andresen [42]:

$$\dot{\varepsilon}_{ct} = 6 \cdot 10^{-14}\ K^4, \quad K \text{ v } \left[\text{ksi}\sqrt{\text{in}}\right], \quad \dot{\varepsilon}_{ct} \text{ v } \left[s^{-1}\right] \tag{4-11}$$

$$\dot{\varepsilon}_{ct} = 8.75 \cdot 10^{-14}\ K^4, \quad K \text{ v } \left[\text{MPa}\sqrt{\text{m}}\right], \quad \dot{\varepsilon}_{ct} \text{ v } \left[s^{-1}\right] \tag{4-12}$$

which, together with eq. (4-10) leads to a *da/dt-K* relation. This means that the film rupture is equivalent to the fracture mechanics model.

Another version of this model also includes crack initiation [45, 47].

4.3.4 Summary of the state of the art

The statistical analysis provides an excellent database for comparison of models, but cannot be adapted to the specific conditions of a given plant. Moreover, only predetermined

inspection intervals can be taken into consideration because the model does not contain an explicit time dependence.

The approach using linear elastic fracture mechanics seems to be most promising since it relies only on material data and can be adopted to plant specific loading conditions. The scatter present in inspection data can be included using probabilistic fracture mechanics.

4.4 Asymmetric crack propagation

Linear elastic fracture mechanics can be used to determine the loading parameters for axial cracks in steam generators tubes for two reasons:

- Under normal operating conditions the K-factor is of the order $K \approx 15\text{-}25$ MPa $m^{1/2}$ [71] whereas linear elastic fracture mechanics can be applied to stress corrosion cracking up to 40 MPa $m^{1/2}$ [19].

- The electro-chemical corrosion process causes the embrittlement of the material [64, 70].

4.4.1 Stress intensity factor

The stress in the neighborhood of the axial cracks in the transition zone is varying considerably in axial (x) direction (see Fig. 4-6). This implies that:

- The stress intensity factors at the crack tips of the axial cracks are different from each other. Hence, the center of the crack alters its position if the crack starts to grow.

- There are regions with high gradients of the stress in x-direction. Hence the K-factors depend strongly on the position of a crack center.

A similar problem was analyzed by Terada and Nakajima [91] who considered a crack in a plate. The method developed in [91] will also be used here. A local coordinate system (ξ, η) is introduced with origin at the center of the crack (see Fig. 4-6). The position of the crack is defined in terms of the distance L from the origin of the stress field. If the variation of the stress field is given in terms of $\sigma(\xi+L)$, the K-factors at both crack tips can be determined using the corresponding Green's function:

$$K_{\pm a} = \left[\frac{1}{\sqrt{\pi a}} \int_{-a}^{+a} \sigma(\xi + L) \sqrt{\frac{a \pm \xi}{a \mp \xi}}\, d\xi \right] m_F(a) \qquad (4\text{-}13)$$

where $m_F(a)$ denotes the bulging factor given in eq. (2-3). The K-factor depends strongly on the crack length $2a$ and the distance L from the stress field origin.

Figs. 4-7 and 4-8 show the results obtained for the crack tips $\pm a$ (see Fig. 4-6). For $L<0$, K becomes negative which implies that cracks can propagate only a small distance towards the tube sheet. Cracks will initiate at $L \approx 4$ mm in the vicinity of the residual stress peak. The cracks will first propagate with high velocity towards the tube sheet an then stop (see Fig. 4-7, K_{-a}) whereas the other crack tip will move at a fairly constant rate (see Fig. 4-8, K_{+a}) because K_{+a} is only slightly influenced by the residual stresses in the transition zone.

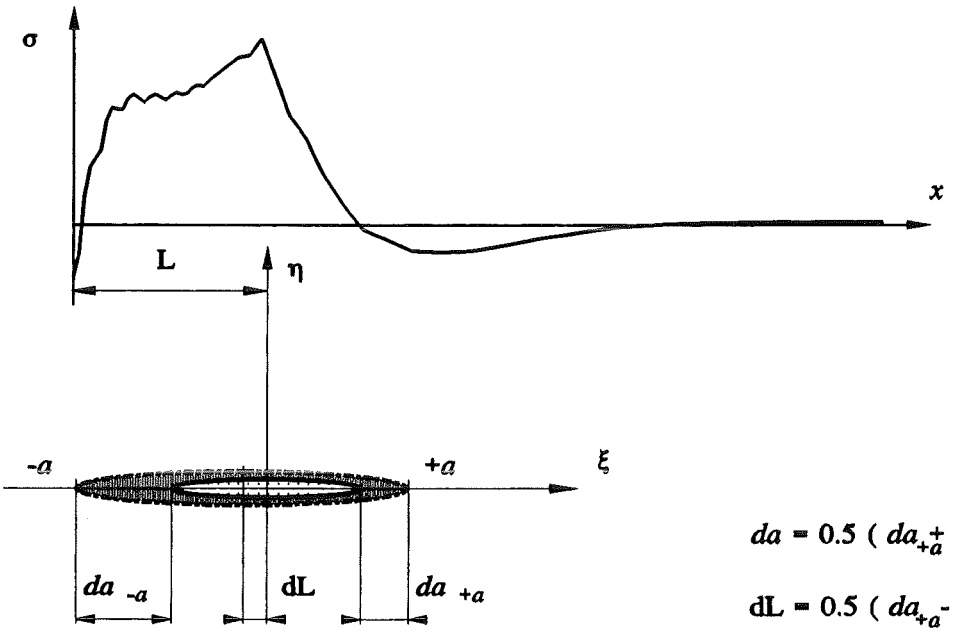

Figure 4-6 Crack position in the residual stress field (asymmetrical propagation)

A Gaussian type integration procedure is used to perform the integration over the stress field. The corresponding formulae are given below [2]:

$$\int_{-a}^{a} \sigma(L+\xi) \frac{\sqrt{a+\xi}}{\sqrt{a-\xi}}\, d\xi = 2a \sum_{j=1}^{N} w_j \sigma(L+y_j) \qquad (4\text{-}14)$$

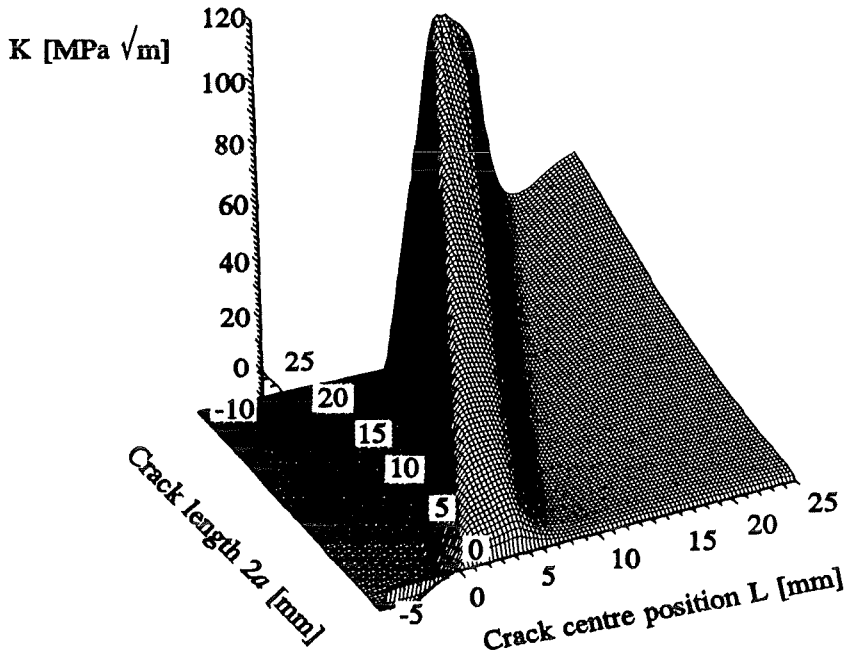

Figure 4-7 Stress intensity factors at the left (-*a*) crack tip

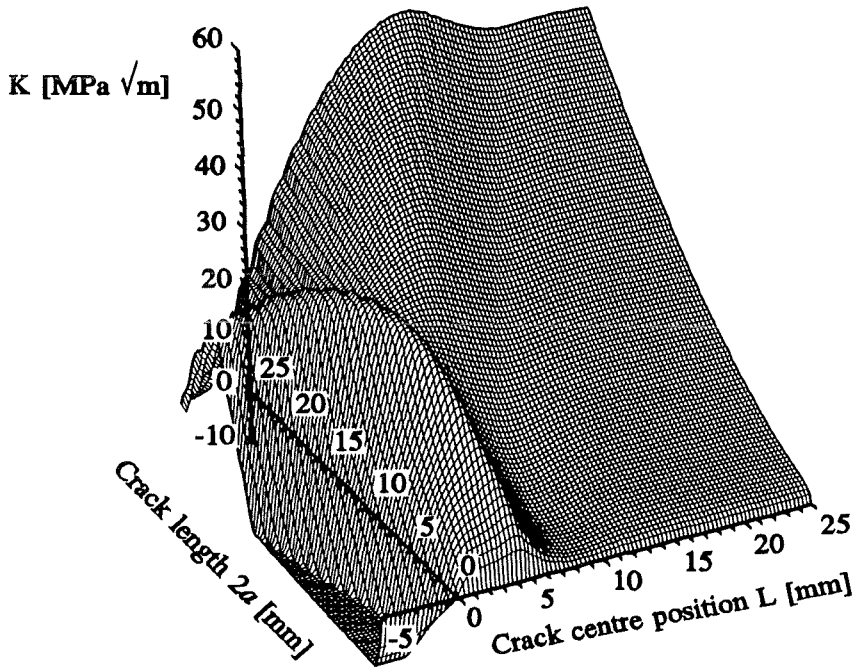

Figure 4-8 Stress intensity factors at the right (+*a*) crack tip

with

$$y_j = -a(1 - 2x_j) \tag{4-15}$$

$$x_j = \cos^2\left(\frac{(2j - 1)\pi}{2(2N + 1)}\right) \tag{4-16}$$

and

$$w_j = \frac{2\pi x_j}{2N + 1} \tag{4-17}$$

N=30 integration points were enough to stabilize the integral value inside the $\pm 5\%$ interval. In order to maintain reasonably continuous derivatives, it was unfortunately not enough to increase the N value to very high values. The bicubic spline approximation was introduced which allows an accurate approximation of the functional values together with fairly stable derivatives.

4.4.2 Asymmetric crack propagation

A stress intensity factor $K_{\pm a}$ is calculated for each crack tip. The corresponding crack growth rates $\dot{a}_{\pm a}$ can then be determined using the crack growth law eq. (4-20). The rate of increase of the average crack length is given by:

$$\dot{a} = \frac{da}{dt} = \frac{1}{2}\left(\dot{a}_{+a} + \dot{a}_{-a}\right) \tag{4-18}$$

whereas:

$$\dot{L} = \frac{dL}{dt} = \frac{1}{2}\left[\dot{a}_{+a} - \dot{a}_{-a}\right] \tag{4-19}$$

describes the migration rate of the crack center.

4.4.3 Position of the crack with known length

Cracks are initiated at the peak value of the stress distribution which follows from the response surface (eq. (3-3)). The corresponding value L_{init} is the initial value of L in the crack growth analysis, whereas the initial crack size a_{init} is equal to zero. Integration of the

crack growth equations (4-18) and (4-19) from a_{init} to a_0 yields the position of crack of size a_0 for a given set of material constants, loading conditions and parameters C and K_{ISCC}.

4.4.4 Crack propagation law

The crack propagation law is given by:

$$\dot{a}_{\pm a} = \left(\frac{da}{dt}\right)_{\pm a} = C_{\pm a}\left(K_{\pm a} - K_{ISCC}\right)^m \geq 0. \qquad (4\text{-}20)$$

The constants $C_{\pm a}$ may be different for each crack tip at $\pm a$. This is because crack tip $-a$ moves into material which has been subjected to cold working whereas crack tip $+a$ is leaving this area. Based on results of Cassagne et al [19], the relation between C_{-a} (cold worked) and C_{+a} is given by:

$$C_{+a} = \frac{1}{\rho_C} C_{-a} \qquad (4\text{-}21)$$

A value of $\rho_C \leq 6$ is consistent with the crack growth data reported in the literature.

The material constants m, C and K_{ISCC} are assumed to be random variables whose mean values correspond to those given in [86] ($m=1.16$, $C_{+a}=2.8 \cdot 10^{-12}$ as lower bound [86] and $K_{ISCC}=9$ MPa $m^{1/2}$). This is in agreement with what has been observed elsewhere. The temperature of 330°C and pressure loading are assumed to be constant under operating conditions.

4.5 Discussion of the crack propagation model results

4.5.1 Stress intensity factors

Figures 4-9 and 4-10 contain the stress intensity factors obtained for both crack tips for various combinations of a and L. The value L=0 corresponds to the last contact point between the rolling tool and the tube. The dashed line (L=3 mm) corresponds to the top of the tube sheet.

For $L > 20$, both K-factors are approximately equal to the ones obtained for a free tube with constant membrane hoop stress, i.e. the effect of the residual stress is essentially limited to $L \leq 20$ mm. No crack can propagate far into the tube sheet because of $K < 0$ for $L < 0$.

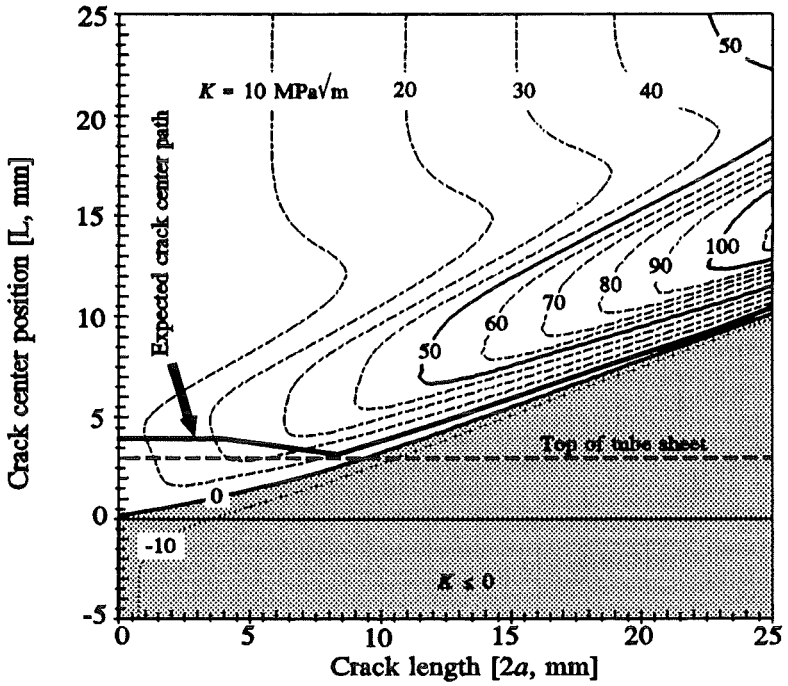

Figure 4-9 Values of K_{-a} as a function of crack center position and length

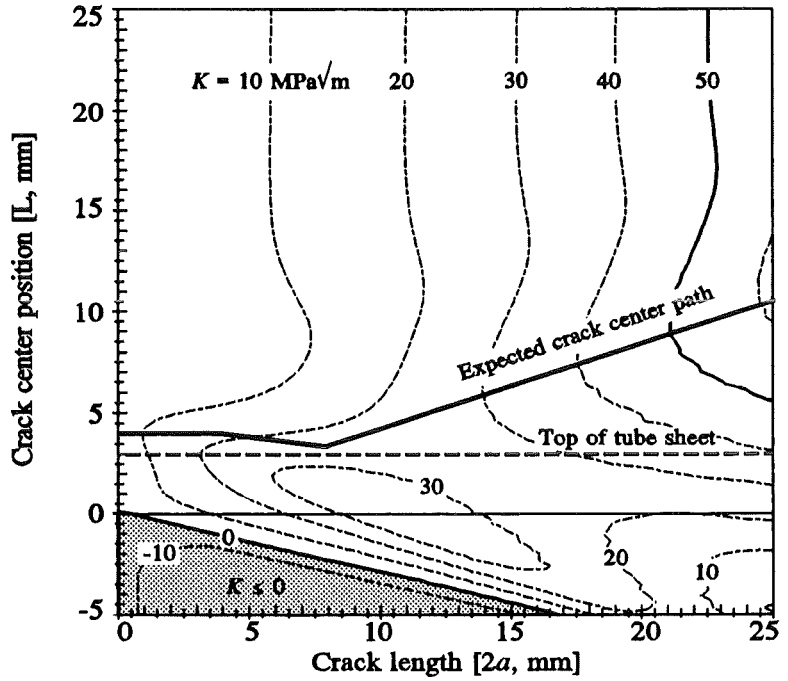

Figure 4-10 Values of K_{+a} as a function of crack center position and length

4.5.2 Movement of the center of a crack

The variation of the stress intensity factor with both the crack length $2a$ and the position L shows (see Figures 4-9 and 4-10) that the center of the crack moves considerably in the course of crack propagation.

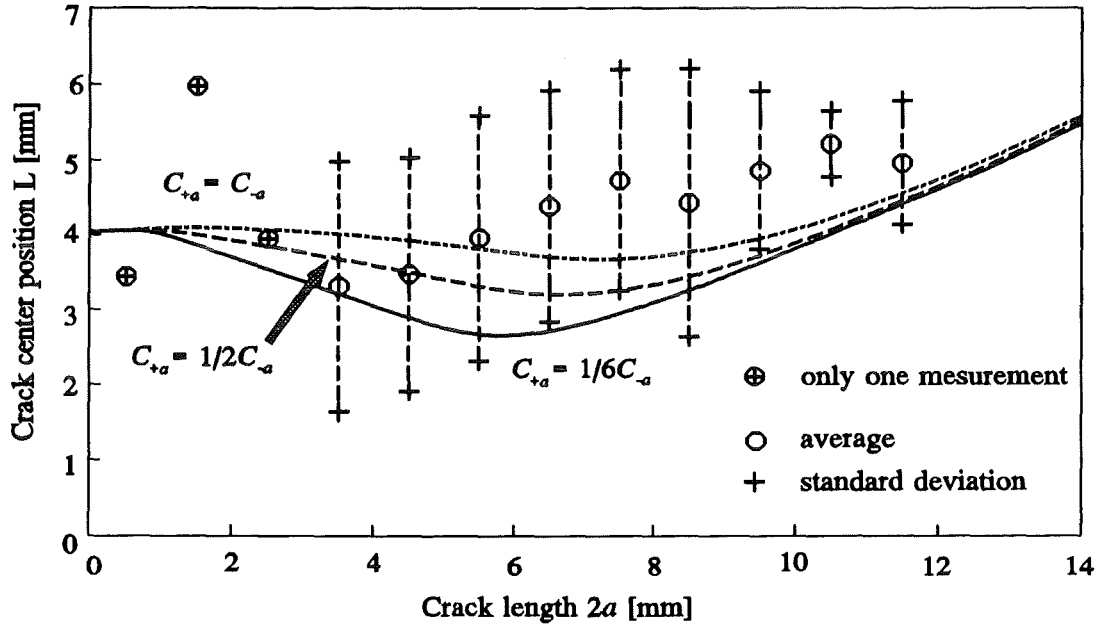

Figure 4-11 Predicted and observed crack center path

The bold line in Figs. 4-9 and 4-10 shows the expected crack path for a crack which is initiated at the point of maximum stress. The value K_{-a} drops below the threshold K_{ISCC}=9 MPa m^{½} at about $2a$=8 mm, then the $-a$ crack tip is arrested. The $+a$ crack tip propagates at maximum growth rate, i.e. follows the maxima of the $K_{+a}(a, \mathrm{L})$ surface.

In Fig. 4-11 the results of the crack propagation model are compared with inspection data from the Krško plant, where mean values were inserted for the parameters of the model. The error bars of the data corresponds to the standard deviation from the inspection data. Only one data point has been obtained for crack lengths of 1, 2 and 3 mm (also shown on Fig. 4-11). The ratio of the constants C_{-a} and C_{+a} at the crack tips corresponding to $-a$ and $+a$, respectively, was varied with ρ_C=1, 2 and 6 (see eq. 4-21). The agreement is quite satisfactory compared to the accuracy of the inspection procedure ($\pm$1.5 mm on crack length, see [31, 32]).

4.5.3 Crack propagation

In the statistical model [58] (see also sect. 4.3.1) the amount of crack propagation Δa depends on the initial crack length a_0. Δa to a_0 relationship was therefore obtained from the fracture mechanics model and compared with inspection data from the Krško plant (Fig. 4-12 for ρ_C=1, Fig. 4-13 for ρ_C=2 and Fig. 4-14 for ρ_C=6). The error bars correspond to the maximum and minimum values observed. The time interval between two inspections was 15 months. Average values ± 10% were used for the parameters of the crack growth law. The best agreement is obtained for ρ_C=2 which will be used in subsequent calculations.

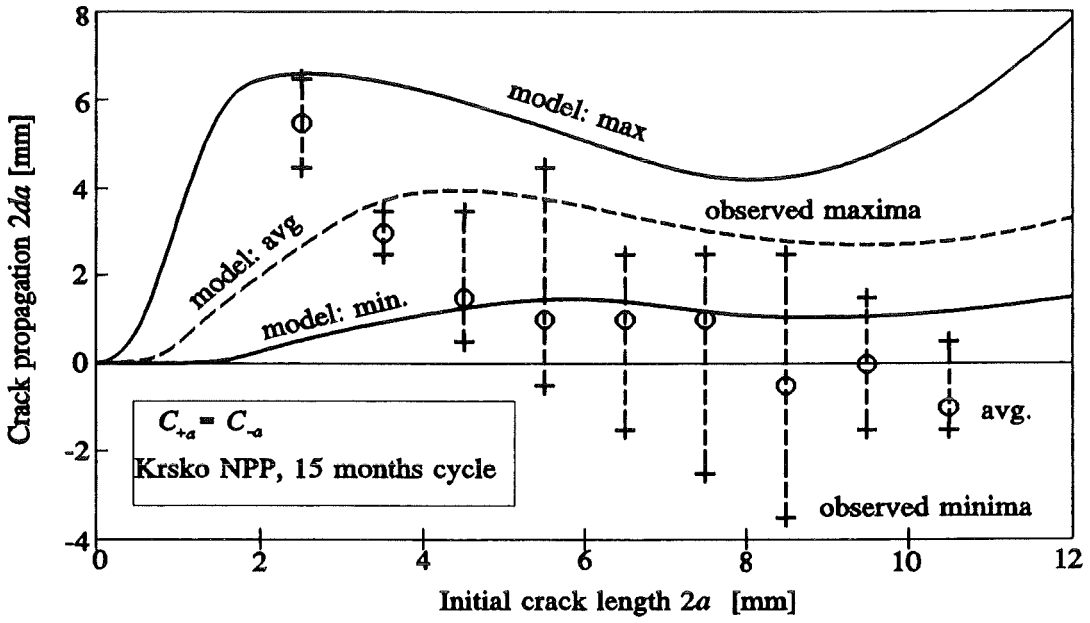

Figure 4-12 Predicted and observed crack growth ($C_{+a}=C_{-a}$)

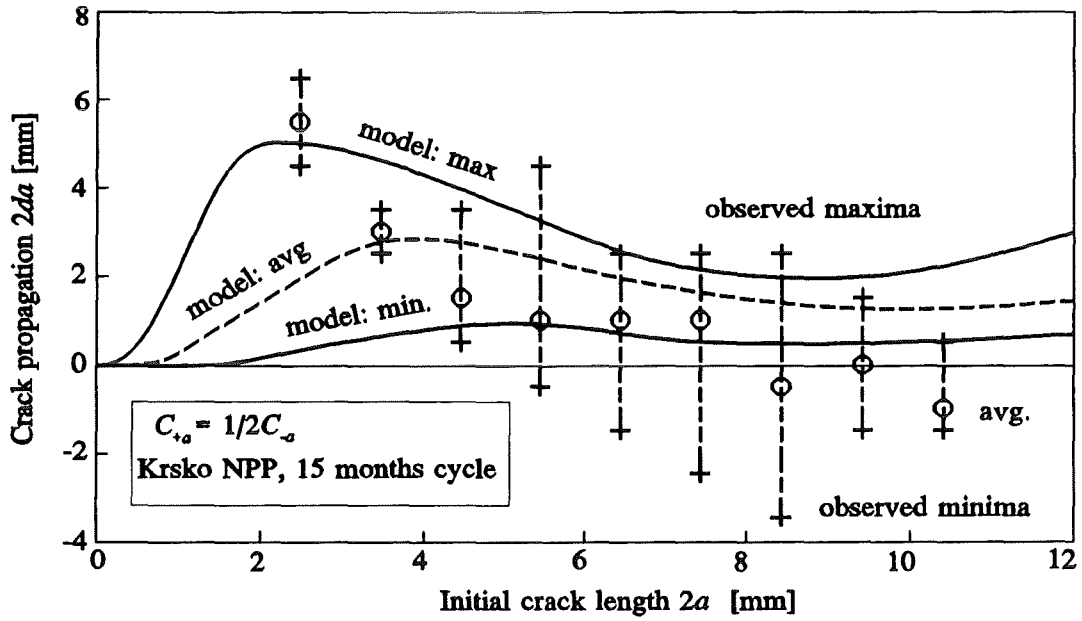

Figure 4-13 Predicted and observed crack growth ($C_{+a}=1/2C_{-a}$)

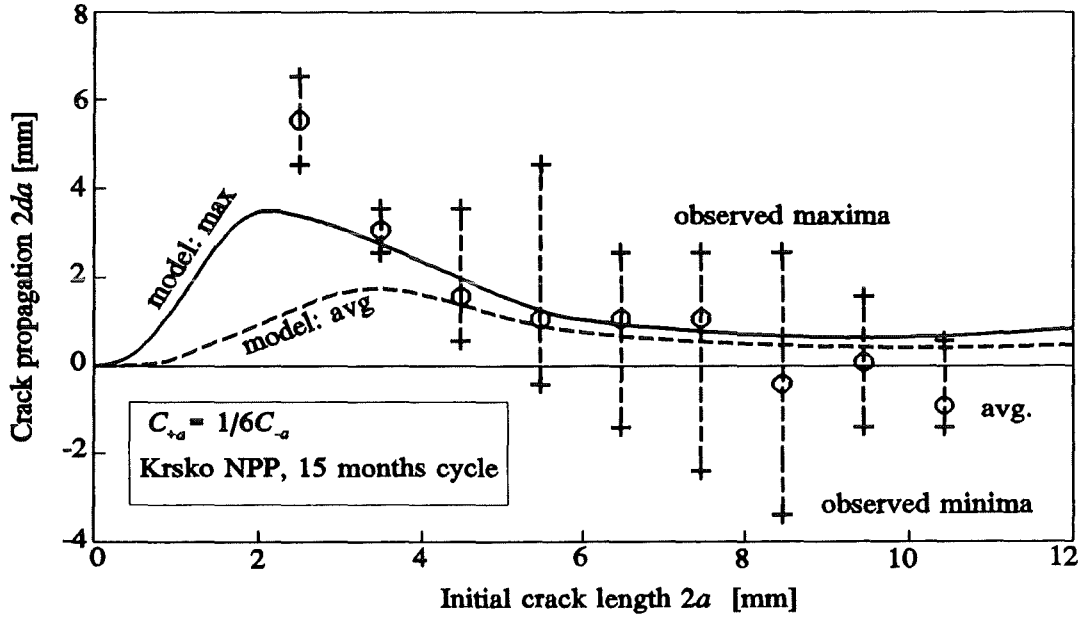

Figure 4-14 Predicted and observed crack growth ($C_{+a}=1/6C_{-a}$)

5 ON NUMERICAL SOLUTION TECHNIQUE FOR THE FAILURE INTEGRAL

In general the failure integral eq. (2-1) has to be evaluated numerically. There are only a few isolated cases where an analytical solution is possible. Conventional numerical methods are not applicable because of the high number of basic variables (5-10) and the low values of P_f. The methods used to evaluate P_f are Monte Carlo simulation and approximate methods [15, 82].

5.1 Monte Carlo family

5.1.1 Direct simulation

The results obtained by direct Monte Carlo simulation are considered to be exact within a given numerical accuracy [12]. However, direct simulation may be very time consuming.

Direct simulation corresponds to a sequence of numerical experiments. The failure function $g(\vec{x})$ is evaluated for n realizations of the random vector $\vec{x}$. Let n_f denote the number of realizations with $g(\vec{x}) < 0$. An estimator of P_f is given by [15]:

$$P_f = \frac{n_f}{n} \tag{5-1}$$

with the standard error:

$$s = \sqrt{\frac{P_f \cdot (1 - P_f)}{n}} \tag{5-2}$$

5.1.2 Other methods

The number of realizations has to be reduced for complicated g-functions. Variance reduction methods have been introduced in the literature. A well known example is latin hypercube sampling. In probabilistic fracture mechanics most efforts were concentrated on introducing some kind of weighted sampling around the failure surface, e.g. importance sampling [15], adaptive sampling [17], efficient sampling [55]. However, the evaluation of the weight factor may also be time consuming.

5.2 Methods using first and second order approximations

First- (FORM) and Second Order Reliability Methods (SORM) were first used in civil engineering [37]. Their applicability to PFM problems including creep and fatigue have been demonstrated in the literature [82]. An upgraded version of the **ZERBERUS** code will be used in this study [83].

5.3 First order reliability method

The failure integral can be solved analytically for standard normal basic available and linear failure functions:

$$P_f = \Phi(-\beta) \tag{5-3}$$

where Φ is the c.d.f. of the standard normal distribution, β is the minimal distance of the origin to the failure surface with:

$$\beta = \frac{g(\vec{x}^*) - \vec{a}\cdot\vec{x}^*}{|\vec{a}|} \tag{5-4}$$

and

$$\vec{a} = \nabla g(\vec{x}^*) = \left(\frac{\partial g(\vec{x}^*)}{\partial x_1}, \ldots, \frac{\partial g(\vec{x}^*)}{\partial x_n} \right) \tag{5-5}$$

β is the reliability index: the point on $g=0$ closest to the origin is the design point.

5.3.1 Non-linear failure function

In this case $g(\vec{x})=0$ is linearized in the design point and the approximate relation is valid:

$$P_f \approx \Phi(-\beta) \tag{5-6}$$

The approximation error is not known in general.

5.3.2 Arbitrarily distributed variables

Standard normal variables are introduced by the transformation:

$$U_i = \Phi^{-1}(F_i(X_i)) \tag{5-7}$$

where F_i is the c.d.f. of random variable X_i with the inverse transformation:

$$X_i = F_i^{-1}\left(\Phi(U_i)\right) \tag{5-8}$$

The transformation is illustrated in Fig. 5-1.

The failure function in u-space $g_u(\vec{u})$ is given by:

$$g(\vec{x}) = g\left(\vec{F}^{-1}(\Phi(\vec{u}))\right) = g_u(\vec{u}) \tag{5-9}$$

Its partial derivatives are evaluated using the chain rule:

$$\frac{\partial g_u}{\partial u_i} = \frac{\partial g}{\partial x_i}\frac{\partial x_i}{\partial u_i} = \frac{\partial g(\vec{x})}{\partial x_i}\frac{\varphi(u_i)}{f_i(x_i)} = \frac{\partial g(\vec{x})}{\partial x_i}\frac{\varphi(\Phi^{-1}(F_i(x_i)))}{f_i(x_i)} \tag{5-10}$$

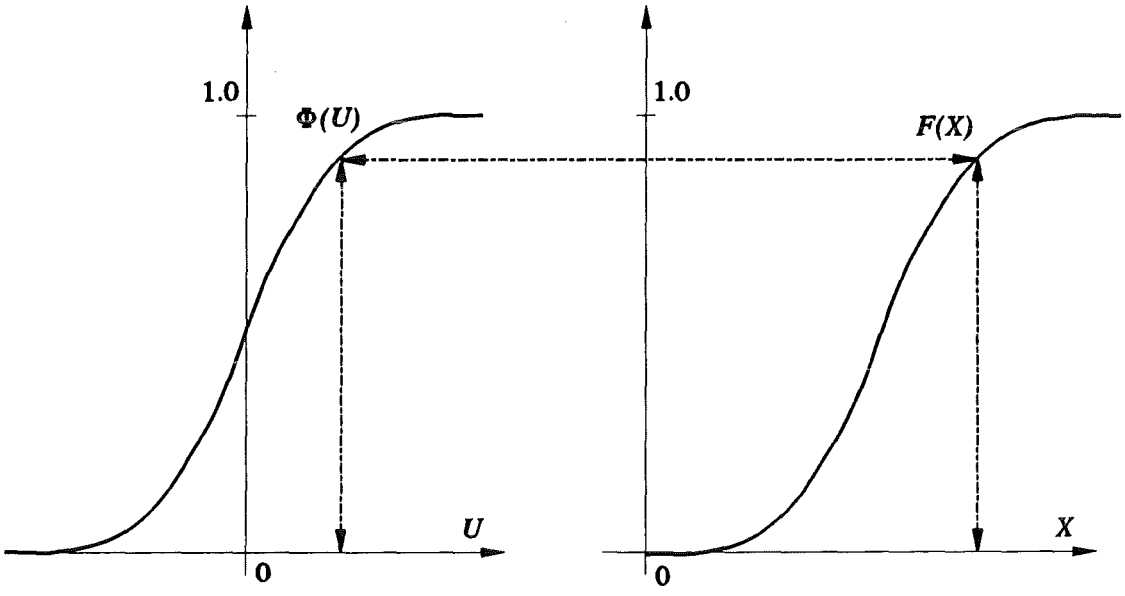

Figure 5-1 Transformation of a basic variable into a standard normal space

5.3.3 The design point determination

The design point is the point in u-space on $g(\vec{u})=0$ with minimal distance to the origin. Hence it is a solution of the constrained optimization problem with:

$$\min\left(\beta^2 = \sum_{i=1}^{n} u_i^2\right) \quad \text{given} \quad g_u(\vec{u}) = 0 \tag{5-11}$$

This non-linear optimization problem can be solved by the following iteration algorithm [66]:

$$\vec{u}^{(m+1)} = \left(\vec{u}^{(m)} \cdot \vec{a}^{(m)}\right) \cdot \vec{a}^{(m)} + \frac{g_u\left(\vec{u}^{(m)}\right)}{\left|\nabla g_u\left(\vec{u}^{(m)}\right)\right|} \cdot \vec{a}^{(m)} \tag{5-12}$$

with

$$\vec{a}^{(m)} = -\frac{\nabla g_u\left(\vec{u}^{(m)}\right)}{\left|\nabla g_u\left(\vec{u}^{(m)}\right)\right|} \tag{5-13}$$

and

$$\nabla g_u(\vec{u}) = \left(\frac{\partial g_u}{\partial u_1}(\vec{u}), \ldots, \frac{\partial g_u}{\partial u_n}(\vec{u})\right) \tag{5-14}$$

The iteration procedure is illustrated in Fig. 5-2

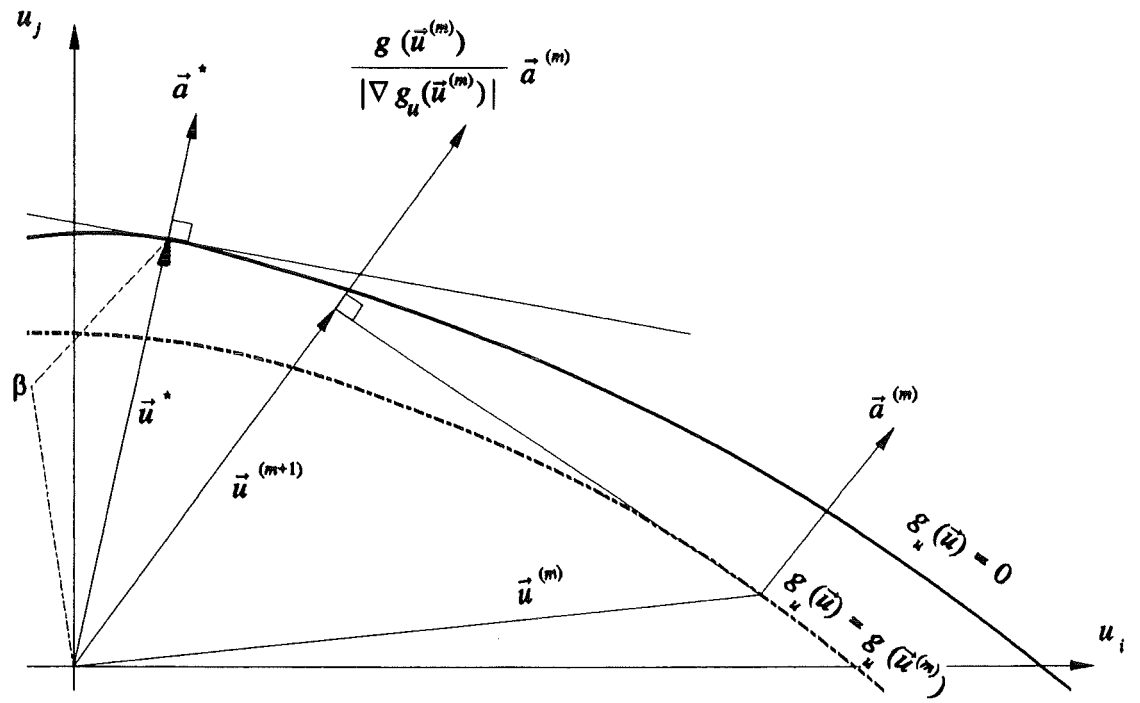

Figure 5-2 Searching for the design point in case of two basic variables

Some numerical examples exhibited two minima of β. This caused the series given by eq. (5-12) to oscillate between two different values instead tending to its limit. The problem has been solved by appropriate selection of starting value $\vec{u}^{(0)}$ and reducing the step between two consecutive design point approximations:

$$\vec{u}^{(m+1)'} = \vec{u}^{(m)} + z \cdot \left(\vec{u}^{(m+1)} - \vec{u}^{(m)}\right) \tag{5-15}$$

Good convergency was obtained by setting $z=0.5$.

5.3.4 Sensitivity analysis

The sensitivity factors

$$\frac{\partial \beta}{\partial u_i} = \frac{\partial}{\partial u_i} \sqrt{\sum_{i=1}^{n} u_j^2} = \frac{u_i^*}{|\vec{u}|} = \alpha_i^* \tag{5-16}$$

determine the dependence of the failure integral on a specific basic variable. The vector of sensitivity factors $\vec{\alpha}^*=(\alpha_1^*, \ldots, \alpha_n^*)$ is a unit vector pointing towards design point.

5.4 Second order reliability method

In SORM the failure surface in the design point is approximated by a quadratic surface with the same values for the principal curvatures κ_j [66]. The failure integral is approximated by:

$$P_f \approx S_1 + S_2 + S_3 \tag{5-17}$$

with

$$S_1 = \Phi(-\beta) \prod_{j=1}^{n-1} (1 - \beta\kappa_j)^{-0.5} \tag{5-18}$$

$$S_2 = [\beta\,\Phi(-\beta) - \varphi(\beta)] \left\{ \prod_{j=1}^{n-1} (1 - \beta\kappa_j)^{-0.5} - \prod_{j=1}^{n-1} (1 - (\beta+1)\kappa_j)^{-0.5} \right\} \tag{5-19}$$

$$S_3 = (\beta + 1)\,[\beta\,\Phi(-\beta) - \varphi(\beta)] \cdot \left\{ \prod_{j=1}^{n-1} (1 - \beta\kappa_j)^{-0.5} - \mathrm{Re}\left[\prod_{j=1}^{n-1} (1 - (\beta + i)\kappa_j)^{-0.5} \right] \right\} \tag{5-20}$$

i is the imaginary unit and $Re()$ denotes the real part. S_1 converges to the exact value of P_f for $\beta \to \infty$. S_2 and S_3 are regarded as correction terms.

In order to evaluate the principal curvatures the standard space is first rotated in y-space such that the position vector of the design point lies in the direction of the n^{th} basic vector. This is obtained by the transformation:

$$Y = \mathbf{D}^T U \tag{5-21}$$

with inverse given by ($\mathbf{D}^{-1}=\mathbf{D}^T$):

$$U = \mathbf{D} Y \tag{5-22}$$

The principal curvatures κ_j are obtain as solutions of the characteristic equation:

$$\det\left(\frac{\mathbf{G}_y}{\partial g(\vec{y}^*)/\partial y_n} - \kappa \mathbf{I} \right) = 0 \tag{5-23}$$

where $\mathbf{G}_y$ represents the matrix of second derivatives of the failure function in the design point in y -space. $\mathbf{I}$ is the unit matrix.

6 NUMERICAL EXAMPLES

Two examples will be considered in the following. The first example corresponds to the one which has also been considered in refs. [25, 68]. The second example is based on the data obtained for the Krško plant on the occasion of the '92 maintenance inspection.

6.1 Comparison with results from literature

The database explained in refs. [25, 68] is used to generate input data for a study using probabilistic fracture mechanics methods along the lines explained in the previous sections. The results are compared with the results given in [25, 68]. There are the following differences between the two approaches:

- The increase in crack length between successive inspections was described in [25, 68] in terms of random variables, whereas asymmetric crack propagation is considered in this study.

- Plugging resulted in a truncated crack length distribution in the model given in [25, 68]. Inspection uncertainties are taken into account here as was explained in section 2.3. This implies that quite long cracks may remain in the tubes after the inspection.

The failure probabilities are calculated using FORM/SORM as in ref. [25]. The Monte Carlo approach used in [68] is not applicable here because of the amount of computing time needed in an extended sensitivity analysis for rare events.

6.1.1 Geometry and material data

The statistical distributions of the input variables which were given in [25, 68] are summarized in table 6-I. The only difference here is that yield strength and ultimate strength are given separately instead of their sum. This was necessary as only σ_y influences the crack propagation law but their sum is needed to evaluate the failure function. The operational load, $\Delta p = 195.6$ bar, was taken from the plant specifications (limiting hypothetical accident - feed line break).

Table 6-I Geometry and material data

Basic variable	Distribution		Unit	Comments
	Type	Parameters		
R_{out}	normal	μ=9.525, σ=0.0254	mm	-
R_h	normal	μ=9.709, σ=0.0106	mm	-
t	normal	μ=1.055, σ=0.0464	mm	-
2 a_m	normal	α=10.3, β=1.0	mm	Assumed
κ	normal	μ=0.545, σ=0.03	-	-
δ_T	normal	μ=0.928, σ=0.003	-	-
σ_Y	normal	μ=362., σ=38.	MPa	-
σ_M	normal	μ=718., σ=38.	MPa	-

Distributions are not truncated

6.1.2 Crack propagation

A Γ-distribution with parameters α=1.25, β=0.8 was introduced in [68] to describe the amount of crack growth within an inspection interval of one year. The mean values of the parameters of the crack propagation law were taken from literature (see Sec. 4). The statistical distributions which were assumed for these parameters are given in table 6-II. The best fit to the inspection data was obtained using ρ_c=3.

Table 6-II Basic variables with direct impact on the crack propagation

Basic variable	Distribution		Unit	Comments
	Type	Parameters		
C_{-a}	normal	$\mu=2.8\cdot10^{-11}$, $\sigma=1.0\cdot10^{-12}$	m/s	Assumed
K_{ISCC}	normal	μ=9.0, σ=0.3	MPa $m^{1/2}$	Assumed
m	normal	μ=1.16, σ=0.03	-	Assumed

Distributions are not truncated

6.1.3 Failure probability

Two different maintenance strategies are compared with each other: the simple model used in [25, 68] leading to eq. (2-7) and the complex model described in Sec. 2.3.3 and [6]. Fig. 6-1 shows the failure probability just before the next yearly inspection as a function of the plugging limit *PL*. The dashed lines are results obtained with the crack propagation model for the different maintenance strategies, whereas the solid line is taken from [25].

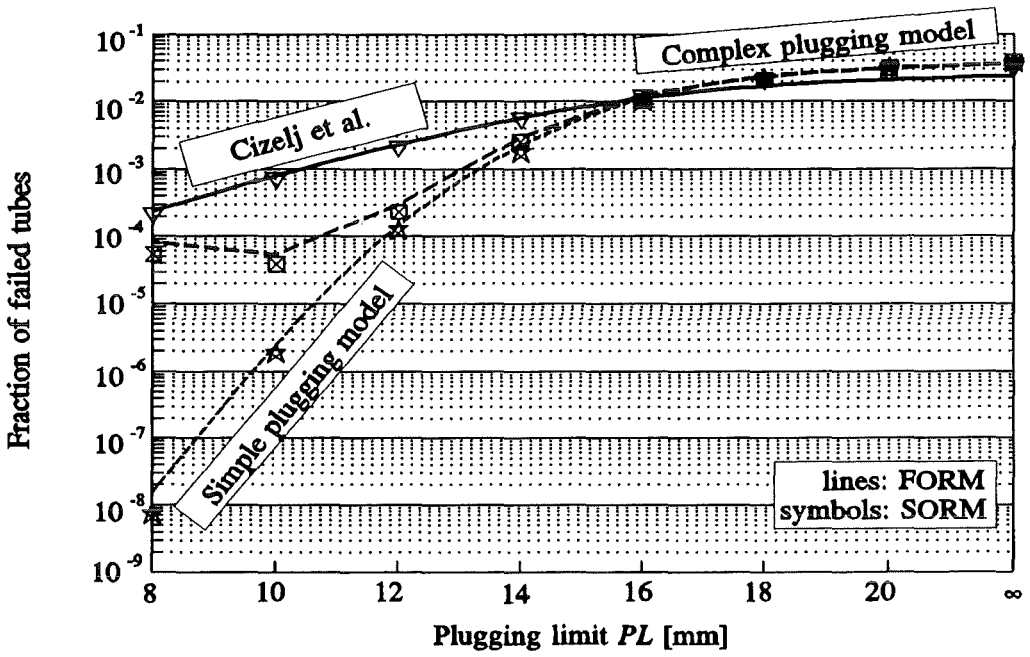

Figure 6-1 Fraction of failed tubes (Cizelj et al [25], simple model eq. (2-7), complex model eq. (2-25))

There is almost no difference in P_f for large values of *PL*. Cracks with lengths below 15 mm are slowed down in the crack propagation model compared to the random variable approach. Hence the failure probability decreases more rapidly, if tubes containing long cracks are plugged. The plateau value of P_f obtained for the complex maintenance strategy in case of $PL < 10$ mm can be attributed to long cracks which are not discovered during the inspection.

Both SORM (symbols) and FORM (lines) results are shown in Fig. 6-1. The relative errors of FORM with respect to SORM is shown in Fig. 6-2. The comparatively large deviations for low values of *PL* can be attributed to the increase of the curvature of the limit state surface with decreasing *PL* and the fact that the second derivatives of the *K*-factors needed

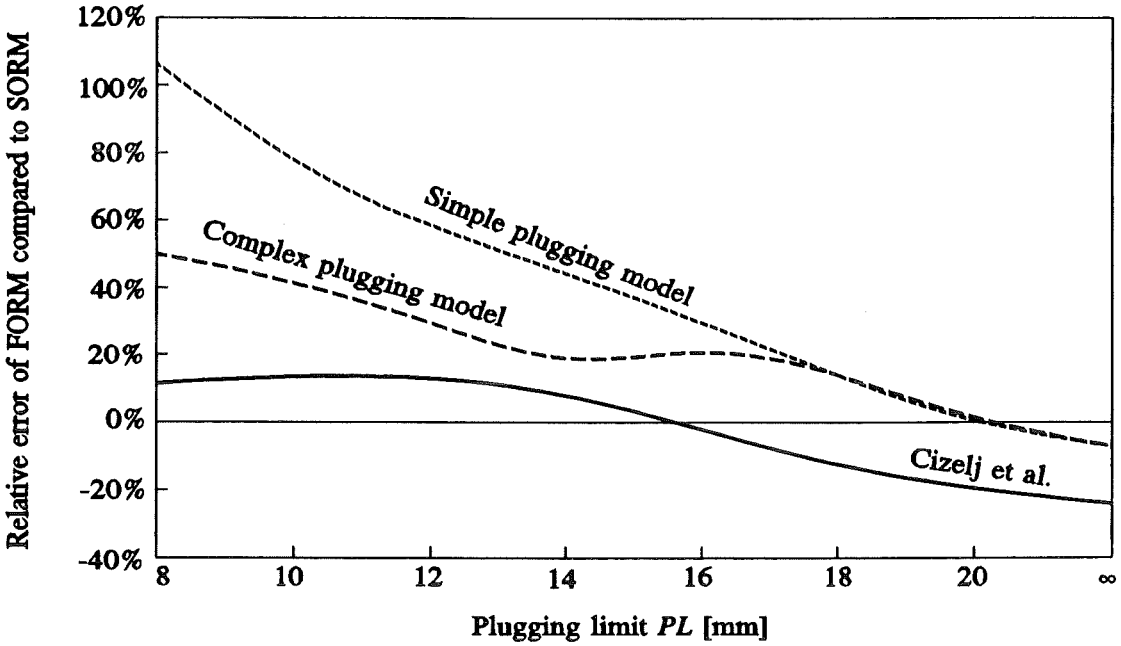

Figure 6-2 Relative error of FORM compared to SORM

in SORM are numerically unstable in many cases. A comparison with Monte Carlo results was given in [25] where FORM- and SORM- results turned out to be upper and lower bounds for the Monte Carlo results.

6.1.4 Sensitivity analysis

The highest sensitivity factors were obtained in [25] for the initial crack length and the crack growth increment. The more complex model described here also yields a high absolute value of the sensitivity factor for the crack length, whereas the crack growth increment is a function of several independent random variables. The following is an ordered list of input quantities with decreasing sensitivity factors: tube wall thickness, flow stress factor, yield stress, ultimate tensile strength, exponent of crack growth law, constant C_a of crack growth law, temperature factor δ_T and outer pipe radius. The influence of the threshold value of the crack growth law is negligible.

6.2 Steam generator No. 1 in Krško power plant

The example is based on data collected during the 1992 inspection. Interest is focused on the effect of the assumed crack length distribution, and of the reliability of the inspection and

plugging procedure. The failure probability at the subsequent inspection is given as well as P_f as a function of the length of the inspection interval.

6.2.1 Geometry and material data

The stochastic input quantities are summarized in table 6-III. Deterministic input quantities are: the crack growth parameter ρ_c=2 (see section 4), the radius of the hole in the tube sheet (=9.709 mm), the pressure difference of the operational loading (=195.6 bar, see Sec. 6.1.1) and the interval between subsequent inspections (1 year unless explicitly stated).

Table 6-III Geometry and material data (Krško steam generator No. 1)

Basic variable	Distribution		Unit
	Type	Parameters	
R_{out}	normal	μ=9.525, σ=0.0254	mm
t	normal	μ=1.0922, σ=0.039	mm
κ	normal	μ=0.545, σ=0.03	-
δ_T	normal	μ=0.928, σ=0.003	-
σ_Y	normal	μ=362., σ=34.	MPa
σ_M	normal	μ=713., σ=25.	MPa

Distributions are not truncated

6.2.2 Crack length distribution

273 indications were found during the 1992 inspection of steam generator #1 in Krško power plant. Fig. 6-3 contains the histogram of the measured crack lengths. The actual crack length distribution can be derived from these data using the procedure described in [6] and Sec. 2.3. This procedure takes into account the sizing uncertainty, the detection probability and the plugging probability.

The detection probability is given by (see ref. [69]):

$$P_{OD}(a) = \left(1 - e^{-0.45 \cdot 2 \cdot a}\right) \cdot \left(1 - \varepsilon_{OD}\right) \qquad \text{(6-1)}$$

which implies that there is a residual probability ε_{OD} of missing very long cracks. The sizing uncertainty is assumed to be independent of the crack length. Only random errors (as

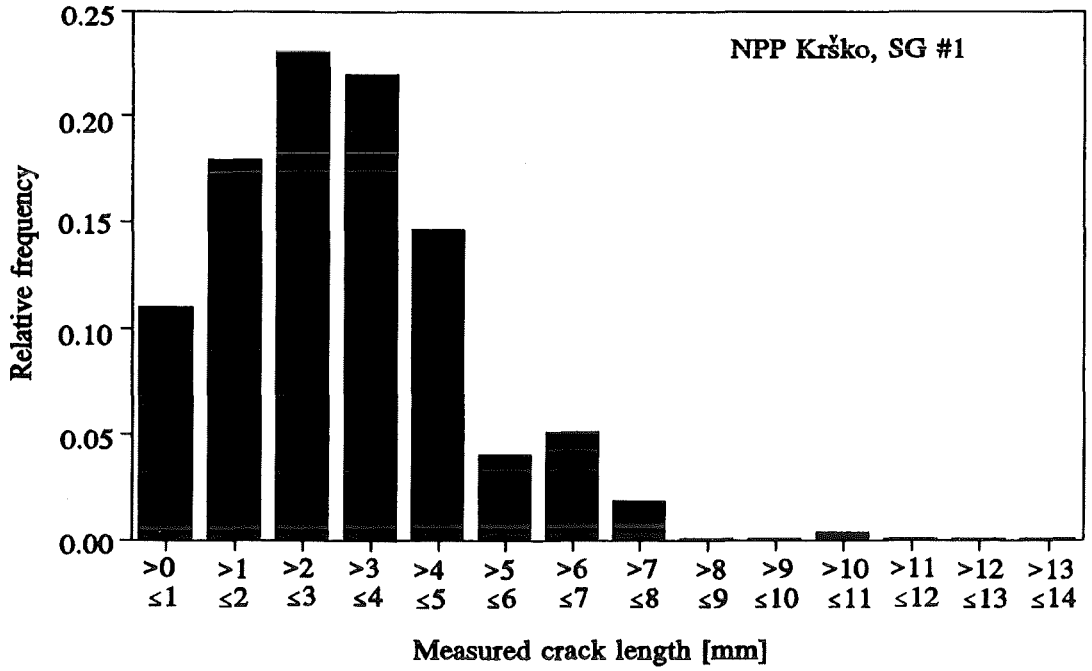

Figure 6-3 Distribution of crack length indications in the tube expansion transition zone of Krško NPP steam generator No. 1 after 1992 inspection

opposed to systematic errors) are considered, and a normal distribution with mean value equal to zero and a standard deviation of 0.75 mm (see [43]) is selected.

Table 6-IV Parameters and quality estimation for assumed real crack length distributions

Distribution	Parameter		χ^2 test		F_{OD} Fraction of detected cracks
	Shape	Scale	χ^2	Significance level	
Lognormal	0.532	1.627	134.760	0.	32.52 %
Exponential	0.489	-	35.2839	$5 \cdot 10^{-5}$	47.94 %
Gamma	0.521	1.244	29.2635	$6 \cdot 10^{-4}$	53.89 %
Weibull	2.063	1.155	27.5182	$1 \cdot 10^{-3}$	48.99 %

The following crack length distributions are considered: lognormal, exponential, Gamma, Weibull. Each set of parameters is fitted to the histogram Fig. 6-3 according to the procedure described in ref. [6] and in Sec. 2.3. The results are summarized in Table 6-IV. The lognormal distribution yields the worst fit, but also the most conservative results as the fraction of cracks detected (F_{OD}) is lowest. Also, the lognormal distribution exhibits the

largest probabilities of long cracks, which has been observed elsewhere [54]. The other three distributions lead to comparable results. None of the distributions is strictly comparable with the data, as they are only accepted in a χ^2 test at a very low significance level.

Fig. 6-4 shows the fitted distributions with special emphasis on their behavior for $2a > 8$mm. Figs. 6-5 and 6-6 show the histograms of measured crack length together with the results of the fitting procedure. All distributions except the Weibull distribution lead to higher numbers of long crack than observed in the inspection.

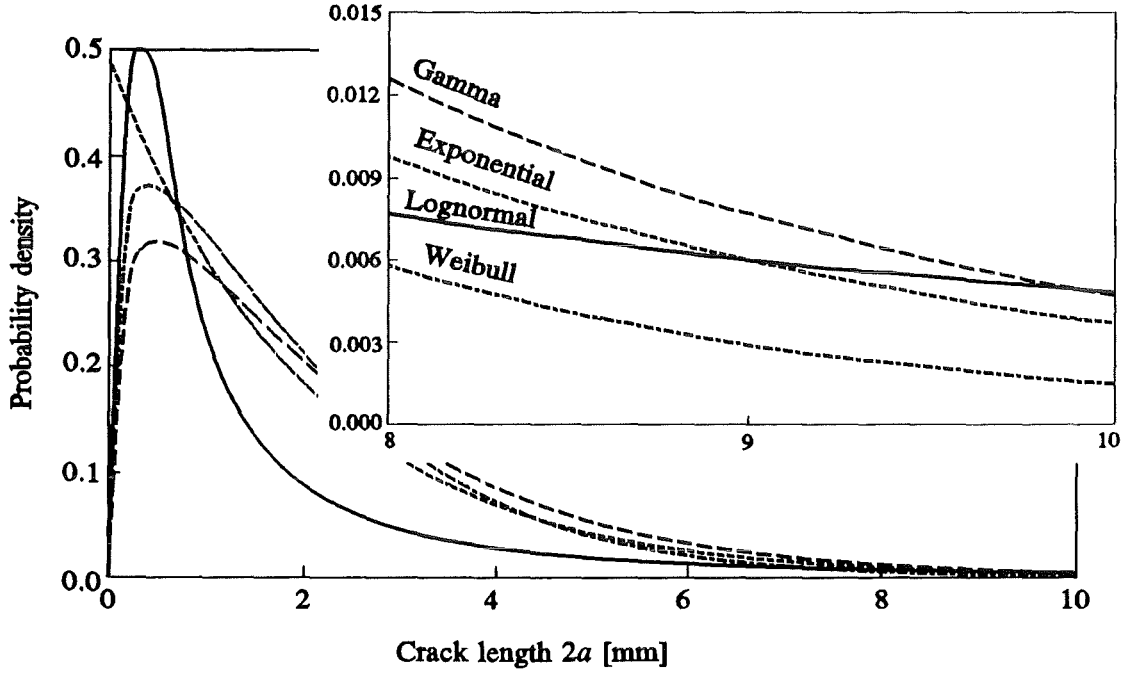

Figure 6-4 Comparison of assumed real crack length distributions

6.2.3 Effects of plugging

In some cases, tubes with long cracks remain unplugged due to the sizing uncertainty and the limited efficiency of the plugging procedure (see eq. (2-16)) and of the inspection given by the detection probability. On the other hand, tubes containing relatively short cracks may be unnecessarily plugged due to the sizing uncertainty. The effect of the inspection procedure on the crack length distribution is shown in Fig. 6-7 which contains both the crack length distribution before inspection (lognormal) as well as the normalized length distribution of those cracks which remain in the operation after inspection and plugging.

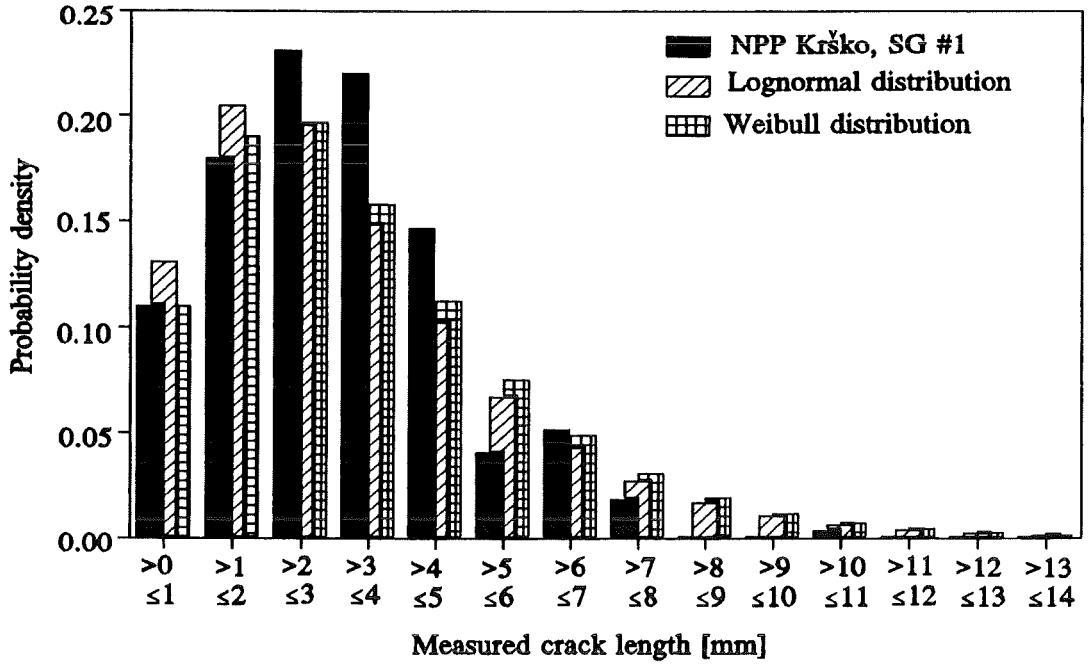

Figure 6-5 Comparison of crack indication length distributions (SG No. 1, exponential and Gamma distribution of real crack lengths)

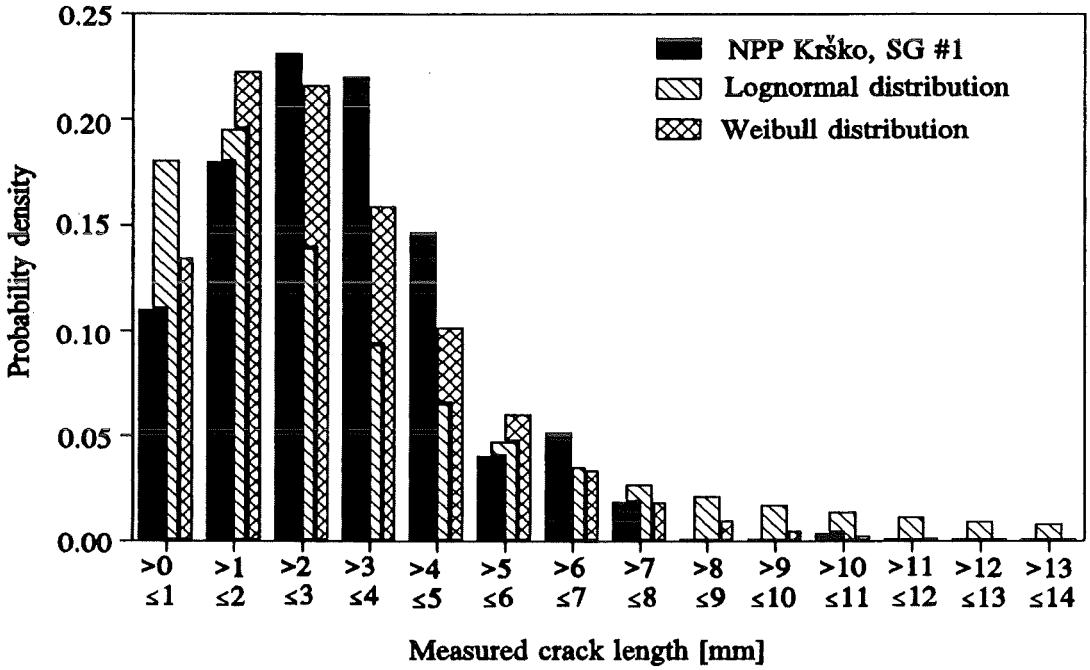

Figure 6-6 Comparison of crack indication length distributions (SG No. 1, lognormal and Weibull distribution of real crack lengths)

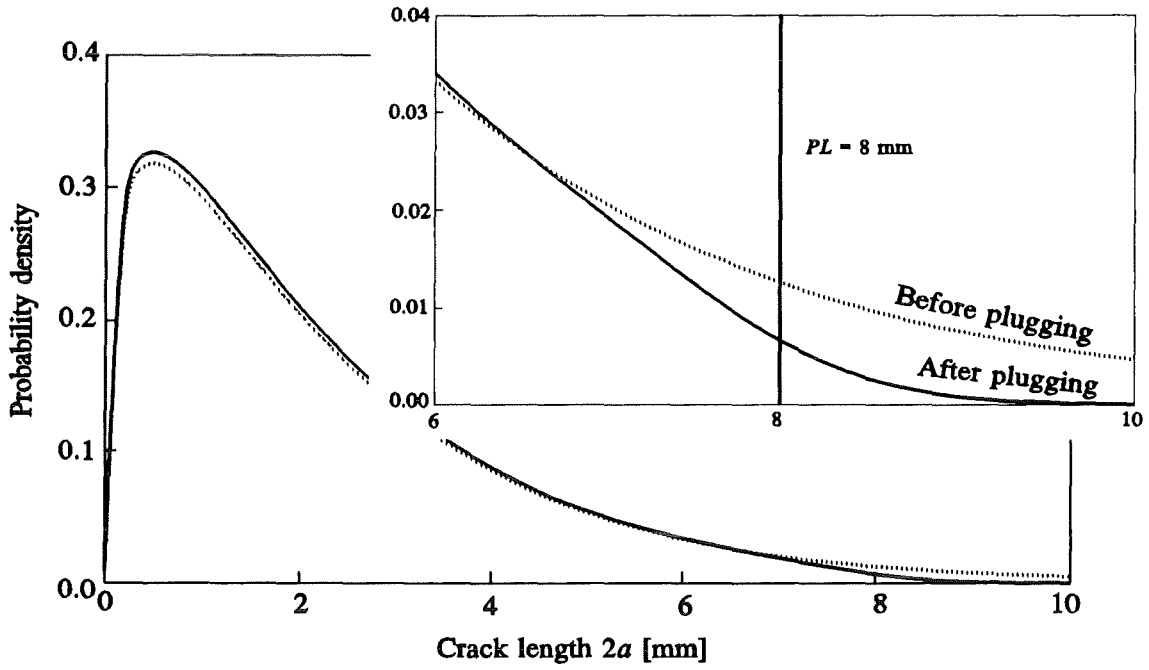

Figure 6-7 Plugging impact on the real crack length distribution

6.2.4 Fraction of failed tubes

The failure probability P_f eq. (2-1) is calculated for four different crack length distributions as a function of the plugging limit *PL* and shown in Fig.6-8. P_f is approximately constant for *PL* larger than 20 mm. This implies that the plugging procedure has no significant effect on the reliability of the steam generator. Cracks below the plugging limit will propagate during the inspection interval and potentially cause failure, whereas cracks exceeding the plugging limit are very scarce.

The failure probability decreases for 10 mm < *PL* < 20 mm with decreasing plugging limit. There are two contributions to the failure probability. First, tubes containing cracks of the size of the plugging limit remain unplugged due to the sizing uncertainty. Second, a certain percentage of the cracks is not detected due to the limited efficiency of the inspection procedure.

The failure probability approaches a constant value for *PL* < 10 mm. This can be explained by the fact that cracks of the order of *PL* (or below) make only a minor contribution to the failure probability as they do not reach a critical crack size within one inspection period. Therefore it is irrelevant whether these cracks are detected and plugged or left in the tubes.

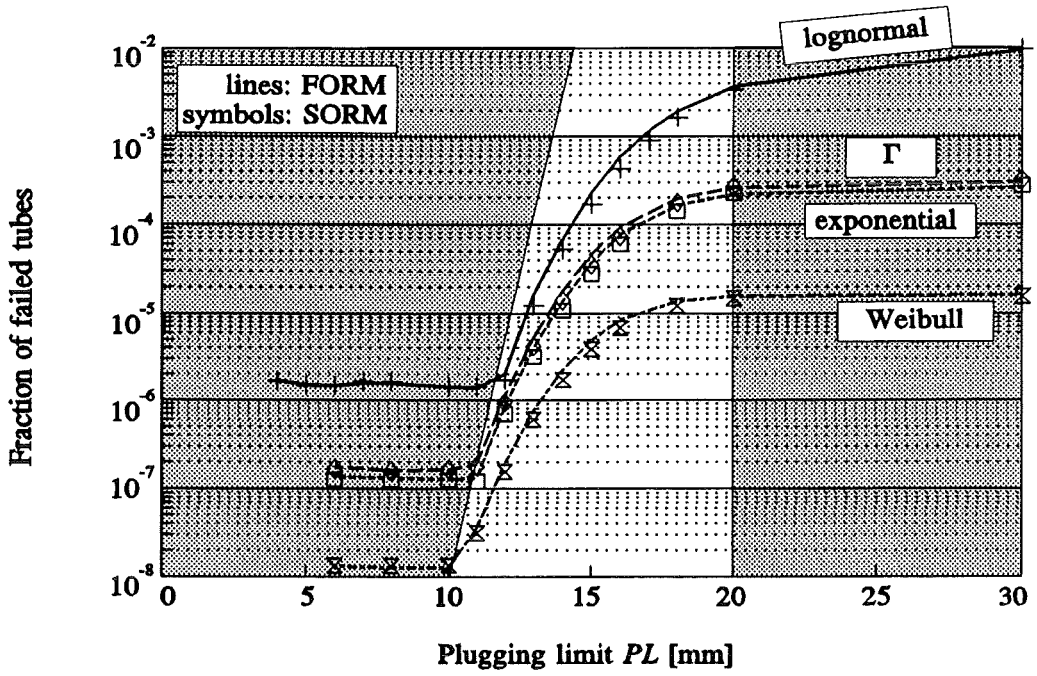

Figure 6-8 Fraction of failed tubes (lines FORM, symbols SORM)

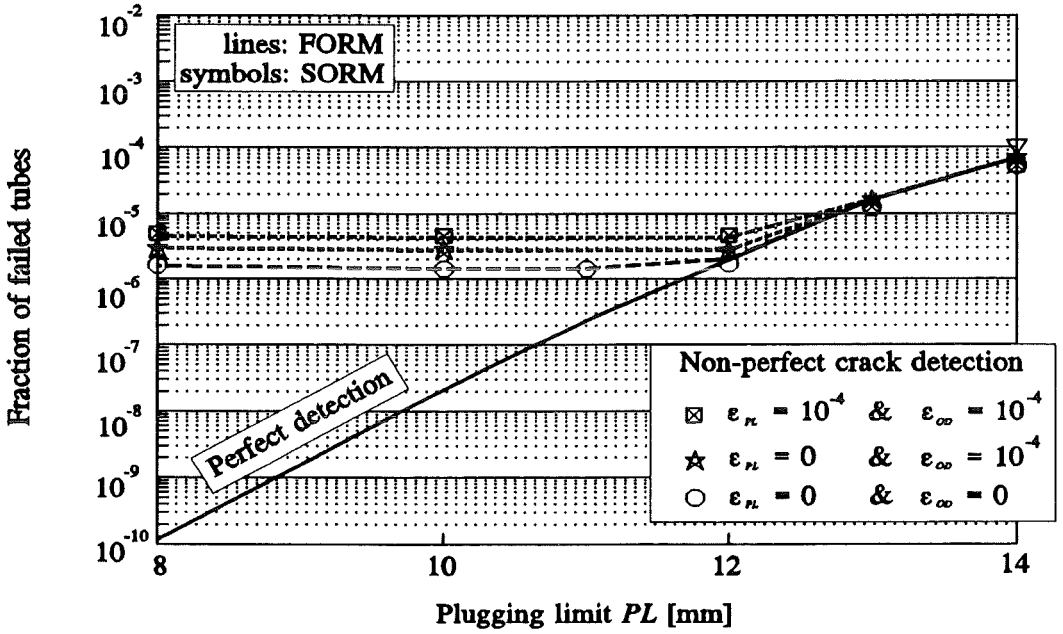

Figure 6-9 Influence of different detection reliability assumptions on the fraction of failed tubes P_f

The most important contribution to the failure probability stems either from those tubes which contain large cracks which are not found or from those tubes which are not plugged.

The absolute value of the failure probability changes by three orders of magnitude depending on the crack length distribution selected. However, the characteristic shape of the $P_f(PL)$-curve remains unchanged with the two plateau-values of P_f for $PL < 10$mm and $PL > 20$mm and the transition zone between.

The effect of the efficiency of the inspection and the plugging procedures is analyzed in Fig. 6-9 for a lognormal crack length distribution. The bold line corresponds to 100% inspection efficiency, whereas the other curves are determined using different values of the plugging probability 1 - ε_{PL} and of the residual non-detection probability ε_{OD}. The behavior of $P_f(PL)$ in Fig. 6-9 can be explained along the same lines as Fig. 6-8 (see Sect. 6.2.4).

We should note here that ε_{PL} and ε_{OD} affect the distribution of crack lengths after plugging in exactly the same way (see eqs. (2-22) and (6-1)).

6.2.5 Relative error of the FORM/SORM results

The relative differences of the FORM and the SORM results for a lognormal crack length distribution are shown in Fig. 6-10. The error is relatively small except a peak for $10\text{mm} < PL < 20$ mm which corresponds to the transition of P_f between the low and the high stationary level. This difference between FORM and SORM results can be partially attributed to problems with the numerical derivatives. These problems can be neglected for $PL > 20$ mm and $PL < 10$ mm, because all sensitivity factors are approximately zero except the sensitivity factor of the crack length (see subsequent section).

Another important consideration considering the relative errors is the observation of two failure modes. This occurs at PL values in the vicinity of 10 mm, where the transition of P_f values starts. FORM tends to detect two design points and consequently two P_f values in this area. The first one actually lies on the perfect detection curve (see Fig. 6-9), whereas the second complies with the plateau value. In most cases, the initial design point estimate controls the design point detected.

The numerical errors affect the shape of the transition curve in Fig. 6-8, but not the fact that there is a transition between two stationary levels of the failure probability in the range of $10 \text{ mm} < PL < 20$ mm.

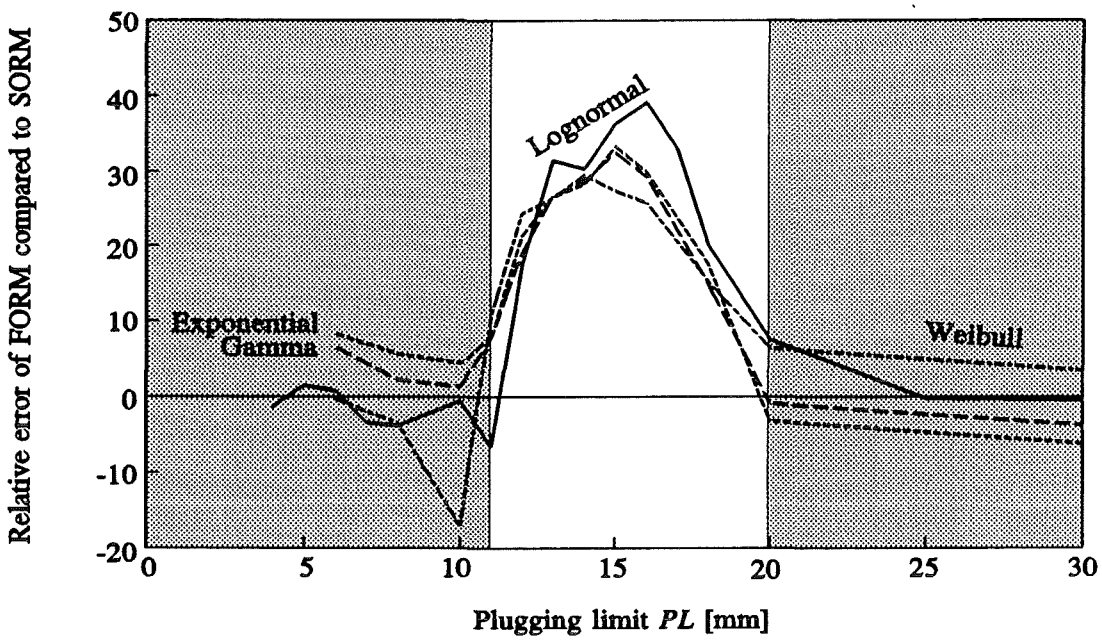

Figure 6-10 Comparison of FORM and SORM results

6.2.6 Sensitivity analysis

Figs. 6-11, 6-12, 6-13 show the sensitivity factors eq. (5-16) obtained using a lognormal crack length distribution as a function of the plugging limit PL for the crack length, the exponent m in the crack growth law, the tube wall thickness, and the flow stress factor κ. These are the dominant input variables. Less important quantities are the constant in the Paris law C_a the outer pipe radius, the yield strength, the ultimate tensile strength and the temperature factor δ_T. The scatter of the threshold for stress corrosion cracking is negligible as in the previous example.

All the sensitivity factors show a characteristic jump at $PL \approx 10$ mm which can be explained along the same lines as in Fig. 6-8 (see Sect. 6.2.4). If higher values of the relative number of unplugged tubes and/or the residual non-detection probability are assumed, the absolute value of the sensitivity factor of the crack length increases.

6.2.7 Dependence of P_f on the length of the inspection interval

Figs. 6-14 and 6-15 show the failure probability as a function of the length of the inspection interval. The optimal value of PL is decreasing with increasing length of inspection interval.

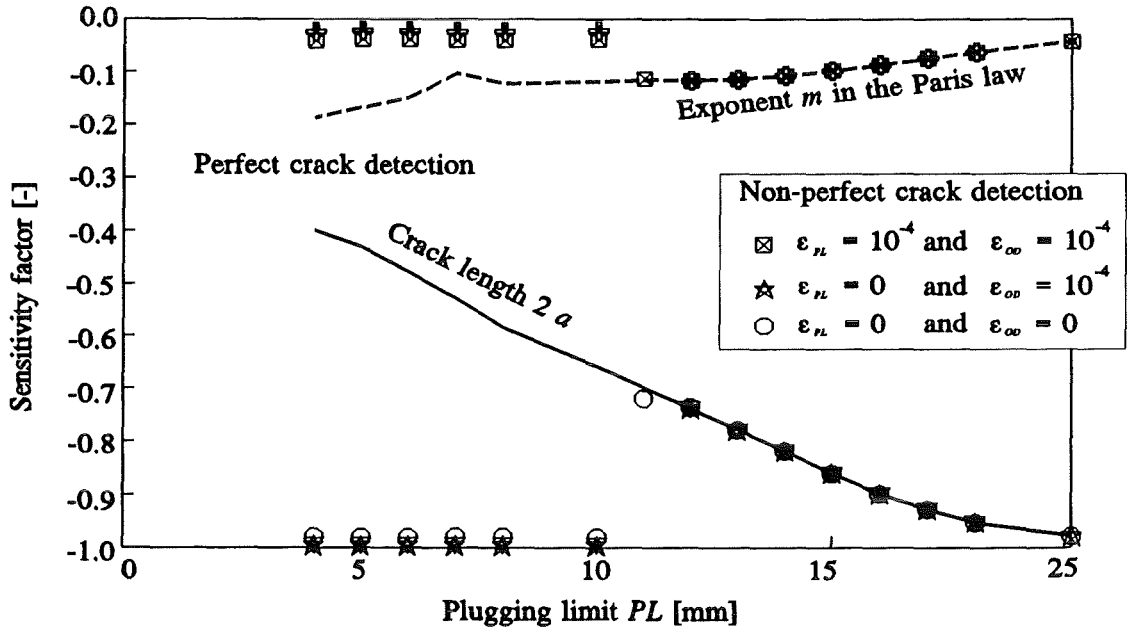

Figure 6-11 Sensitivity factors of crack length ($2 \cdot a$) and Paris law exponent (m)

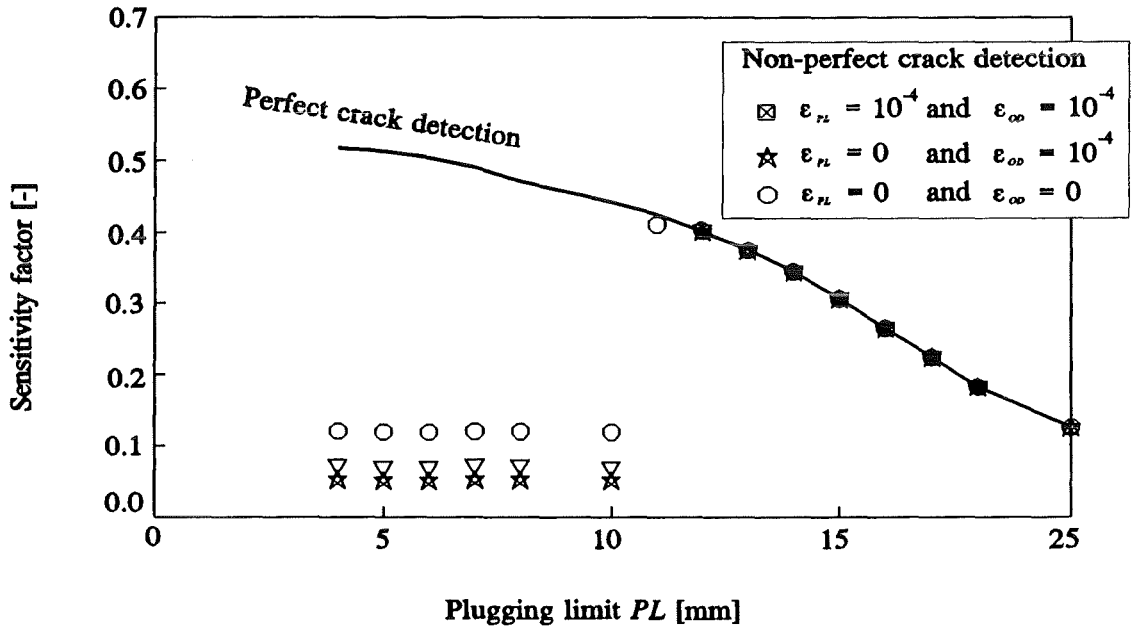

Figure 6-12 Sensitivity factor of tube wall thickness (t)

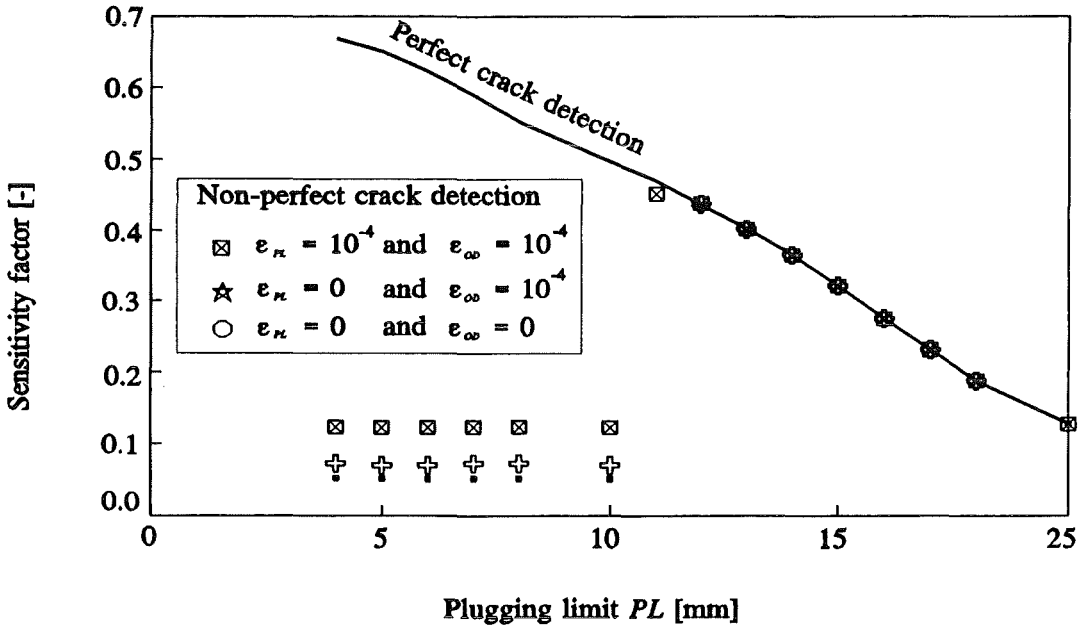

Figure 6-13 Sensitivity factor of flow stress factor (κ)

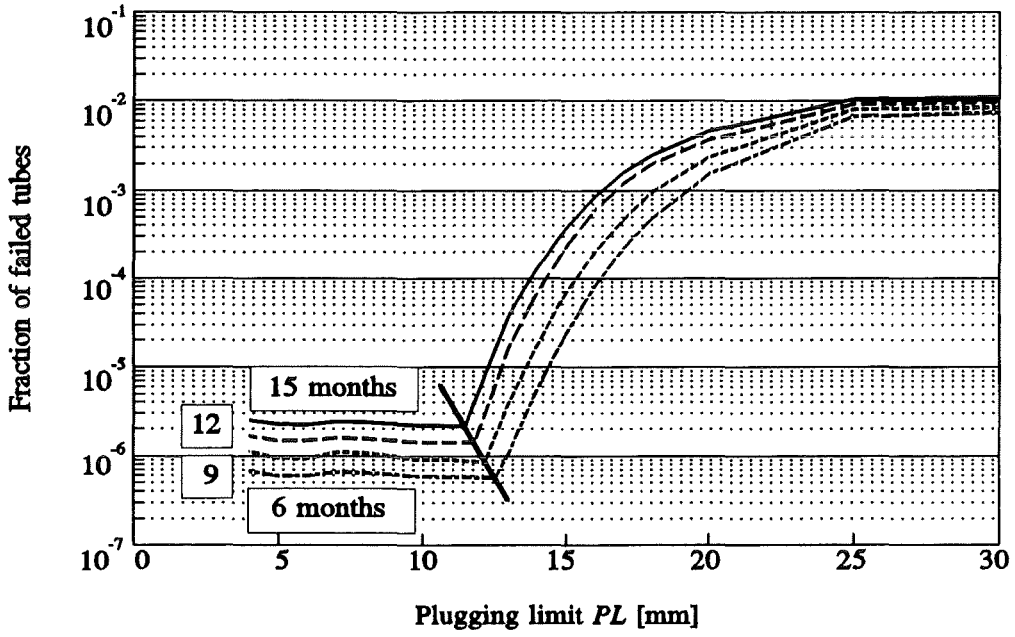

Figure 6-14 Influence of time between two consecutive inspections on the fraction of failed tubes P_f

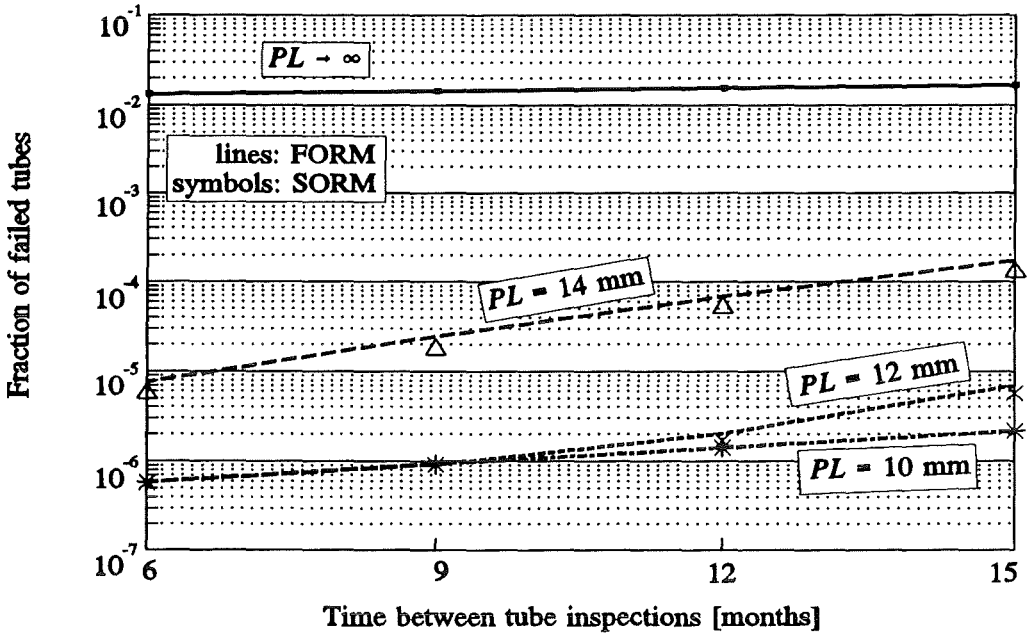

Figure 6-15 Development of fraction of failed tubes P_f in time

6.2.8 Single vs multiple tube failure (rupture)

The probability for multiple tube failure (rupture) was determined in Sect. 2.4. Table 6-V summarizes the results obtained. The total number of cracked tubes N is estimated to be 841 based on the information that 273 flawed tubes were found and on the formula for the inspection uncertainty (see Sect. 2). The number of plugged tubes N_{PL} follows by multiplying eq. (2-23) with N, whereas the number of remaining flawed tubes N_R is equal to the difference between N and N_{PL}.

The probability that exactly i tubes fail during the inspection interval is given in eq. (2-31). For high values of PL, multiple tube failure becomes highly probable. At PL=6.4 mm (Krško plant), single tube rupture is dominating failure mode.

The predicted number of plugged tubes given in Table 6-V can be compared with the findings of the 1992 inspection of the Krško plant. Altogether 43 tubes were plugged. Since the reason for the plugging was not recorded, the effect of other degradation mechanisms is included in this number, and the agreement is considered satisfactory.

Table 6-V Single and multiple tube rupture probability

PL [mm]	N_{PL}	P_f		N_R	$P(i \geq 1)$ [%]		$P(i=1)$ [%]	
		FORM	SORM		FORM	SORM	FORM	SORM
6	18	$.146 \cdot 10^{-5}$	$.145 \cdot 10^{-5}$	823	0.12	0.12	0.12	0.12
6.4	17*	$.145 \cdot 10^{-5}$	$.147 \cdot 10^{-5}$	798	0.12	0.12	0.12	0.12
8	12	$.156 \cdot 10^{-5}$	$.162 \cdot 10^{-5}$	829	0.13	0.13	0.13	0.13
10	9	$.141 \cdot 10^{-5}$	$.142 \cdot 10^{-5}$	832	0.12	0.12	0.12	0.12
12	8	$.199 \cdot 10^{-5}$	$.17 \cdot 10^{-5}$	833	0.17	0.14	0.17	0.14
14	7	$.687 \cdot 10^{-4}$	$.527 \cdot 10^{-4}$	834	5.57	4.30	5.41	4.21
16	5	$.592 \cdot 10^{-3}$	$.425 \cdot 10^{-3}$	836	39.05	29.94	30.18	24.93
18	4	$.196 \cdot 10^{-2}$	$.163 \cdot 10^{-2}$	837	80.61	74.44	31.81	34.87
20	3	$.369 \cdot 10^{-2}$	$.343 \cdot 10^{-2}$	838	95.46	94.35	14.04	16.23
∞	0	$.142 \cdot 10^{-1}$	$.142 \cdot 10^{-1}$	841	100.00	100.00	0.01	0.01

* Theoretical prediction. 43 tubes were plugged in SG #1 in Krško plant. However, those tubes have been damaged also on other locations not accounted for in this study.

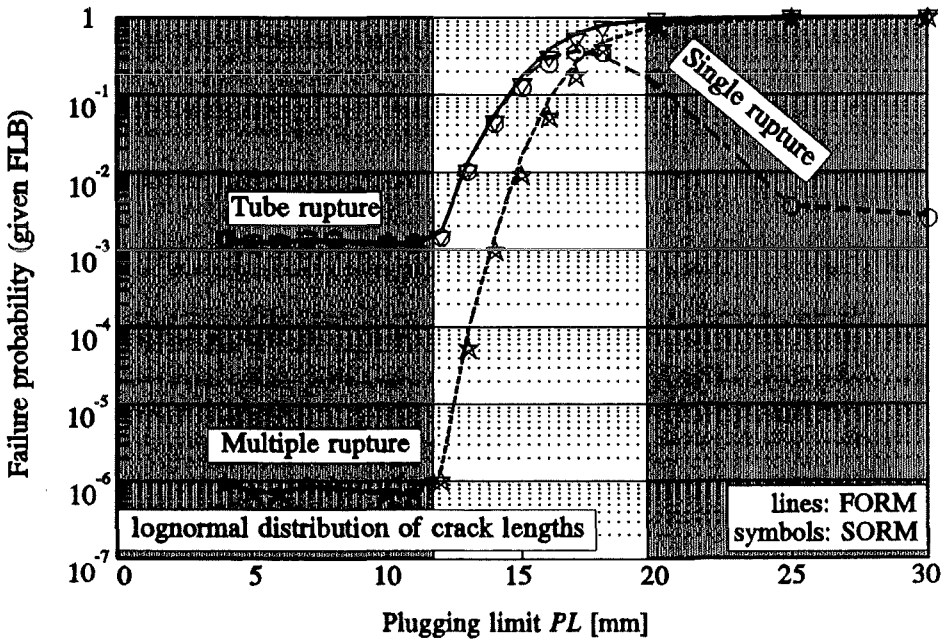

Figure 6-16 Single and multiple tube rupture probabilities

In Fig. 6-16 the probabilities $P(i \geq 1)$, $P(i=1)$, and $P(i \geq 2)$ are compared with each other as a function of the plugging limit. Figure (6-17) shows the ratio of the probabilities of single

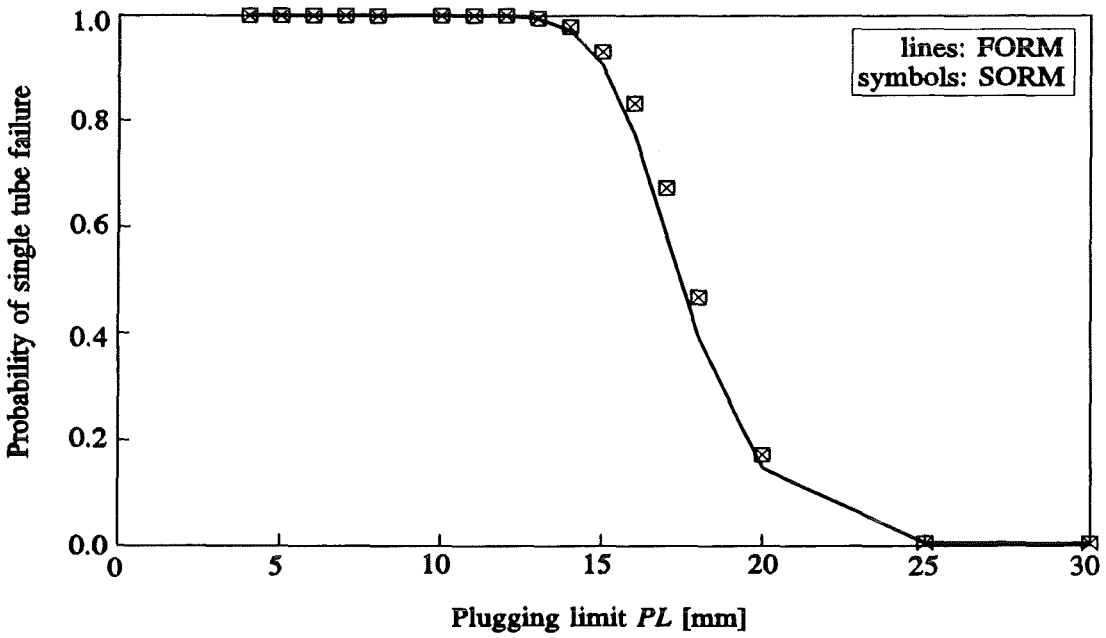

Figure 6-17 Single tube rupture probability (given a tube rupture)

tube rupture and of multiple tube rupture, which decreases rapidly for $PL > 12$ mm, i.e. multiple tube rupture becomes the dominant failure mode.

6.3 Optimizing the steam generator life time

6.3.1 Comparison of different plugging strategies

Two different strategies are compared with each other:

- bobbin coil inspection and plugging based on crack depth criterion;
- MRPC inspection and plugging based on crack length criterion.

Table 6-VI Comparison of defect length and defect depth plugging criterion

	No. of plugged tubes	Probability of tube rupture	Probability of multiple tube rupture
Length criterion	17 - 43*	$1.20 \cdot 10^{-3}$-$1.16 \cdot 10^{-3}$	$7.22 \cdot 10^{-7}$-$6.78 \cdot 10^{-7}$
Depth criterion	3	1.00	0.99

17 is a theoretical prediction; 43 of tubes have been plugged in Krško SG No. 1 in 1992

Table 6-3 shows the number of plugged tubes and the probabilities $P(i \geq 1)$ and $P(i \geq 2)$. The probabilities for the crack depth criterion have been calculated assuming that very poor correlation between the crack length as measured by the MRPC inspection and crack depth as measured by the bobbin coil inspection exists [34]. Therefore, plugging the tubes following the crack depth criterion assumes the P_f at $PL \rightarrow \infty$.

The crack length criterion dramatically reduces the probability of multiple tube rupture.

6.3.2 Number of plugged tubes vs failure probability

Figure 6-18 shows the number of plugged tubes and the failure probability as a function of the plugging limit. As the failure probability is almost constant for $PL < 12$mm and the number of plugged tubes decreases monotonically with increasing PL, an optimum value of PL is around 10-12 mm.

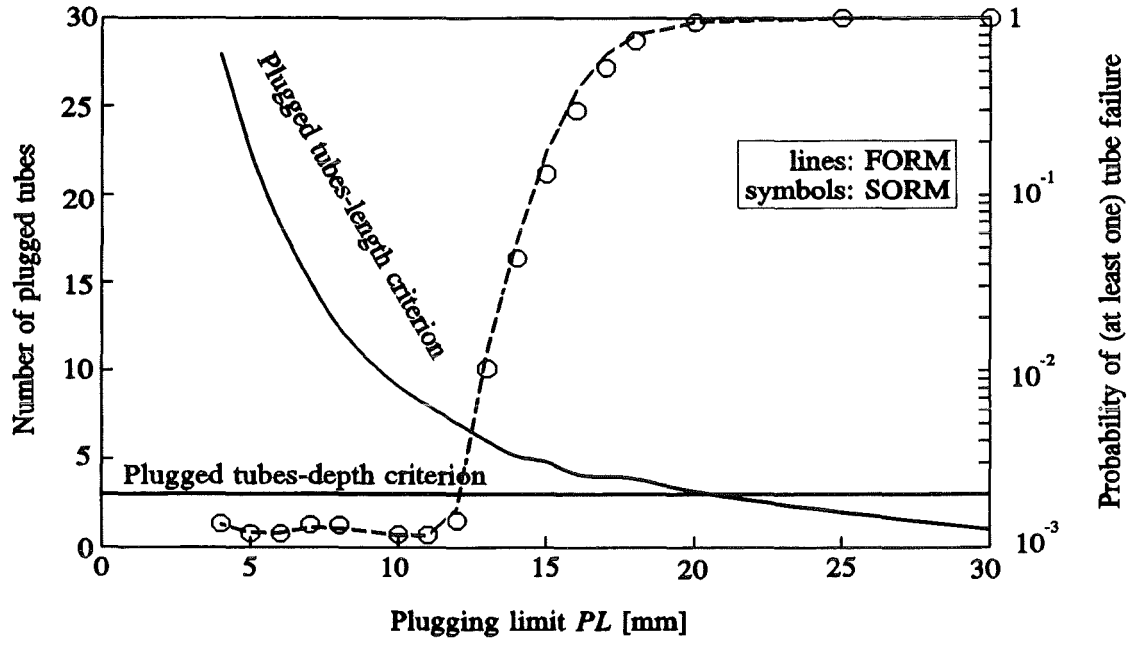

Figure 6-18 Optimizing the steam generator life time

The plugging limit can be adjusted during each inspection using the following procedure:

- inspection;
- determination of crack length distribution from inspection results;

- calculation of the failure probability and of $P(i \geq 1)$ as a function of the plugging limit; determination of optimum value for PL;
- plugging of tubes.

Such approach enables the most efficient use of all available information about the steam generator state. This enables reduction in conservativities, which are built in the maintenance procedures and the steam generator life-time optimization at given risk of tube failure.

7 CONCLUDING REMARKS

Ageing of steam generator tubes made of Inconel 600 may severely affect their structural reliability and reduce the steam generator life-time. The main objective of the present study was to develop and propose a procedure to estimate the tube failure probability, based on scatter of geometry, material data, defect size and growth rate and the efficiency of applied maintenance strategy. As the particular ageing mechanism studied, the axially oriented through-wall stress corrosion cracking in the residual stress field in the tube expansion transition zone has been selected.

7.1 Summary of the proposed procedure

The probabilistic fracture mechanics provided the basis for the reliability model. Unstable crack propagation has been assumed to occur at hypothetical accidental conditions and predicted by the plastic limit load concept. Stable crack propagation during normal operation between the two consecutive tube inspections has been modelled using linear-elastic fracture mechanics theory. Residual stresses have been estimated using the non-linear finite element techniques (code **ABAQUS** [1]). The scatter in residual and operational stresses driving the crack has been accounted for by the response surface method. The efficiency of the maintenance strategy consisted of detection reliability, sizing accuracy and probability of plugging the tube containing long crack. The reliability calculations have been performed using the First- and Second order reliability methods (FORM and SORM) using the modified **ZERBERUS** [83] code.

7.2 Experience using the proposed procedure

Two numerical examples were studied. The first one was selected based on the results available in the literature and showed reasonable agreement. The second considered the Krško power plant steam generator after the 1992 maintenance activities. The numerical results assumed the use crack length tube plugging criterion and 100% tube inspection by motorized rotating pancake coil eddy current technique. In both cases, the conditional tube failure probabilities have been calculated assuming the hypothetical feed line break accident as an initiating event.

The failure probability of the steam generator considered depends strongly on the assumed crack length distribution and applied allowable crack length (plugging limit *PL*). Considering

the failure probability as a function of plugging limit, two plateau regions are obtained at low (< 10 mm) and high plugging limit (> 20 mm) values. The intermediate *PL* values exhibit a transition region extending over four orders of magnitude in the numerical example considered. The high *PL* value plateau failure probability is controlled exclusively by the probability of having long cracks. Nearly identical situation occurs at low *PL* values, where the reliability of the inspection and plugging methods completely controls probability of long cracks.

Similar conclusions are obtained from the FORM sensitivity analysis. It has been shown that the scatter in crack length dominates the overall uncertainty and therefore the failure probability both at the low (< 10 mm) and high (> 20 mm) *PL* values. At the intermediate *PL* values, the uncertainty in the flow stress factor and the tube wall thickness are also shown to be important.

Two different maintenance strategies have been compared based on the Krško steam generator No. 1 analysis. It has been shown that the use of the suitable crack length plugging limit with appropriate inspection technique significantly reduces the tube failure probability. Furthermore, the probability of multiple tube rupture tends to vanish with decreasing *PL* value. On the other hand, application of the crack depth plugging strategy with bobbin coil inspection technique tends to result in multiple tube rupture.

Some results concerning the risk based steam generator life time optimization are also provided. The model is namely able to predict the number of plugged tubes and the tube failure probability given the value of plugging limit. The optimal *PL* value in the numerical example considered is estimated to be between 10 and 12 mm.

7.3 Weak points of the analysis

The probabilistic fracture mechanics and the First- and Second order reliability methods have been shown to enable relatively easy and accurate analysis of reliability problem studied. The relative errors of both numerical methods were limited to 40% in the transition region at intermediate *PL* values and 10% in the plateau regions (low and high *PL* values) in the analysis of the Krško steam generator. The main cause of observed discrepancy between FORM and SORM results is considered to be relatively unstable numerical differentiation of stress intensity factors, which lead to similar instabilities in the derivatives of failure function. In addition to that, two failure modes have been observed at the failure probability plateau at low *PL* values. This caused some difficulties in FORM convergence. However,

the errors observed affected the quantitative results only. The qualitative behavior of the systems analyzed was consistent regardless of the method used in range of parameters analyzed. Therefore, the results obtained are considered to be reliable.

7.4 Future work

The future work is related mainly to some weak points of the procedure proposed:

- increasing the accuracy of stress intensity factor calculation, leading to "more continuous" first and second order failure function derivatives,

- implementing two-dimensional crack propagation instead of one-dimensional. This should enable more accurate description of crack propagation kinetics. Also, the full leak-before-break and leak rate analysis can be developed, which has not been considered here. To solve this problem, stochastic finite elements techniques may be used.

The formulation of the procedure allows for relatively easy modifications in order to investigate other failure mechanisms in steam generator tubes, such as intergranular attack at the tube to tube support plate intersections.

7.5 Recommendations for the steam generator maintenance

Based on the results obtained in the analysis of the Krško steam generator No. 1, the following activities are recommended to be performed in the framework of tube maintenance:

- inspection;
- determination of crack length distribution from inspection results;
- calculation of the single and multiple tube rupture probabilities as a function of the plugging limit; determination of optimum value for *PL*;
- plugging of tubes.

Such approach enables the most efficient use of all available information about the steam generator state. This enables reduction in conservativities, which are built in the maintenance procedures and the steam generator life-time optimization at given risk of tube failure.

8 REFERENCES

[1] **ABAQUS User's Manual** Ver. 4.9, Hibbit, Karlsson and Sorrensen, Inc., Providence, USA.

[2] Abramowitz, M., I.A.Stegun, eds.: **Handbook of Mathematical Functions**, 9th Edition, Dover Publication Inc, New York.

[3] American Society of Mechanical Engineers: **Boiler and Pressure Vessel Code**, Section III, Edition 1986.

[4] American Society of Mechanical Engineers: **Boiler and Pressure Vessel Code**, Section II, Edition 1972.

[5] Andresen, P.L.: *Fracture Mechanics Data and Modeling of Environmental Cracking of Nickel-Base Alloys in High Temperature Water*, The NACE Annual Conference and Corrosion Show (1991), Cincinnati, Ohio, USA, paper No. 44.

[6] Barnier, M., P.Pitner, T.Riffard: *Estimation of Crack Size Distribution from In-Service Inspection Data for the Calculation of Failure Probabilities*, Safety and Reliability 92, Copenhagen, June 10-12, 1992, p. 527-538.

[7] Becher, P.E., A.Pedersen: *Application of Statistical Linear Elastic Fracture Mechanics to Pressure Vessel Reliability Analysis*, Nuclear Engineering and Design, Vol. 27 (1974), No. 3, pp. 413-425.

[8] Berge, Ph., J.M.Fiquet: *Present Status of Water Chemistry in Nuclear Power Plants*, JAIF Int Conf on Water Chemistry in NPP, Fukui City, Japan (1991).

[9] Berge, Ph.: *Moddeling Corrosion for Life Prediction of Nuclear Reactor Components*, 3rd NACE International Symposium, Cambridge, UK (1991).

[10] Berge, Ph., P.Saint Paul: *An Overview of R and D Support of PWR Steam Generators*, Steam Generator and Heat Exchanger Conference, Toronto (1990).

[11] Besuner, P.M.: *Probabilistic Fracture Mechanics*, in: J.W. Provan, ed(s).: **Probabilistic Fracture Mechanics and Reliability**, Martinus Nijhoff Publishers (1987), pp. 387-436.

[12] Bjerager, P.: *Probability Computation Methods in Structural and Mechanical Reliability*, in: W.K.Liu, T.Belytscko, ed(s).: **Computational Mechanics of Probabilistic and Reliability Analysis**, Elmpress International, Laussane, Switzerland (1991), pp. 49-67.

[13] Bowen, W.M., P.G.Heasler, R.B.White: **Evaluation of Sampling Plans for In-Service Inspection of Steam Generator Tubes**, NUREG/CR-5161, Vol. 1 (1989).

[14] Broek, D.: **Elementary Engineering Fracture Mechanics**, 4th revised edition, Martinus Nijhoff Publishers (1986), The Netherlands.

[15] Brueckner, A.: *Numerical Methods in Probabilistic Fracture Mechanics*, in: J.W. Provan, ed(s).: **Probabilistic Fracture Mechanics and Reliability**, Martinus Nijhoff Publishers (1987), pp. 351-386.

[16] Bucher, C.G., U.Bourgund: *A Fast and Efficient Response Surface Approach for Structural Reliability Problems*, Structural Safety, Vol. 7 (1990), pp. 57-66.

[17] Bucher, C.G.: *Adaptive Sampling - An Iterative Fast Monte Carlo Procedure*, Struct Safety, Vol. 5 (1988), pp. 119-126.

[18] Cameron, R.F, G.O.Johnston, A.B.Lidiard: *The Reliability of Pressurized Reactor Vessels*, in: J.W. Provan, ed(s).: **Probabilistic Fracture Mechanics and Reliability**, Martinus Nijhoff Publishers (1987), pp. 269-324.

[19] Cassagne, T.B., P.Combrade, M.A.Foucault, A.Gelpi: *The Influence of Mechanical and Environmental Parameters on the Crack Growth Behaviour of Alloy 600 in PWR Primary Water*, Proc. of 12th Scandinavian Corrosion Congress & Eurocorr '92, Espoo, Finland (1992), pp. 55-67.

[20] Cassagne, T.B., A.Gelpi: *Crack Growth Rate Measurements on Alloy 600 Steam Generator Tubes in Steam and Primary Water*, Proc. of 5th Symposium on Environmental Degradation of Materials in NPP Systems, Monterey, Ca., USA, 25.-29.8.1991, pp. 518-524.

[21] Chapra, S.C., R.P.Canale: **Numerical methods for Engineers**, 2nd Edition, McGraw-Hill, 1988.

[22] Cizelj, L., B.Mavko: *Sampling Inspection Schemes and Steam Generator Tube Rupture Probability*, CSNI/UNIPEDE Specialist Meeting on Operating Experience with Steam Generators, Brussels, Belgium (1991), paper 5.3.

[23] Cizelj, L., B.Mavko: *On the Risk-Based Steam Generator Life Time Optimisation*, to be published in Theoretical and Applied Fracture Mechanics (1993).

[24] Cizelj, L., B.Mavko, H.Riesch-Opperman, A.Brückner-Foit: *Propagation of Stress Corrosion Cracks in Steam Generator Tubes*, Trans of 11th Conf on SMiRT (1993), Stuttgart, paper DG07/2.

[25] Cizelj, L., B.Mavko, H.Riesch-Oppermann: *Application of First and Second Order Reliability Methods in the Safety Aseessment of Cracked Steam Generator Tubing*, Nuclear Engineering and Design, Vol. 147 (1994), p.359-368.

[26] Cizelj, L. H.Riesch-Oppermann: *ZERBERUS-the Code for Reliability Analysis of Crack Containing Structures*, Report KfK 5019, Kernforschungszentrum Karlsruhe, Germany (1991).

[27] Clark, R.A., R.J.Kurtz: *Compendium and Comparison of International Practice for Plugging, Repair and Inspection of Steam Generator Tubing*, NUREG/CR-5016 (1988).

[28] Cochet, B., B.Flesch: *Crack Stability Criteria in Steam Generator Tubes*, in: F.H.Wittmann, ed(s).: **Experience with Structures and Components in Operating Reactors**, Trans of 9th Int Conf on SMiRT, Lausanne, Switzerland, Vol. D (1987), pp. 413-419.

[29] Degreve, D., D.Dobbeni: *Inspection of Steam Generators and Reactor Vessel Components*, Trans. of the 1st Int. Conf. on Engineering Support to NPP Operation, Belgatom, Brussels (1990), paper 4.2.

[30] DerKiureghian, A., Jyh-Bin Ke: *The stochastic Finite Element Method in Structural Reliability*, Probabilistic Engineering Mechanics, Vol. 3 (1988), pp. 83-91.

[31] Dobbeni, D.: *Eddy Current & Ultrasonic Inspections of SG Tubes via Rotating Probes*, Nuclear Europe Worldscan, Vol. 5 (1991), pp. 11-12.

[32] Dobbeni, D.: *Eddy Current Inspection Methodology*, NEA-CSNI-UNIPEDE Specialist Meeting on Operating Experience with Steam Generators, Brussels, Belgium (1991), paper 6.3.

[33] Duc, M.H., H.Churier-Bosnec, C.Faidy: *Computation of Stresses in French Steam Generator Tubes*, Transactions of 11th Conference on SMiRT, Vol. F, Tokyo, Japan (1991), pp. 361-370.

[34] Dvoršek, T., L.Cizelj, B.Mavko: *Recent Experience with Krško Steam Generators*, ASME International Joint Power Generation Conference, Kansas City, USA, Oct. 1993, paper No. 93-JPGC-NE-2.

[35] Erdogan, F.: *Ductile Fracture Theories for Pressurized Pipes and Containers*, Int J Press V & Piping, Vol. 4 (1976), pp. 253-283.

[36] Fabjan, L., L.Cizelj, B.Mavko: *Ageing of Steam Generators in Nuclear Power Plants (in Slovene)*, Strojniški vestnik, Vol. 38 (1992), No. 10-12, pp. 249-262.

[37] Fiessler, B., H.-J.Neumann, R.Rackwitz: *Quadratic Limit States in Structural Reliability*, J Eng Mech ASCE, Vol. 105 (1979), pp. 661-677.

[38] Flesch, B., P.Vidal, D.Buisine, B.Cochet: *Operating Stresses and Stress Corrosion Cracking in Steam Generator Transition zones (900-MWe PWR)*, Transactions of 11th Conference on SMiRT, Vol. F, Tokyo, Japan (1991), pp. 371-376.

[39] Flesch, B., P.Vidal, J.M.Proix, F.Voldoire, B.Granger, A.Gelpi, B.Cochet: *Contraintes en service et sur-contraintes de denting dans les zones de transition des generateurs de vapeur des reacteurs 900 MWe et 1300 MWe*, SFEN International Symposium, Fontevraud, Vol. 2 (1990), pp. 268-280.

[40] Flesch, B., P.Pitner, T.Riffard: *Failure Ananlysis Module for the PFM Code for PWR Steam Generator Tube Maintenence*, Transactions of 11th International Conference on SMIRT 11, Tokyo, Vol. G (1991), pp. 307-312.

[41] Folias, E.S.: *An Axial Crack in A Pressurized Cyllindrical Shell*, Int. J. of Fracture Mech, Vol. 1 (1965), No. 1, pp. 104-113.

[42] Ford, F.P., P.L.Andresen: *Development and Use of a Predictive Model of Crack Propagation in 304/316L, A533B/A508 and Inconel 600/182 Alloys in 288 C Water*, in: G.J.Theus, J.R.Weeks, ed(s).: **Environmental Degradation of Materials in Nuclear Power Systems-Water Reactors**, Proc of 4th Int Symp on Environmental Degradation of Materials in NPP Systems, Traverse City, USA (1988), pp. 789-800.

[43] Frederick, G., J.Mathonet, P.Hernalsteen, D.Dobbeni: **Development and Justification of New Plugging Criteria Applicable to the Cracking Phenomena in the Tubing of Steam Generators**, Belgatom, Brussels (1989).

[44] Garud, Y.S., T.L.Gerber: **Intergranular Stress Corrosion Cracking of Ni-Cr-Fe Alloy 600 Tubes in PWR Primary Water-Review and Assessment for Model Development**, EPRI-NP-3057 (1983).

[45] Garud, Y.S: *An Incremental Damage Formulation for Stress Corrosion Cracking and Its Application to Crack Growth Interpretation Based on CERT Data*, Corrosion, Vol. 46 (1990), No. 12, pp. 968-974.

[46] Garud, Y.S.: **Development of a Model for Predicting Intergranular Stress Corrosion Cracking of Alloy 600 Tubes in PWR Primary Water**, EPRI-NP-3791 (1985).

[47] Garud, Y.S.: *Quantitative Evaluation of Environmentally Assisted Cracking: A survey of Development and Applications of Modelling Concepts*, J Pressure Vessel Technology, Vol. 113 (1991), pp. 1-9.

[48] Garud, Y.S.: *Service Stresses within the Expansion Transition of Tubes in a PWR U-Tube Heat-exchanger Design Including Local Discontinuity and Geometry Effects*, Transactions of 11th Conference on SMiRT, Vol. F, Tokyo, Japan (1991), pp. 355-360.

[49] Gillot, E., B.Cochet, P.Richard, C.F.Faidy: *Validation of Leak Before Break Analysis for Steam Generator Tubes*, in: F.H.Wittmann, ed(s).: **Experience with Structures and Components in Operating Reactors**, Trans of 9th Int Conf on SMiRT, Lausanne, Switzerland, Vol. D (1987), pp. 405-411.

[50] Gortnar, O.: **An Analysis of the Heat Transfer in a Steam Generator in Nuclear Power Plant (in Slovene)**, Graduate Student Report, University of Ljubljana, Slovenia, 1991.

[51] Granger, B., P.Pitner, D.Crouzet, B.Flesch: *A Practical Study of I.G.S.C.C. in Operating P.W.R. Steam Generators with the Help of A Probabilistic Fracture Mechanics Code for Maintenance*, 12th Scandinavian Corrosion Congress & Eurocorr '92 (1992), Espoo, Finska, pp. 1-10.

[52] Granger, B., P.Pitner, T.Riffard: *Probabilistic Fracture Mechanics Code for PWR Steam Generator Tube Maintenance*, NEA-CSNI-UNIPEDE Specialist Meeting on Operating Experience with Steam Generators, Brussels, Belgium (1991).

[53] Gunsell, L.: **Allowed Crack Length in SG Based on Probabilistic Safety Assessment**, private communication (1992).

[54] Häberer, R., A.Brückner, D.Munz: **Zuverlässigkeitsberechnung mit Hilfe der probabilistischen Bruchmechanik am Beispiel des Sicherheitseinschlusses von Druckwasserreaktoren**, Teil 1, KfK-Report 3458 (1982).

[55] Harbitz, A.: *An Efficient Sampling Method for Probability of Failure Calculation*, Structural Safety, Vol4. (1986), pp. 109-115.

[56] Hernalsteen, P.: *Statistical Treatment of non Destructive Testing of Steam Generator Tubes to Modelize their Future Behaviour*, SFEN International Symposium, Fountevraud, Vol. 2 (1990), pp. 303-312.

[57] Hernalsteen, P.: *The Influence of Testing Conditions on Burst-Pressure Assessment for Inconel Tubing*, Int. J. Pres. Ves. & Piping, Vol. 52 (1992), pp.41-57.

[58] Hernalsteen, P.: *Prediction Models for the PWSCC Degradation Process in Tube Roll Transitions*, NEA-CSNI-UNIPEDE Specialist Meeting on Operating Experience with Steam Generators, Brussels, Belgium (1991), paper 5.2.

[59] Hernalsteen, P.: *A Predictive Model for Steam Generator Degradation Through PW SCC in Roll Transitions*, Trans of 10th Int Conf on SMiRT, Annaheim, Ca., USA, Vol. D (1989), pp. 183-188.

[60] Hutin, J.P., D.Miniere, R.Serres: *Safety Assessment and Inservice Inspection Program*, in: F.H.Wittmann, ed(s).: **Experience with Structures and Components in Operating Reactors**, Trans of 9th Int Conf on SMiRT, Lausanne, Switzerland, Vol. D (1987), pp. 141-146.

[61] Jawad, M.H., E.J.Clarkin, R.E.Schuessler: *Evaluation of Tube-to-Tubesheet Junctions*, Journal of Pressure Vessel Technology ASME, Vol. 109 (1987), pp. 19-26.

[62] Johnston, G.O.: *A Review of Probabilistic Fracture Mechanics Literature*, Reliability Engineering, Vol. 3 (1982), pp. 423-448.

[63] Kalnins, A., D.P.Updike, S.M.Caldwell: *Contact Pressure in Rolled Tube-Tubesheet Transitions*, Transactions of 9th conference on SMiRT, Annaheim, Vol. L (1989), pp. 195-200.

[64] Krausz, A.S., K.Krausz: **Fracture Kinetics of Crack Growth**, Kluwer Academic Publishers (1988), Dordrecht, The Netherlands.

[65] Lawrence, M.: *An Introduction to Reliability Methods*, in: W.K.Liu, T.Belytscko, ed(s).: **Computational Mechanics of Probabilistic and Reliability Analysis**, Elmepress International, Lausanne, Switzerland (1991), pp. 10-46.

[66] Madsen, H.O., S.Krenk, N.C.Lind: **Methods of Structural Safety**, Prentice Hall, Englewood Cliffs (1986).

[67] Martin, P.W.: *Factors that Affect Tube-Tubesheet Joint Integrity*, Trans on 11th Conf on SMiRT (1991), Tokyo, Vol. F, pp. 283-293.

[68] Mavko, B., L.Cizelj: *Failure Probability of Axially Cracked Steam Generator Tubes: A Probabilistic Fracture Mechanics Model*, Nuclear Technology, Vol. 98 (1992), No. 2, pp. 171-177.

[69] Mavko, B., L.Cizelj, G.Roussel: *Steam Generator Tubes Rupture Probability Estimation - Study of the Axially Cracked Tube Case*, NEA-CSNI-UNIPEDE Specialist Meeting on Operating Experience with Steam Generators, Brussels, Belgium (1991).

[70] McEvily, A.J.Jr.: **Atlas of Stress-Corrosion and Corrosion Fatigue Curves**, ASM International (1990), ISBN:0-87170-374-2.

[71] McIlree, A.R., R.B.Rebak, S.Smialowska: *Relationship of Stress Intensity to Crack Growth Rate of Alloy 600 in Primary Water*, SFEN International Symposium, Fontevraud, Vol. 2 (1990), pp. 258-267.

[72] Middlebrooks, W.B., D.L.Harrod, R.E.Gold: *Residual Stresses Associated with the Hydraulic Expansion of Steam Generator Tubing into Tubesheets*, Transactions of 11th Conference on SMiRT, Vol. F, Tokyo, Japan (1991), pp. 343-354.

[73] Mills, A.F.: **Heat Transfer**, Irwin, Boston, USA, 1992.

[74] Myers, R.H.: **Response Surface Methodology**, Allyn and Bacon, Inc. (1971), Boston, USA.

[75] Nuklearna Elektrarna Krško: **Updated Final Safety Analysis Report**, 1992.

[76] Petersen, R.G.: **Design and Analysis of Experiments**, Marcel Dekker, Inc. (1985), New York, USA.

[77] Pitner, P.: *PRA of STEAM Generator Tubes Cracks at Dampierre 1 EDF Plant*, Proceedings of PSA 89 Conference, Pittsburgh, USA, Vol. 1 (1989), pp. 1055-1059.

[78] Pitner, P., T.Riffard, H.Proccacia, B.Granger, C.Faidy, B.Flesch: *Probabilistic Fracture Mechanics Code for PWR Steam Generator Tube Maintenance*, Transactions of 11th International Conference on SMiRT, Tokyo, Vol. G (1991), pp. 302-306.

[79] Press, W.H., B.P.Flannery, S.A.Teukolsky, W.T.Vetterling: **Numerical Recipes (Fortran Version)**, Cambridge University Press, (1989).

[80] Provan, J.W.: **Probabilistic Fracture Mechanics and Reliability**, Martinus Nijhoff Publishers (1987).

[81] Rebak, R.B., A.R.McIlree, Z.Sklarska-Smialowska: *Effects of pH and Stress Intensity on Crack Growth Rate in Alloy 600 in Lithiated + Borated Waters at High Temperatures*, Proc. of 5th Symposium on Environmental Degradation of Materials in NPP Systems, Monterey, Ca., USA, 25.-29.8.1991, pp. 511-517.

[82] Riesch-Oppermann, H., A.Brueckner-Foit: *First- and Second-Order Approximations of Failure Probabilities in Probabilistic Fracture Mechanics*, Reliab Eng Syst Saf, Vol. 23 (1988), No. 3, pp. 183-194.

[83] Riesch-Oppermann, H.: **Anwendung von Naeherungsmethoden zur Berechnung der Ausfallwahrscheinlichkeit rissbehafteter Strukturen unter Ermuedungs- und Kriechbeanspruchung**, Dissertation, University of Karlsruhe (1989).

[84] Riesch-Oppermann, H., A.Brueckner-Foit: *Probabilistic Fracture Mechanics Applied to High Temperature Reliability*, Nucl Eng Design, Vol. 128 (1991), pp. 193-200.

[85] Roussel, G., P.Mignot: *Behaviour of Steam Generator Tubes in Belgium and their Consequences Roll Transitions*, Trans of 10th Int Conf on SMiRT, Annaheim, Ca., USA, Vol. D (1989), pp. 167-175.

[86] Scott, P.M.: *An Analysis of Primary Water Stress Corrosion Cracking in PWR Steam Generators*, NEA-CSNI-UNIPEDE Specialist Meeting on Operating Experience with Steam Generators, Brussels, Belgium (1991).

[87] Shen, Y., P.G.Shewmon: *A Mechanism for Hydrogen-Induced Intergranular Stress Corrosion Cracking*, Metalurgical Transactions A, Vol. 21 (1990), pp. 1261-1271.

[88] Shen, Y., P.G.Shewmon: *Intergranular Stress Corrosion Cracking of Alloy 600 and X-750 in High-Temperature Deaerated Water/Steam*, Metallurgical Transactions A, Vol. 22 (1991), pp. 1857-1864.

[89] Speidel, M.O., R.Magdowski: *Stress Corrosion Crack Growth of Cold Worked Nickel Base Alloy 600*, Proc. of the International Conference on Corrosion-Deformation-Interactions, Fontainebleau, France (1992).

[90] Stubbe, J., P.Hernalsteen: *The Efficiency of Peening on Initiation and Propagation of PWSCC in Roll Transition*, NEA-CSNI-UNIPEDE Specialist Meeting on Operating Experience with Steam Generators, Brussels, Belgium (1991).

[91] Terada, H., T.Nakajima: *Analysis of Stress Intensity Factor of a Crack Approaching Welding Bead*, Int. J. of Fracture, Vol. 27 (1985), pp. 83-90.

[92] Timoshenko, S.: **Theory of Elasticity**, 2nd Edition, McGraw-Hill, 1951.

[93] US Nuclear Regulatory Commission: **Bases for Plugging Degraded PWR Steam Generator Tubes**, Regulatory Guide 1.121 (1976).

[94] US Nuclear Regulatory Commission: **Inservice Inspection of Pressurized Water Reactor Steam Generator Tubes**, Regulatory Guide 1.83, Rev. 1 (1975).

[95] US Code of Federal Regulations, Title 10, Part 50, Appendix A: **General Design Criteria for Nuclear Power Plants**, Washington, USA (1974).

[96] Vyve, J.van, P.Hernalsteen: *Tube Plugging Criteria for Axial and Circumferential Cracks in the Tubesheet Area*, NEA-CSNI-UNIPEDE Specialist Meeting on Operating Experience with Steam Generators, Brussels, Belgium (1991).

[97] Wellein, R.: *Application of PFM in the Nuclear Industry to Reactor Pressure Vessel, Main Coolant Piping and Steel Containment*, in: J.W. Provan, ed(s).: **Probabilistic Fracture Mechanics and Reliability**, Martinus Nijhoff Publishers (1987), pp. 325-350.

[98] Westinghouse Electric Corporation: **Certificates for NPP Krško**, C.O. 545-5316-400 TO 5344.

[99] Westinghouse Electric Corporation: **Vertical Steam Generator for Krško Nuclear Power Plant**, Westinghouse Technical Manual 1440-C298 (1976).

[100] Westinghouse Electric Corporation: **Krško Tubesheet Region Plugging Criterion for Full Depth Hardroll Expanded Tubes**, NS-RCSCL-C/L-85-200, Rev.1, (1985).

[101] Yahsi, O.S., F.Erdogan: *A Pressurized Cylindrical Shell with a Fixed End Which Contains an Axial Part-Through or Through Crack*, International Journal of Fracture, Vol. 28 (1985), pp. 161-187.